

**NICKEL SUPPORTED CATALYST FOR  
HYDRODEOXYGENATION OF BIO-OIL MODEL  
COMPOUNDS**

**SHARAFADEEN GBADAMASI**

**INSTITUTE OF GRADUATE STUDIES  
UNIVERSITY OF MALAYA  
KUALA LUMPUR**

**2016**

**NICKEL SUPPORTED CATALYST FOR  
HYDRODEOXYGENATION OF BIO-OIL MODEL  
COMPOUNDS**

**SHARAFADEEN GBADAMASI**

**DISSERTATION SUBMITTED IN FULFILMENT OF  
THE REQUIREMENTS FOR THE DEGREE OF  
MASTERS OF PHILOSOPHY**

**INSTITUTE OF GRADUATE STUDIES  
UNIVERSITY OF MALAYA  
KUALA LUMPUR**

**2016**

**UNIVERSITY OF MALAYA**  
**ORIGINAL LITERARY WORK DECLARATION**

Name of Candidate: SHARAFADEEN GBADAMASI

Registration/Matric No: HGA130019

Name of Degree: MASTERS OF PHILOSOPHY

Title of Dissertation (“this Work”): NICKEL SUPPORTED CATALYST FOR  
HYDRODEOXYGENATION OF BIO-OIL MODEL COMPOUNDS

Field of Study: CHEMICAL ENGINEERING (ENERGY)

I do solemnly and sincerely declare that:

- (1) I am the sole author/writer of this Work;
- (2) This Work is original;
- (3) Any use of any work in which copyright exists was done by way of fair dealing and for permitted purposes and any excerpt or extract from, or reference to or reproduction of any copyright work has been disclosed expressly and sufficiently and the title of the Work and its authorship have been acknowledged in this Work;
- (4) I do not have any actual knowledge nor do I ought reasonably to know that the making of this work constitutes an infringement of any copyright work;
- (5) I hereby assign all and every rights in the copyright to this Work to the University of Malaya (“UM”), who henceforth shall be owner of the copyright in this Work and that any reproduction or use in any form or by any means whatsoever is prohibited without the written consent of UM having been first had and obtained;
- (6) I am fully aware that if in the course of making this Work I have infringed any copyright whether intentionally or otherwise, I may be subject to legal action or any other action as may be determined by UM.

Candidate’s Signature

Date:

Subscribed and solemnly declared before,

Witness’s Signature

Date:

Name: Prof. Dr. Sharifah Bee O. A. Abd Hamid

Designation: Professor

## ABSTRACT

The continuous depletion of crude oil reserves and environmental concern has made the search for alternative energy source more imperative. Biomass, which is abundant and carbon neutral energy source has been identified as a potential feedstock for the production of fuel, chemicals and carbon-based materials. Bio-oil, a liquid product of fast pyrolysis of biomass, has gained substantial interest in recent decades with the aim of mitigating and subsequently substituting transport fuel. The combustion of bio-oil produces negligible amount of harmful emissions, such as nitrogen oxides (NO<sub>x</sub>), sulphur dioxide (SO<sub>2</sub>) and soot. Additionally, emitted carbon dioxide (CO<sub>2</sub>) is being recycled into the plant by photosynthesis, hence preventing global warming effect. However, bio-oil possesses undesirable properties such as high polarity, viscosity and acidity, and chemical instability due to its high oxygen and water contents. Consequently, this study investigated the first time application of Ni/Al-SBA-15 catalysts in hydrodeoxygenation of bio-oil model compounds (dibenzofuran and guaiacol). Ni/Al-SBA-15 catalysts with different Si/Al (Si/Al = 50, 60, 70 and 80) mole ratios were synthesized and their catalytic performance was tested for hydrodeoxygenation of dibenzofuran and guaiacol as bio-oil model compounds in a batch reactor. The catalysts were synthesized using the impregnation method and systematically characterized using XRD, N<sub>2</sub>-adsorption desorption, Raman, H<sub>2</sub>-TPR, NH<sub>3</sub>-TPD, XRF, and FESEM techniques. The characterization results reveal that all the synthesized catalysts are mesoporous (pore size range = 3.80–5.20 nm) and possess high surface areas ranging from 665–740 m<sup>2</sup>/g. Further, the incorporation of Al<sup>3+</sup> into the SBA-15 matrix generates weak acidic sites and the total acidity generated increases with decrease in the Si/Al mole ratio (i.e. increase in amount of Al<sup>3+</sup> incorporated). The activity results showed that the hydrodeoxygenation of dibenzofuran proceeds via hydrogenation of the benzene rings on the Ni sites followed by cleavage of C-O bonds on the acidic sites of the catalyst to yield unsaturated

hydrocarbons. Further hydrogenation of unsaturated hydrocarbons on the Ni sites gives bicyclohexyl as the major product. A remarkable 100.00% dibenzofuran conversion was found for all the catalysts except for Ni/SBA-15 and Ni/Al-SBA-15 (80) (Si/Al mole ratio = 80) catalysts, which showed 97.97% and 99.31%, respectively. Among the synthesized catalysts, the Ni/Al-SBA-15(50) (Si/Al mole ratio = 50) catalyst showed the highest efficiency (due to its high acidity), with superior selectivity of ~87.00% for bicyclohexyl and ~96.00% degree of deoxygenation at 10 MPa, 260 °C and 5 h. The obtained activity results reveal the synergetic effect of Ni and support in the hydrodeoxygenation of dibenzofuran reaction: the concentration of acidic sites has a significant effect on the selectivity of the desired products. Further, the activity of Ni/Al-SBA-15(50) (being the most effective catalyst) was investigated for hydrodeoxygenation of guaiacol in a batch reactor at 5 MPa. The activity results showed that the reaction proceeded via demethoxylation of guaiacol to produce phenol, followed by direct hydrogenolysis to produce benzene. Subsequent hydrogenation of the benzene produces cyclohexane. After 3 h of reaction at 250 °C, 89.00% conversion, 74.97% degree of deoxygenation and 60.40% cyclohexane selectivity were achieved.

## ABSTRAK

Pengurangan rizab minyak mentah secara berterusan serta kesan negative bahan tersebut terhadap alam sekitar menjadikan pencarian sumber tenaga alternatif sangat penting. Sisa biomas yang banyak dan merupakan sumber tenaga yang neutral karbon menjadikannya sebagai bahan mentah yang berpotensi sebagai sumber pengeluaran bahan api, bahan kimia dan bahan-bahan berasaskan karbon. "Bio-oil" yang merupakan produk yang dihasilkan apabila biomas melalui proses pirolisis cecair secara pantas, telah mendapat perhatian ramai sejak beberapa dekad yang lalu dalam usaha untuk mengurangkan dan seterusnya menggantikan bahan api pengangkutan. Pembakaran bahan bio-minyak hanya menghasilkan jumlah bahan merbahaya kecil seperti oksida nitrogen ( $\text{NO}_x$ ), sulfur dioksida ( $\text{SO}_2$ ) dan jelaga dalam jumlah yang kecil. Malah, karbon dipancarkan dioksida ( $\text{CO}_2$ ) yang dihasilkan juga akan dikitar semula menerusi proses fotosintesis seterusnya mencegah kesan pemanasan global. Namun, "bio-oil" mempunyai ciri-ciri yang tidak diingini seperti kekutuban yang tinggi, kelikatan dan keasidan, serta ketidakstabilan kimia yang disebabkan kandungan oksigen dan air yang tinggi. Justeru, kajian ini menjurus kepada aplikasi Ni/Al-SBA-15 untuk proses "hydrodeoxygenation" buat pertama kali bagi kompaun model untuk minyak bio iaitu dibenzofuran dan guaiacol. Ni/Al-SBA-15 dengan nisbah mol Si/Al yang berbeza ( $\text{Si/Al} = 50, 60, 70$  dan  $80$ ) telah disediakan dan prestasi setiap sampel sebagai pemangkin telah diuji menerusi proses hydrodeoxygenation ke atas dibenzofuran dan guaiacol sebagai sebatian model yang dilaksanakan dalam reaktor. Pemangkin telah disediakan menggunakan kaedah pengisitepuan dan dianalisa secara sistematik menggunakan teknik-teknik seperti XRD,  $\text{N}_2$ -adsorption desorption, Raman,  $\text{H}_2$ -TPR,  $\text{NH}_3$ -TPD, XRF, and FESEM. Keputusan analisa mendedahkan bahawa semua pemangkin yang disediakan adalah mesoporous (saiz liang antara 3.8–5.2 nm) dan mempunyai kawasan permukaan yang tinggi antara 665-740  $\text{m}^2 / \text{g}$ . Di samping itu, pengenalan  $\text{Al}^{3+}$  ke dalam matriks SBA-15 telah menjana

laman asid lemah dan jumlah keasidan meningkat apabila nisbah mol Si/Al menurun (iaitu apabila terdapat peningkatan dalam jumlah  $Al^{3+}$ ). Keputusan turut menunjukkan bahawa hydrodeoxygenation terhadap dibenzofuran terhasil melalui penghidrogenan pada cincin benzena pada laman Ni diikuti oleh pemotongan jalinan C-O pada laman berasid pada pemangkin untuk menghasilkan hidrokarbon tidak tepu. Turut dapat diperhatikan adalah kesan penghidrogenan lanjut terhadap hidrokarbon tidak tepu tersebut pada laman Ni memberikan “bicyclohexyl” sebagai produk utama. Kadar 100% penukaran dibenzofuran telah dicapai bagi semua pemangkin kecuali Ni/SBA-15 dan Ni/Al-SBA-15 (80) (nisbah mol Si/Al = 80) dengan kedua-dua pemangkin tersebut menunjukkan 97.97% dan 99.31%. Di antara pemangkin yang disediakan, Ni/Al-SBA-15 (50) (Si/Al nisbah mol = 50) menunjukkan kadar kecekapan tertinggi (disebabkan keasidan yang tinggi), dengan kadar pemilihan sekitar ~ 87% untuk bicyclohexyl dan ~ 96 % tahap “deoxygenation” pada 10 MPa, 260 ° C dan 5 jam. Keputusan aktiviti yang diperoleh turut mendedahkan kesan sinergi Ni dan penyokong dalam tindak balas hydrodeoxygenation ke atas dibenzofuran: kepekatan laman berasid mempunyai impak yang besar ke atas pemilihan produk yang dikehendaki. Di samping itu, aktiviti Ni/Al-SBA-15 (50) (menjadikannya sebagai pemangkin yang paling berkesan) telah dikaji lebih lanjut sebagai pemangkin bagi hydrodeoxygenation daripada guaiacol dalam reaktor pada 5 MPa. Keputusan aktiviti menunjukkan bahawa tindak balas akan berterusan dan guaiacol akan melalui “demethoxylation” untuk menghasilkan fenol, diikuti oleh “hydrogenolysis” bagi menghasilkan benzena. Penghidrogenan berikutnya terhadap benzena menghasilkan “cyclohexane”. Selepas 3 jam, tindak balas pada 250 °C, memberi kadar penukaran sebanyak 89%, tahap “deoxygenation” pada 74.97% dan kadar pemilihan “cyclohexane” sebanyak 60.4% telah berjaya dicapai.

## ACKNOWLEDGEMENTS

I am grateful for the financial support of the research grant from Ministry of Higher Education (grant number: HIR – F000032), Malaysia, and financial assistance from national research institute for chemical technology (NARICT), Zaria.

I would like to express my deepest sense of gratitude and appreciation to my main supervisor Prof. Dr Sharifah Bee O. A. Abd. Hamid, for her support and guidance throughout my studies. Her valuable advices and constructive criticism were of great help at all stages of my studies. Also, to my second supervisor Dr Lee Hwei Voon, I would like to say thank you for your contribution towards my success. It is a great privilege to have been supervised by both of them for which and I am grateful.

My sincere gratitude and warm thanks to Dr Azman bin Maamor for his guidance in operating some of the equipment used during this study. To Dr Tammar Hussein Ali, I am grateful for his mentorship during the short time stint at NANOCAT. My appreciation also goes to Nur Atiqah Bint Da'ud for her assistance and guidance in operating the equipment used during this studies. A big thank you to all members of NANOCAT, (both academic and non-academic staff) for their assistance and support throughout my studies in University of Malaya. It would not have been possible without them.

My special appreciation goes to Prof. Idris Muhammad Bugaje, Dr Abdulazeez Yusuf Atta and Dr Nurudeen Yusuf for giving me the support and opportunity of pursuing my studies in Malaysia. Words of mouth alone cannot express my sincere gratitude. All I can say is 'May Almighty Allah in His infinite mercy reward you all abundantly'. Also, my

sincere gratitude and warm thanks to Dr Yahaya Muhammad Sani for his support, guidance and assistance during this studies.

Warm regards also goes to Ahmad Khalil and Murtala Maidamma Ambursa for their friendship and brotherhood, which gave me a lot of motivations and support during this studies. I am also thankful to Dr M. T. Isa, Abdulazeez Isa Rbed, Nasir Ibrahim Lawal, Ope Fasanya, Dr Babangida Sarki Yandoka, Sirajudeen Abdulazeez Olayiwola, Murtala Muhammad, Abideen Abdulazeez, Yusuf Adeleke, Bashir Abdulazeez, Shefiu Abdulsalam, Idris Adewale, Abubakar Abdulsalam Abdurashed Adewale, Abbas Lawal, Abdullah Abdul Rauf, Adamu Abbas, all members of Nigerian Students Community in University of Malaya (NISCUM), all my colleagues at national research institute for chemical technology (NARICT), Zaria, and all members of club 60 for their supports, concerns and prayer.

My final appreciation goes to my family. To my Mum and Dad, Mrs. Sidikat Mustapha Gbadamasi and Mr. Mustapha Gbadamasi; I am grateful for my moral up bringing to become the man that I am today. I am grateful for raising me with a strong work ethics and a drive and tenacity to succeed. I am grateful for your continuous prayer and unflinching support. I am grateful for raising me to be a man that is always happy and who only seeks for support from Almighty Allah. I pray to Allah to give you both long life and prosperity in good health and faith in Allah, so that you can reap the fruit of your labour. My warmest appreciations to my siblings, Rashidah, Lukman, Shakirah, Abdurashed, Muhyideen, and my nephew and niece, Abdulsamad, Rofiah and Fatima – I love you all. Finally, to my fiancé, Amina Muhammad Sani, thank you for your love, prayers, encouragement and for being patient with me – I love you.

## TABLE OF CONTENTS

|   |          |
|---|----------|
| Abstract .....                              | iii      |
| Abstrak .....                               | v        |
| Acknowledgements .....                      | vii      |
| Table of Contents .....                     | ix       |
| List of Figures .....                       | xiii     |
| List of Tables.....                         | xvi      |
| List of Symbols and Abbreviations.....      | xvii     |
| List of Appendices .....                    | xx       |
| <br>  |          |
| <b>CHAPTER 1: INTRODUCTION.....</b>         | <b>1</b> |
| 1.1 Research background.....                | 1        |
| 1.2 Statement of the research problem ..... | 4        |
| 1.3 Justification for the study .....       | 4        |
| 1.4 Aim and objective of the research ..... | 5        |
| 1.5 Scope of the research.....              | 5        |
| 1.6 Outline of the dissertation.....        | 6        |
| <br>  |          |
| <b>CHAPTER 2: LITERATURE REVIEW.....</b>    | <b>8</b> |
| 2.1 Bio-oil.....                            | 8        |
| 2.2 Bio-oil upgrading.....                  | 8        |
| 2.2.1 Zeolite cracking.....                 | 9        |
| 2.2.2 Hydrodeoxygenation .....              | 10       |
| 2.3 Bio-oil model compounds .....           | 12       |
| 2.3.1 Guaiacol.....                         | 14       |
| 2.3.2 Anisole.....                          | 17       |

|   |  |           |
|---|--|-----------|
| 2.3.3                                       | Phenol .....   | 18        |
| 2.3.4                                       | Dibenzofuran .....   | 20        |
| 2.3.5                                       | Ketones, aldehydes, and acids .....  | 21        |
| 2.4   | Catalysts.....   | 22        |
| 2.4.1                                       | Transition metal sulfides (TMS) .....  | 22        |
|   | 2.4.1.1 Challenges associated with the use of sulfided catalysts .....                 | 24        |
| 2.4.2                                       | Noble metal catalysts.....   | 25        |
|   | 2.4.2.1 Challenges associated with the use of supported noble metal<br>catalysts ..... | 28        |
| 2.4.3                                       | Non-noble transition metal catalysts .....   | 28        |
| 2.5   | Catalyst supports.....   | 31        |
| 2.5.1                                       | Alumina .....  | 32        |
| 2.5.2                                       | Metal oxides .....   | 32        |
| 2.5.3                                       | Mesoporous silica.....   | 34        |
| <b>CHAPTER 3: RESEARCH METHODOLOGY.....</b> |  | <b>35</b> |
| 3.1   | Materials .....  | 35        |
| 3.2   | Catalysts preparation .....  | 35        |
|   | 3.2.1 Synthesis of SBA-15 .....  | 35        |
|   | 3.2.2 Synthesis of Al-SBA-15 .....   | 37        |
|   | 3.2.3 Synthesis of supported Ni-based catalysts .....                                  | 38        |
| 3.3   | Catalysts characterization .....   | 38        |
|   | 3.3.1 X – Ray diffraction (XRD) analysis .....   | 38        |
|   | 3.3.1.1 Background .....   | 38        |
|   | 3.3.1.2 Procedure.....   | 40        |
|   | 3.3.2 X – Ray fluorescence (XRF) analysis .....  | 41        |
|   | 3.3.2.1 Background .....   | 41        |

|   |  |           |
|---|--|-----------|
| 3.3.2.2                                       | Procedure.....   | 42        |
| 3.3.3   | BET and BJH analysis.....  | 42        |
| 3.3.3.1                                       | Background .....   | 42        |
| 3.3.3.2                                       | Procedure.....   | 43        |
| 3.3.4   | Field Emission Scanning Electron Microscopy (FESEM) analysis .....                       | 43        |
| 3.3.4.1                                       | Background .....   | 43        |
| 3.3.4.2                                       | Procedure.....   | 44        |
| 3.3.5   | Raman spectroscopy analysis .....  | 44        |
| 3.3.5.1                                       | Background .....   | 44        |
| 3.3.5.2                                       | Procedure.....   | 45        |
| 3.3.6   | H <sub>2</sub> -Temperature-Programmed Reduction (H <sub>2</sub> -TPR) analysis .....    | 45        |
| 3.3.6.1                                       | Background .....   | 45        |
| 3.3.6.2                                       | Procedure.....   | 46        |
| 3.3.7   | NH <sub>3</sub> -Temperature-Programmed Desorption (NH <sub>3</sub> -TPD) analysis ..... | 46        |
| 3.3.7.1                                       | Background .....   | 46        |
| 3.3.7.2                                       | Procedure.....   | 46        |
| 3.4   | Catalysts activity study .....   | 47        |
| 3.4.1   | Catalysts activation.....  | 47        |
| 3.4.2   | Reactor set-up.....  | 49        |
| 3.4.3   | Hydrodeoxygenation reaction .....  | 50        |
| 3.5   | Product analysis .....   | 51        |
| 3.5.1   | GC analysis.....   | 51        |
| 3.5.2   | Conversion and selectivity calculation.....  | 52        |
| <b>CHAPTER 4: RESULTS AND DISCUSSION.....</b> |  | <b>53</b> |
| 4.1   | Catalysts characterization .....   | 53        |
| 4.1.1   | Surface area and porosity measurement .....  | 53        |

|  |   |           |
|--|---|-----------|
| 4.1.2  | Morphological properties .....  | 58        |
| 4.1.3  | Powder XRD analysis.....  | 60        |
| 4.1.4  | Elemental composition determination.....                                  | 66        |
| 4.1.5  | Raman spectroscopy analysis .....   | 67        |
| 4.1.6  | H <sub>2</sub> -TPR analysis .....  | 70        |
| 4.1.7  | NH <sub>3</sub> -TPD analysis.....  | 72        |
| 4.2  | Catalytic activity results .....  | 74        |
| 4.2.1  | HDO of DBF .....  | 74        |
| 4.2.1.1  | Effect of reaction temperature on HDO of DBF .....                        | 78        |
| 4.2.1.2  | Effect of reaction time on HDO of DBF .....                               | 80        |
| 4.2.1.3  | Possible reaction pathways in HDO of DBF.....                             | 82        |
| 4.2.2  | HDO of guaiacol.....  | 83        |
| 4.2.2.1  | Effect of reaction temperature on HDO of guaiacol .....                   | 85        |
| 4.2.2.2  | Reaction pathways and effect of reaction time on HDO of<br>guaiacol ..... | 87        |
| <b>CHAPTER 5: CONCLUSION AND RECOMMENDATIONS .....</b> |   | <b>90</b> |
| 5.1  | Conclusion.....   | 90        |
| 5.2  | Recommendations for future work .....                                     | 92        |
| References.....  |   | 93        |
| List of Publications and Papers Presented .....        |   | 108       |
| Appendix.....  |   | 109       |

## LIST OF FIGURES

|  |    |
|--|----|
| Figure 2.1: Structure of guaiacol.....   | 14 |
| Figure 2.2: Guaiacol HDO reaction pathways .....   | 15 |
| Figure 2.3: Anisole HDO reaction pathways .....  | 18 |
| Figure 2.4: Phenol HDO reaction pathways over Pd/HY catalyst .....   | 19 |
| Figure 2.5: Phenol HDO reaction pathways to bicyclic compounds over Pt/HY catalyst .....   | 19 |
| Figure 2.6: HDO reaction pathways of DBF .....   | 20 |
| Figure 2.7: HDO reaction pathways of carbonyl group into alkanes.....  | 21 |
| Figure 2.8: Mechanism of 2-ethylphenol HDO over MoS <sub>2</sub> -based catalyst .....   | 24 |
| Figure 2.9: Possible mechanism of guaiacol HDO over non-noble metal catalysts .....  | 29 |
| Figure 3.1: Flow chart for the synthesis of SBA-15 .....   | 36 |
| Figure 3.2: Flow chart for the synthesis of Al-SBA-15 .....  | 37 |
| Figure 3.3: Flow chart for the catalysts synthesis .....   | 39 |
| Figure 3.4: Pretreatment set-up for catalysts activation.....  | 48 |
| Figure 3.5: Bulb sealing with a torch in the encapsulation unit and catalysts bulbs after sealing .....                                | 49 |
| Figure 3.6: A workstation that consist 12 independent batch reactors .....   | 50 |
| Figure 4.1: (a) N <sub>2</sub> adsorption-desorption isotherms (b) pore size distribution of SBA-15 and Ni/SBA-15.....                 | 54 |
| Figure 4.2: (a) N <sub>2</sub> adsorption-desorption isotherms (b) pore size distribution of Al-SBA-15(50) and Ni/ Al-SBA-15(50) ..... | 55 |
| Figure 4.3: (a) N <sub>2</sub> adsorption-desorption isotherms (b) pore size distribution of Al-SBA-15(60) and Ni/ Al-SBA-15(60) ..... | 56 |
| Figure 4.4: (a) N <sub>2</sub> adsorption-desorption isotherms (b) pore size distribution of Al-SBA-15(70) and Ni/ Al-SBA-15(70) ..... | 56 |

|  |    |
|--|----|
| Figure 4.5: (a) N <sub>2</sub> adsorption-desorption isotherms (b) pore size distribution of Al-SBA-15(80) and Ni/ Al-SBA-15(80) .....         | 56 |
| Figure 4.6: FESEM images of (a) SBA-15 (b) Al-SBA-15(50) (c) Al-SBA-15(60) (d) Al-SBA-15(70) (e) Al-SBA-15(80); magnification = x 10,000 ..... | 59 |
| Figure 4.7: (a) Small angle and (b) wide angle XRD analysis of the synthesized supports .....  | 61 |
| Figure 4.8: (a) Small angle and (b) wide angle XRD analysis of the synthesized catalysts .....   | 64 |
| Figure 4.9: Raman spectra of the synthesized (a) SAB-15 and Al-SBA-15 supports, and (b) Ni/SBA-15 and Ni/Al-SBA-15(n) catalysts .....          | 68 |
| Figure 4.10: TPR profiles of all the synthesized catalysts .....   | 71 |
| Figure 4.11: NH <sub>3</sub> -TPD profiles of the synthesized catalysts .....  | 73 |
| Figure 4.12: Products distribution obtained over supported Ni catalysts at 250 °C and 2 h .....  | 77 |
| Figure 4.13: DBF conversion and degree of deoxygenation (HDO) over synthesized catalysts at 260 °C and 2 h .....                               | 80 |
| Figure 4.14: Effect of reaction time on (a) DBF conversion and selectivity, and (b) product selectivity .....                                  | 81 |
| Figure 4.15: Proposed reaction scheme of DBF HDO over the synthesized catalysts ...  | 83 |
| Figure 4.16: Guaiacol and degree of HDO at 250 °C and 2 h of reaction .....  | 84 |
| Figure 4.17: Products distribution from HDO of guaiacol at 250 °C and 2 h of reaction .....  | 84 |
| Figure 4.18: Guaiacol conversion and degree of HDO as a function of temperature at 5 MPa and 3 h of reaction .....                             | 86 |
| Figure 4.19: product selectivity obtained over Ni/Al-SBA-15(50) as a function of temperature at 5MPa and 3 h of reaction .....                 | 87 |
| Figure 4.20: Guaiacol conversion and degree of HDO as a function of reaction time at 5 MPa and 250 °C .....                                    | 88 |
| Figure 4.21: Product selectivity obtained over Ni/Al-SBA-15(50) as a function of reaction time at 5 MPa and 250 °C .....                       | 88 |

Figure 4.22: Proposed reaction scheme of guaiacol HDO over Ni/SBA-15 and Ni/Al-SBA-15(50)..... 89

University of Malaya

## LIST OF TABLES

|  |    |
|--|----|
| Table 2.1: Comparison between bio-oil and crude oil .....  | 9  |
| Table 2.2: Comparison of characteristics of bio-oil, catalytically upgraded bio-oil and crude oil.....                       | 11 |
| Table 2.3: Overview of catalysts investigated for bio-oil upgrading via HDO and ZC .   | 13 |
| Table 2.4: Components of wood-based bio-oil .....  | 14 |
| Table 2.5: Overview of results obtained for HDO of bio-oil model compounds over supported noble metal catalysts .....        | 27 |
| Table 2.6: Overview of some recent results for HDO of bio-oil model compounds over supported non-noble metal catalysts ..... | 30 |
| Table 3.1: List of chemicals used in this study, their suppliers and purity .....  | 35 |
| Table 4.1: Textural properties of the synthesized catalysts .....  | 57 |
| Table 4.2: Summary of extract from small angle XRD analysis .....  | 62 |
| Table 4.3: Summary of extract from wide-angle XRD analysis .....   | 65 |
| Table 4.4: Amount of Ni metal present in the catalysts .....   | 67 |
| Table 4.5: Raman band assignment for the synthesized supports and catalysts .....  | 69 |
| Table 4.6: Summary of total acidity .....  | 74 |
| Table 4.7: Conversion of DBF over the synthesized catalysts at 250 °C and 2 h.....   | 74 |
| Table 4.8: Products distribution in HDO of DBF at 2 h and varying temperature over the synthesized catalysts .....           | 79 |

## LIST OF SYMBOLS AND ABBREVIATIONS

|        |   |                          |
|--------|---|--------------------------|
| HDO    | : | Hydrodeoxygenation       |
| ZC     | : | Zeolite cracking         |
| HHV    | : | High heating value       |
| $\rho$ | : | Density                  |
| $\mu$  | : | Viscosity                |
| wt.%   | : | Weight percentage        |
| C      | : | Carbon                   |
| O      | : | Oxygen                   |
| H      | : | Hydrogen                 |
| S      | : | Sulphur                  |
| N      | : | Nitrogen                 |
| FCC    | : | Fluid catalytic cracking |
| Y      | : | Yield                    |
| t      | : | Time                     |
| P      | : | Pressure                 |
| T      | : | Temperature              |
| DOD    | : | Degree of deoxygenation  |

|       |   |                          |
|-------|---|--------------------------|
| DME   | : | Demethylation            |
| DH    | : | Direct hydrogenolysis    |
| DMO   | : | Demethoxylation          |
| MT    | : | Methyl transfer          |
| HYD   | : | Hydrogenation            |
| DBF   | : | Dibenzofuran             |
| TMS   | : | Transition metal sulfide |
| TEOS  | : | Tetraethylorthosilicate  |
| AIP   | : | Aluminum isopropoxide    |
| BET   | : | Brunauer–Emmett–Teller   |
| BJH   | : | Barrett-Joyner-Halenda   |
| BCH   | : | Bicyclohexyl             |
| CHCHE | : | Cyclohexyl-cyclohexene   |
| CHB   | : | Cyclohexyl-benzene       |
| DHDBF | : | Dodecahydro-dibenzofuran |
| PCHOH | : | Phenyl-cyclohexanol      |
| CHPOH | : | Cyclohexyl-phenol        |
| HHDBF | : | Hexahydro- dibenzofuran  |

THDBF : Tetrahydro- dibenzofuran

CHCHOH : Cyclohexyl-cyclohexanol

CHCHO : Cyclohexyl-cyclohexanone

University of Malaya

## **LIST OF APPENDICES**

Appendix A: GC-FID Chromatograms for product analysis at various reaction time for HDO of DBF at 10 MPa and 260 °C

Appendix B: Calculation for dibenzofuran conversion at 2 h and 10 MPa

University of Malaya

## CHAPTER 1: INTRODUCTION

### 1.1 Research background

Owing to the increasing emissions of greenhouse gases such as carbon dioxide (CO<sub>2</sub>), human life and the ecological environment have been affected by global warming and climate changes. Also, increasing concerns about depletion of fossil fuel reserves, instability in crude oil prices and the fact that crude oil is only concentrated in few regions of the globe has resulted in research into alternative energy sources. The development of synthetic fuels and biofuels technologies using alternative energy sources has become increasingly important in recent years (Bui *et al.*, 2012; Hahn-Hägerdal *et al.*, 2006; Song, 2006; Subramani & Gangwal, 2008; Wang *et al.*, 2011). Biomass, which is the only carbon-based renewable resource on the earth, has emerged as a potential alternative feedstock to fossil fuels for the production of high-value chemicals and fuels (Wang *et al.*, 2012). Bio-oil, a complex mixture of oxygenated compounds produced from fast pyrolysis of biomass, in particular, have the potential of substituting petrol and diesel. The combustion of bio-oil produces negligible amounts of harmful emissions, such as nitrogen oxides (NO<sub>x</sub>), sulphur dioxide (SO<sub>2</sub>) and soot. This is because the source of biomass contains a negligible amount of sulphur, nitrogen and ash. Additionally, emitted carbon dioxide (CO<sub>2</sub>) is being recycled into the plant by photosynthesis, hence preventing global warming effect (He & Wang, 2012; Jacobson *et al.*, 2013; Mortensen *et al.*, 2011; Ruddy *et al.*, 2014). However, despite its advantages, bio-oil contains undesirable properties like high water and oxygen content that results into low heating value and pH, high viscosity and polarity, and poor thermal and chemical stability (Bui *et al.*, 2012; He & Wang, 2012; Ruddy *et al.*, 2014; Wang *et al.*, 2015). To address these challenges (i.e. bio-oil undesirable properties), there is a need for post-production upgrading of bio-oil.

In open literature, there have been reports on different upgrading techniques (such catalytic hydrodeoxygenation, zeolite cracking, etc.) of bio-oil to biofuel or chemicals. However, catalytic hydrodeoxygenation (HDO) is considered as the most effective upgrading technique to produce high quality fuel. HDO involve the removal of oxygen from bio-oil by the cleavage of C–O bond under high temperature and H<sub>2</sub> pressure to produce water as by-product in the presence of a catalyst. The technique is similar to hydrodesulfurization (HDS) technique used in conventional petroleum refineries (Bridgwater, 1994; Bridgwater, 1996; Jacobson *et al.*, 2013; Mortensen *et al.*, 2011; Ruddy *et al.*, 2014). However, design of efficient catalyst(s) for HDO of bio-oil has been extremely challenging due to the complex nature bio-oil. Hence, recent studies have been focused on the use of bio-oil model compounds, such as guaiacol, dibenzofuran, phenol, furfural, etc. to gain insight into the chemistry that could provide useful information for effective catalyst(s) design (He & Wang, 2012; Honkela *et al.*, 2010; Lee *et al.*, 2015). For example, Lee *et al.*, (2012) studied the HDO of guaiacol over noble metal dispersed on acidic support in a batch reactor at 40 bar and 250 °C. They reported that since the reaction proceeds via hydrogenation (HYD) – hydrogenolysis- hydrogenation (HYD) routes, therefore, HDO process requires bifunctional catalyst(s).

In recent time, the most studied HDO catalysts have been the supported noble metal–based catalysts. There have been reports on the use of noble metals such as Pd (Hong *et al.*, 2014), Pt (Wang *et al.*, 2015), Ru (Wang *et al.*, 2014) and Rh (Gutierrez *et al.*, 2009) in the literature and the targeted products have been saturated hydrocarbons. The supported noble metal-based catalysts show excellent catalytic activity both in conversion of the substrate used and in the selectivity to alkanes. For example, Wang *et al.*, (2012) studied the HDO of guaiacol in an autoclave reactor at 200 °C and 40 bar. They reported high catalytic activity with cyclohexane, methylcyclohexane and methylcyclopentane being the products formed. Although the use of supported noble metal catalysts yield

excellent result, but noble metals are prone to poisoning and are relatively expensive (Honkela *et al.*, 2010; Zhang *et al.*, 2013). Thus, the development of less expensive catalysts will be more attractive to the global market.

Another key component that dictates the activity of HDO catalysts is the support. Al<sub>2</sub>O<sub>3</sub> was the earliest studied support for HDO catalysts because of its performance in HDS. However, in the HDO of bio-oil and its model compounds, phenolics like phenol and guaiacol chemisorbed to the surface of the Al<sub>2</sub>O<sub>3</sub> to form phenate species at room temperature. Consequently, there is coke formation on the catalysts surface (Bui *et al.*, 2011; Popov *et al.*, 2010). In addition, Al<sub>2</sub>O<sub>3</sub> is metastable in the presence of water, and water forms about 30% of bio-oil (Laurent & Delmon, 1994). To overcome these challenges, supports like carbon (Zhao & Lercher, 2012), SiO<sub>2</sub> (Bykova *et al.*, 2012), ZrO<sub>2</sub> (Ardiyanti *et al.*, 2011), TiO<sub>2</sub> (Bui *et al.*, 2011) and zeolites (Zhang *et al.*, 2014) have been studied in recent years. All these supports showed enhanced metal dispersion and good stability in HDO reaction in the presence of water. However, these supports have small surface areas, thus limiting the adsorption of reactant molecules on the active sites of the metal species dispersed on the supports and consequently, low reaction rates. To this note, the use of mesoporous materials, such as SBA-15 (Wang *et al.*, 2014), mesoporous zeolites (Yuxin Wang *et al.*, 2011) and alumina-silicates, Al-SBA-15 (Sankaranarayanan *et al.*, 2015) has attracted much attention because they exhibit superior surface areas and porosity.

The catalytic HDO of bio-oil model compounds have been studied extensively over the last decade and many reports on this topic have been published. However, more insight into catalytic roles of each heterogeneous catalyst components and the interplay between these components need more investigations. Better understanding of the

catalysts and the model compounds chemistry will aid the design of highly active and selective catalysts.

## **1.2 Statement of the research problem**

The prospect of complimenting conventional petro-fuel with bio-oil as a means of mitigating global warming have been met with challenges over the last decade. These challenges are the unwanted bio-oil properties such as high polarity, viscosity and acidity, and chemical instability associated with bio-oil. These properties are due to the presence of high oxygen and water content present in bio-oil and they are distributed across various functionalities. To curtail these challenges, researchers have been studying the upgrading of bio-oil by focusing on the use of model compounds. Furthermore, development of economically feasible HDO catalysts with better performance is another challenge for the upgrading of bio-oil. HDO is an hydrogenolysis process that involves saturating the double bonds present in the bio-oil on the metallic sites of the catalyst, and followed by cleavage of oxygen from carbon heteroatom on the catalyst acidic sites. Therefore, modifying the catalysts properties by using a less expensive transition metal supported on a highly mesoporous material that possesses sufficient acidity can lead to enhanced activity and desired selectivity. In addition, the operating conditions of the upgrading technique are an expensive process, as it requires high temperature and pressure. To overcome these challenges, there is a need for development of cheap and effect catalysts that can replace the most studied sulfided and noble metal based catalysts.

## **1.3 Justification for the study**

Cheap and robust HDO catalyst(s) that can withstand the rigorous operating conditions of bio-oil upgrading process will (without doubt) improve the economic feasibility of use of bio-oil in automobile engines. Therefore, development of a cheap and enhance catalyst(s) with high activity and selectivity to hydrocarbons will (without doubt) bring

the prospect of using bio-oil in automobile engines a step closer to reality. In addition, the study is expected to give more insight into the chemistry of bio-oil model compounds.

#### **1.4 Aim and objective of the research**

The aim of this study is in twofold: first, to synthesize supported mesoporous solid acid catalyst(s), while the second is to investigate the effectiveness in the hydrodeoxygenation of bio-oil model compound(s).

The main research objectives of this study are as follows:

1. To synthesize and characterize supported non-noble transition metal catalyst(s) that possesses surface acidity and mesopores.
2. To investigate the activity of the synthesize catalyst(s) in the hydrodeoxygenation of bio-oil model compound(s) towards biofuel production in a batch reactor.

#### **1.5 Scope of the research**

The scope of the present study is to synthesize supported nickel-based catalyst(s) and investigate the activity in the hydrodeoxygenation of dibenzofuran and guaiacol in batch reactor. The intention is to reduce the expensive cost of the catalyst material(s). The major theme of the present research is synthesis of mesoporous catalyst with potential use in upgrading of bio-oil at a cheaper cost in the future. This would be achieved by synthesizing mesoporous silica (SBA-15) and subsequently incorporating  $\text{Al}^{3+}$  into the silica matrix to obtain Al-SBA-15. It is an established fact that the presence of acidity influences HDO reaction, as such, the incorporation of  $\text{Al}^{3+}$  into the matrix of SBA-15 will generate both Lewis and Brønsted acidic sites.

## **1.6 Outline of the dissertation**

### **Chapter 1**

This chapter consists of introduction that gave a detailed background to the issues in which the research is concerned with, including the statement of the research problem, justification for the study, the aim and objectives of the study, scope of the research , as outlined in the dissertation.

### **Chapter 2**

This chapter presents a review of literature on bio-oil, challenges associated with its direct usage automobile engines as transport fuel, different bio-oil upgrading techniques and comparison of the techniques. It also includes detailed review on different bio-oil model compounds that have been studied to understand the bio-oil upgrading chemistry and the possible reaction routes. Other reviewed aspects include detailed elucidation on the types of catalysts that have been used, how they influence the reaction routes and mechanisms, and challenges associated with the use of each catalyst.

### **Chapter 3**

This chapter describes and explains the catalysts synthesis procedure, characterization equipment, importance of the characterization and the corresponding characterization method used. Other aspect includes a comprehensive description of the autoclave reactor (oleobed) used as well as the catalysts pretreatment/activation unit. It also describes the catalysts activity test using the autoclave reactors as well as the method of product analysis using both the GC-MS and GC-FID.

## **Chapter 4**

This chapter presents the result of the research. The results for both the catalysts characterization and activity test are presented in the form of figures and tables. It also presents the interpretation of the obtained results as well as how the results compared to those in open literature.

## **Chapter 5**

This chapter presents the summary of the entire research as well as recommendations for future studies.

University of Malaya

## CHAPTER 2: LITERATURE REVIEW

### 2.1 Bio-oil

Bio-oil (or pyrolysis oil) is a dark brown liquid obtained from pyrolysis of biomass and contains approximate the same elemental composition as the source biomass. It is a complex mixture of oxygenated hydrocarbons with high water content and compositionally different from crude oil. The composition and properties of bio-oil varies with chemical composition of feedstock, moisture content, particle size, and pyrolysis conditions (temperature, heating rate and time). Detailed analysis of bio-oil revealed that it contains more than 300 compounds and oxygen content accounting for over 38 wt% (Bridgwater, 2010; Debdoubi *et al.*, 2006; Demirbas, 2007; He & Wang, 2012; Jacobson *et al.*, 2013). The oxygen is present in all the compounds across a variety of functional groups, such as alcohols, ketones, aldehydes, esters, sugars, phenolics, furans, ethers and acids. These functional groups present challenges for utilization as alternative liquid fuel in automobile engines. The challenges associated with using bio oil directly in automobile engines include: (i) Chemical instability, (ii) High viscosity, (iii) Immiscibility with conventional petro-fuels due to its polarity, and (iv) Low Heating Value. Due to these challenges, there is need for bio-oil post-production upgrading before it can be used as alternative to petro-fuel in automobile engines (Bridgwater, 2010; Jacobson *et al.*, 2013; Ruddy *et al.*, 2014). Table 2.1 present a comparison between bio oil and crude oil.

### 2.2 Bio-oil upgrading

The properties of crude bio-oil shows that it is inferior to conventional petro-fuel, thus, there is need for post-production upgrading. There have been reports of different upgrading techniques in the literature and they include physical, chemical and catalytic methods. Upgrading to conventional gasoline, kerosene or diesel required total bio-oil deoxygenation. However, partial deoxygenation produces products that are compatible

with existing refinery and taking this advantage is of economic benefits (Bridgwater, 2010). Further, the combustion advantages associated with burning fuel that contains chemically bounded oxygen buttress the benefits of partial deoxygenation. For example, in the U.S. gasoline contains about 10–15 wt.% blended ethanol (3.5–5.2 wt% oxygen) (Hansen *et al.*, 2005; Jacobson *et al.*, 2013; Ruddy *et al.*, 2014). In open literature, there have been series of detailed review on physical and chemical upgrading techniques of bio-oil and reported elsewhere (Bridgwater, 1994; Bridgwater, 2011; Chiaramonti *et al.*, 2003; Czernik & Bridgwater, 2004; Ikura *et al.*, 2003; Zhang *et al.*, 2007). Hydrodeoxygenation (HDO) and zeolite cracking (ZC) are the catalytic upgrading methods for bio-oil and produces fully or partially deoxygenated hydrocarbon depending on the target.

**Table 2.1: Comparison between bio-oil and crude oil**

| <b>Properties</b>                           | <b>Bio-oil</b> | <b>Crude oil</b> |
|---|----------------|------------------|
| Water (wt.%)                                | 15 – 30        | 0.1              |
| pH  | 2.8 – 3.8      | -                |
| $\rho$ (kg/l)                               | 1.05 – 1.25    | 0.86             |
| $\mu$ at 50 °C (cP)                         | 40 – 100       | 180              |
| HHV (MJ/kg)                                 | 16 – 19        | 44               |
| <b>Elemental and ash composition (wt.%)</b> |                |                  |
| C   | 55 – 65        | 83 – 86          |
| O   | 28 – 40        | < 1              |
| H   | 5 – 7          | 11 – 14          |
| S   | < 0.05         | < 4              |
| N   | < 0.4          | < 1              |
| Ash   | < 0.2          | 0.1              |

[Adapted from (Jacobson *et al.*, 2013; Mortensen *et al.*, 2011; Venderbosch *et al.*, 2010)]

### 2.2.1 Zeolite cracking

Zeolite cracking method for upgrading bio-oil is similar to fluid catalytic cracking (FCC) process used in the refinery since zeolite is also used. The method involves the use of acidic zeolites (including transition metal modified and non-modified zeolites) to eliminate oxygen as CO and CO<sub>2</sub> at elevated temperature (> 400 °C) and atmospheric pressure (Bridgwater, 2010; Zacher *et al.*, 2014). The reactions involved in this method

include cracking of C–C bond, methyl transfer, decarboxylation, isomerization, decarbonylation and dehydration. Although this method is efficient in removing oxygen from bio-oil, but the loss of carbon during the process lowers the quality of the produced fuel (Mortensen *et al.*, 2011; Ruddy *et al.*, 2014; Zacher *et al.*, 2014).

High temperature requirement to achieve proper deoxygenation implies increase in cracking rate to produce undesirable lighter gases (Bridgwater, 2010; Ruddy *et al.*, 2014; Zacher *et al.*, 2014). In addition, there is high coke formation on the catalyst surface and resulting to high catalyst deactivation. For example, the study by Samolada *et al.*, (1998) revealed formation 20 wt.% of coke while Bertero & Sedran (2013) reported a lower amount (14 wt.%) of coke formation on the catalysts surface. Although, the challenges associated with coke formation can be overcome by continuous catalyst regeneration via oxidation of the coke in a conventional FCC arrangement (Bridgwater, 2010). However, the products quality and process cost are not competitive with conventional petro-fuel (Bridgwater, 2010; Bridgwater & Cottam, 1992).

### **2.2.2 Hydrodeoxygenation**

The HDO method of upgrading bio-oil is similar to the hydrodesulphurization (HDS) process used in the refinery. It involve saturating bonds of C=O, C=C and aromatic rings present in bio-oil, then subsequently cleavage of carbon heteroatoms in the presence of a catalyst. The process eliminates oxygen in the form of water and produce high quality fuel as compare to ZC since all carbon atoms are conserve. The process requires high temperature (250 – 450 °C), high pressure (70 – 200 bar) and catalyst. The reactions involve in this process include hydrogenation, direct deoxygenation, dehydration, hydrogenolysis hydrocracking, dealkoxylation, demethoxylation, and demethylation. In order to achieve efficient HDO, an efficient catalyst that contains both metallic sites for hydrogenation and acid sites for dehydration is required. The initial tested catalysts were

the conventional HDS catalysts (sulfided NiMo or CoMo supported on Al<sub>2</sub>O<sub>3</sub>) and conditions similar to HDS process. However, for the catalysts to remain active during the reaction there is need for continuous re-sulfurization, which consequently contaminate the final products. In addition, the support (Al<sub>2</sub>O<sub>3</sub>) is unstable in the bio-oil environment because of its high water content. Advantageously, the HDO process is compatible with existing HDS unit in the refinery and produces higher quality fuel than the ZC process. Therefore, HDO is considered a better process for bio-oil upgrading. The properties of upgraded bio-oil via ZC and HDO processes are compared to that of crude oil and presented in Table 2.2, as adapted from (Mortensen *et al.*, 2011).

**Table 2.2: Comparison of characteristics of bio-oil, catalytically upgraded bio-oil and crude oil**

|                            | Bio-oil     | ZC        | HDO       | Crude oil |
|----------------------------|-------------|-----------|-----------|-----------|
| Upgraded bio-oil (wt.%)    |             |           |           |           |
| Y <sub>oil</sub>           | 100         | 12 – 28   | 21 – 65   | –         |
| Y <sub>water phase</sub>   | –           | 24 – 28   | 13 – 49   | –         |
| Y <sub>gas</sub>           | –           | 6 – 13    | 3 – 15    | –         |
| Y <sub>carbon</sub>        | –           | 26 – 39   | 4 – 26    | –         |
| <b>Oil Characteristics</b> |             |           |           |           |
| Water (wt.%)               | 15 – 30     | –         | 1.5       | 0.1       |
| pH                         | 2.8 – 3.8   | –         | 5.8       | –         |
| P (kg/l)                   | 1.05 – 1.25 | –         | 1.2       | 0.86      |
| μ at 50 °C (cP)            | 40 – 100    | –         | 1 – 5     | 180       |
| HHV (MJ/kg)                | 16 – 19     | 21 – 36   | 42 – 45   | 44        |
| C (wt.%)                   | 55 – 65     | 61 – 79   | 85 – 89   | 83 – 86   |
| O (wt.%)                   | 28 – 40     | 13 – 24   | < 5       | < 1       |
| H (wt.%)                   | 5 – 7       | 2 – 8     | 10 – 14   | 11 – 14   |
| S (wt.%)                   | < 0.05      | –         | < 0.005   | < 4       |
| N (wt.%)                   | < 0.4       | –         | –         | < 1       |
| Ash (wt.%)                 | < 0.2       | –         | –         | 0.1       |
| H/C                        | 0.9 – 1.5   | 0.3 – 1.8 | 1.3 – 2.0 | 1.5 – 2.0 |
| O/C                        | 0.3 – 0.5   | 0.1 – 0.3 | < 0.1     | ~ 0       |

[Adapted from (Mortensen *et al.*, 2011)]

Although, the fuel quality obtain via HDO process is attractive, however, its excess hydrogen requirement makes its economically unfriendly. For example, Bridgwater (1996) estimated that 62 g of H<sub>2</sub> is required for total deoxygenation of 1 kg of bio-oil. In

addition, excess of 100 – 200% of the H<sub>2</sub> will be required for processing to maintain high partial pressure. Therefore, the major challenge confronting researchers on the use of HDO process is developing catalysts that will work at low pressure near H<sub>2</sub> stoichiometric condition. Table 2.3 presents an overview of catalysts investigated for bio-oil upgrading via HDO and ZC process, as adopted from (Mortensen *et al.*, 2011). The complex nature of bio-oil has made it more difficult for an effective catalysts design and development, thus, to overcome this challenge, there is need to understand in detail the basic chemistry of bio-oil model compounds.

### **2.3 Bio-oil model compounds**

The complex nature of bio-oil has made it difficult for successful development of effective catalysts for HDO of bio-oil. Therefore, researchers have resulted into studying model compounds in order to understand the chemistry of bio-oil. It is worth mentioning that even HDO of same model compound over different catalysts proceed via different route, producing different products. Therefore, studying different model compounds and detail understanding of the reaction chemistry will enable proper catalysts development with selectivity to desired products (He & Wang, 2012). Table 2.4 presents the components of wood-based bio-oil. Some of the studied bio-oil model compounds include dibenzofuran, guaiacol, phenol, anisole, cresol, furfural, etc. The phenolics components of the bio-oil have the highest resistance in terms of oxygen removal and this is due to their high chemical stability (Furimsky, 2000; Honkela *et al.*, 2010).

**Table 2.3: Overview of catalysts investigated for bio-oil upgrading via HDO and ZC**

| Substrate  | Reactor    | Catalyst  | t (h) | P (bar) | T (°C) | DOD (%) | Y <sub>oil</sub> (wt%) | Reference                          |
|------------|------------|---|-------|---------|--------|---------|------------------------|------------------------------------|
| <b>HDO</b> |            |   |       |         |        |         |                        |                                    |
| Bio-oil    | Batch      | Co-MoS <sub>2</sub> /Al <sub>2</sub> O <sub>3</sub> | 4     | 200     | 350    | 81      | 26                     | (Wildschut <i>et al.</i> , 2009)   |
| Bio-oil    | Continuous | Co-MoS <sub>2</sub> /Al <sub>2</sub> O <sub>3</sub> | 4     | 300     | 370    | 100     | 33                     | (Baldauf <i>et al.</i> , 1994)     |
| Bio-oil    | Batch      | Ni-MoS <sub>2</sub> /Al <sub>2</sub> O <sub>3</sub> | 4     | 200     | 350    | 74      | 28                     | (Wildschut <i>et al.</i> , 2009)   |
| Bio-oil    | Continuous | Ni-MoS <sub>2</sub> /Al <sub>2</sub> O <sub>3</sub> | 0.5   | 85      | 400    | 28      | 84                     | (Sheu <i>et al.</i> , 1988)        |
| Bio-oil    | Continuous | Pd/C  | 4     | 140     | 340    | 64      | 48                     | (Elliott <i>et al.</i> , 2009)     |
| Bio-oil    | Continuous | Pt/Al <sub>2</sub> O <sub>3</sub> /SiO <sub>2</sub> | 0.5   | 85      | 400    | 45      | 81                     | (Sheu <i>et al.</i> , 1988)        |
| Bio-oil    | Batch      | Ru/Al <sub>2</sub> O <sub>3</sub>                   | 4     | 200     | 350    | 78      | 36                     | (Wildschut <i>et al.</i> , 2009)   |
| Bio-oil    | Continuous | Ru/C  | 0.2   | 230     | 350    | 73      | 38                     | (Venderbosch <i>et al.</i> , 2010) |
| Bio-oil    | Batch      | Ru/C  | 4     | 200     | 350    | 86      | 53                     | (Wildschut <i>et al.</i> , 2009)   |
| <b>ZC</b>  |            |   |       |         |        |         |                        |                                    |
| Bio-oil    | Continuous | H-mordenite   | 0.56  | 1       | 330    | -       | 17                     | (Adjaye & Bakhshi, 1995)           |
| Bio-oil    | Continuous | H-Y   | 0.28  | 1       | 330    | -       | 28                     | (Adjaye & Bakhshi, 1995)           |
| Bio-oil    | Continuous | HZSM-5  | 0.91  | 1       | 500    | 53      | 12                     | (Williams & Horne, 1994)           |
| Bio-oil    | Continuous | MgAPO-36  | 0.28  | 1       | 370    | -       | 16                     | (Katikaneni <i>et al.</i> , 1995)  |
| Bio-oil    | Continuous | SAPO-11   | 0.28  | 1       | 370    | -       | 20                     | (Katikaneni <i>et al.</i> , 1995)  |
| Bio-oil    | Continuous | SAPO-5  | 0.28  | 1       | 370    | -       | 22                     | (Katikaneni <i>et al.</i> , 1995)  |

**Table 2.4: Components of wood-based bio-oil**

| Components   | Mass (%) |
|--|----------|
| Water  | 20 – 30  |
| Lignin fragments: Insoluble pyrolytic lignin   | 15 – 30  |
| Aldehydes: Formaldehyde, acetaldehyde, hydroxyacetaldehyde, glyoxal, and methylglyoxal           | 10 – 20  |
| Carboxylic acids: Formic, acetic, propionic, butyric, pentanoic, hexanoic, and glycolic          | 10 – 15  |
| Carbohydrates: Cellobiosan, $\alpha$ -D-levoglucosan, oligosaccharides, and anhydroglucofuranose | 5 – 10   |
| Phenolics: Phenol, cresol, anisole, guaiacol, and syringol                                       | 2 – 5    |
| Furfurals  | 1 – 4    |
| Alcohols: methanol, and ethanol  | 2 – 5    |
| Ketones: Acetol (1-hydroxy-2-propanone), and cyclopentanone                                      | 1 – 5    |

[Adapted from (Honkela *et al.*, 2010)]

### 2.3.1 Guaiacol

Guaiacol (i.e. 2-methoxyphenol) has  $-\text{OH}$  and  $-\text{OCH}_3$  groups attached to aromatic ring and it is the most abundant phenolic form of bio-oil model compound (Roberts *et al.*, 2011). It contains three types of C–O bonds, which are  $\text{C}(\text{sp}^3)\text{--OAr}$ ,  $\text{C}(\text{sp}^2)\text{--OMe}$ , and  $\text{C}(\text{sp}^2)\text{--OH}$  (Figure 2.1) with bond dissociation energy of 262 – 276, 409 – 421, and 466  $\text{kJmol}^{-1}$ , respectively. Evidently, from the bond dissociation energies, cleavage of the  $\text{C}(\text{sp}^2)\text{--OMe}$  and  $\text{C}(\text{sp}^2)\text{--OH}$  are more difficult as compared to the  $\text{C}(\text{sp}^3)\text{--OAr}$  bond (Song *et al.*, 2015).

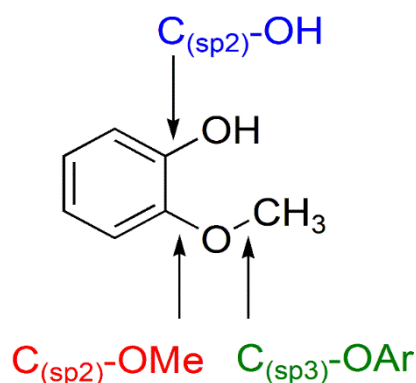


**Figure 2.1: Structure of guaiacol**

[Adapted from (Song *et al.*, 2015)]

The deoxygenation of guaiacol and other phenolics via HDO is believed to proceed via different routes which depends on the catalyst and operating conditions used (Zhao *et al.*, 2011). The HDO of guaiacol could proceed via six (6) possible routes as shown in Figure 2.2 and these six routes include:

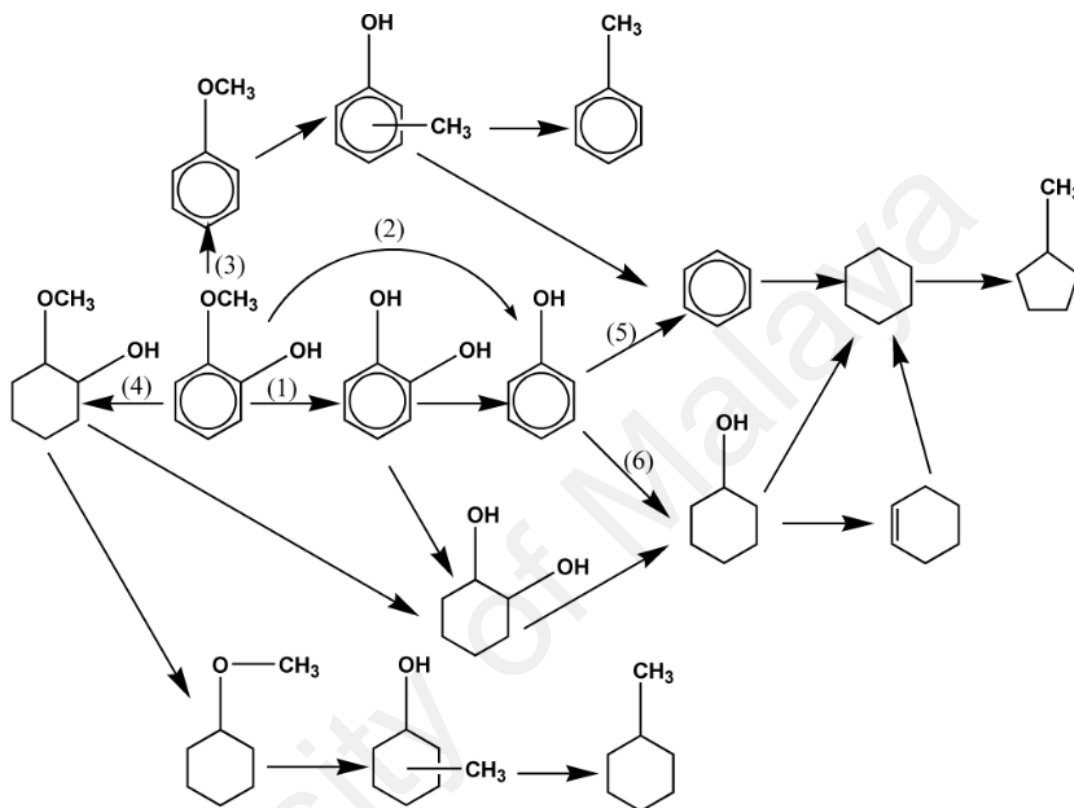


**Figure 2.2: Guaiacol HDO reaction pathways**

[Adapted from (He & Wang, 2012)]

1. Demethylation (DME) to produce benzene-1, 2-diol (catechol), which subsequently undergoes direct hydrogenolysis (DH) to produce phenol.
2. Direct demethoxylation (DMO) to produce phenol.
3. DH to produce anisole, which can subsequently undergoes methyl transfer (MT) to produce cresol.
4. Benzene ring hydrogenation (HYD) to produce 2-methoxy-cyclohexanol which can subsequently undergoes either DME or DH to produce cyclohexane-1, 2-diol or methoxy-cyclohexane respectively

5. DH of phenol to produce benzene and subsequently HYD to produce cyclohexane
6. HYD of phenol to produce cyclohexanol followed by DH to produce cyclohexane

The HDO of guaiacol over sulfided NiMo and CoMo supported on Al<sub>2</sub>O<sub>3</sub> catalysts (i.e. conventional hydrodesulfurization catalysts) proceeds via routes 1, 2 and 3 of Figure 2.2 (Bui *et al.*, 2011a; Bui *et al.*, 2011b; Bui *et al.*, 2009; Hong *et al.*, 2014b; Lin *et al.*, 2011; Romero *et al.*, 2010). In addition to the products and intermediates shown in Figure 2.2, there is report on formation of sulphur containing intermediates. For example, Gutierrez *et al.*, (2009) studied the HDO of guaiacol in a batch reactor at 300 °C and 8 MPa over sulfided CoMo/Al<sub>2</sub>O<sub>3</sub> catalyst. They reported formation of extra compounds like methanethiol and dimethyl sulfide, and cyclohexanethiol and methylthiocyclohexane in the gaseous and liquid phases of the product respectively. They attributed the formations of these undesirable products to contamination caused by sulphur leaching from the catalyst.

Unlike the sulfided catalysts, the HDO of guaiacol over non-sulfided noble metal-based (Pd, Pt, Ru and Rh) catalysts proceeds via route 4 of Figure 2.2 (Gutierrez *et al.*, 2009; Hong *et al.*, 2014a; Lee *et al.*, 2012; Lin *et al.*, 2011; Zhang *et al.*, 2014). Noble metals with acidic supports exhibits higher catalytic activities than the sulfided CoMo and NiMo based catalysts in HDO of guaiacol (Zhao *et al.*, 2011). The route 4 (Figure 2.2) followed by these types of catalysts is attributable to their high hydrogenating ability. Massoth *et al.*, (2006) reported that this route is energetically favourable than routes 1, 2, and 3 (Figure 2.2) since it involve hydrogenating the double bonds of the benzene rings on the metal surface to produce C(sp<sup>3</sup>)–O bonds from the C(sp<sup>2</sup>)–OMe and C(sp<sup>3</sup>)–OH bonds of the guaiacol. The produced C(sp<sup>3</sup>)–O bonds can subsequently be cleave easily of the metal surface of the through dehydration on the acidic supports. Therefore, the use of bifunctional catalysts (e.g. Ru/ZSM-5, Pt/H-Beta, etc.) is paramount since

hydrogenation and dehydration occur on the metal and acidic sites respectively (Zhang *et al.*, 2014; Zhu *et al.*, 2011). In addition, the final product from HDO of guaiacol over noble metals on acidic supports depends on the operating temperature and pressure. If the operating temperature is adequately high, the final product will be cyclohexane and more high hydrogen would be consumed (Zhao *et al.*, 2011).

The HDO of guaiacol over non-noble transition metals like Ni supported on metal oxides like SiO<sub>2</sub>, or mixed metal oxides like SiO<sub>2</sub>-ZrO<sub>2</sub>, SiO<sub>2</sub>-ZrO<sub>2</sub>-La<sub>2</sub>O<sub>3</sub>, etc. proceeds via either routes 1, 2, or 3 of Figure 2.2 (Bykova *et al.*, 2012; Bykova *et al.*, 2014; Zhang *et al.*, 2013). For example, Bykova *et al.*, (2012) studied the HDO of guaiacol over Ni and NiCu supported on CeO<sub>2</sub>-ZrO<sub>2</sub>, SiO<sub>2</sub>-ZrO<sub>2</sub>-La<sub>2</sub>O<sub>3</sub>, Al<sub>2</sub>O<sub>3</sub>, and SiO<sub>2</sub> catalysts in an autoclave reactor operating at 320 °C and hydrogen pressure of 17 MPa. All the synthesized catalysts followed either the route 1, 2, or 3 (Figure 2.2) with the exception of NiCu/ CeO<sub>2</sub>-ZrO<sub>2</sub> which followed route 4 of Figure 2.2. Interestingly, the products formed were not limited to cyclohexane, cyclohexene, cyclohexanol and benzene. There was report of formation of bicyclic compounds like bicyclohexyl, cyclohexyl-phenol, cyclohexyl-benzene and, cyclohexyl-cyclohexanol which are products of two rings condensation.

### 2.3.2 Anisole

Anisole (methoxybenzene) is a benzene ring with attached methoxy group. It contains two types of C-O bonds which are C(sp<sup>3</sup>)-OAr and C(sp<sup>2</sup>)-OMe and the C(sp<sup>2</sup>)-OMe is more stronger (Honkela *et al.*, 2010). There have been reports of anisole HDO in the literature and the sequence of the reaction is believed to proceed via DME, MT or benzene ring HYD (González-Borja & Resasco, 2011; Li *et al.*, 2011; Prasomsri *et al.*, 2011; Saidi *et al.*, 2015; Sankaranarayanan *et al.*, 2015; Yang *et al.*, 2014). Yang *et al.*, (2014) studied the HDO of anisole in a fixed-bed tubular reactor at 290 °C and 3 bar of hydrogen pressure

over Ni-based catalysts. They reported that the reaction proceeds via DME to produce phenol and subsequently HYD and DH to produce cyclohexanol and cyclohexane respectively. In addition, there was formation of benzene and they attributed it to the DH of phenol. Deutsch & Shanks (2012) reported the formation of methoxycyclohexane and attributed it to HYD of the benzene ring of anisole. Also, Viljava *et al.*, (2000) reported MT to benzene ring to form cresol (methylphenol) and subsequently DH to produce toluene while Huuska & Rintala (1985) ruled out direct cleavage of methoxy group from anisole. Figure 2.3 shows the reaction pathway of anisole HDO.

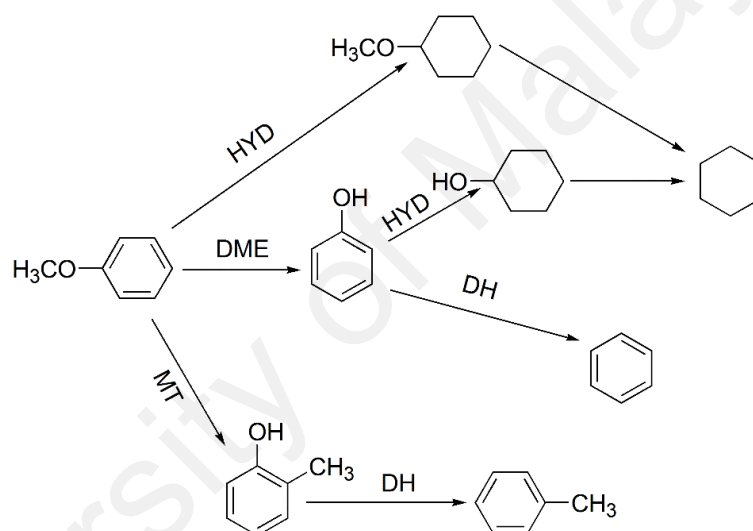


**Figure 2.3: Anisole HDO reaction pathways**

[Adapted from Viljava *et al.*, 2000 and Yang *et al.*, 2014]

### 2.3.3 Phenol

Phenol, the simplest of the phenolics component of bio-oil has a phenyl group bonded to a hydroxyl group. It is formed as an intermediate during the HDO of guaiacol, anisole, catechol, and cresol. The HDO of phenol proceeds via either HYD of the benzene ring to produce cyclohexanol or cyclohexanone, or DH to produce benzene or both HYD and DH (Echeandia *et al.*, 2014; Hong *et al.*, 2010; Massoth *et al.*, 2006; Song *et al.*, 2015). For example, Echeandia *et al.*, (2014) studied the HDO of phenol in a fixed-bed reactor

at 250 °C and 15 bar over Pd supported on zeolite HY mixed with alumina and compared the catalyst performance with sulfided NiMo/Al<sub>2</sub>O<sub>3</sub>. They reported that each catalysts exhibited HYD and HD (Figure 2.4), and are occurring competitively. In addition to the HYD and DH, there was isomerization reaction taking place, which led to the formation of methylcyclopentane. Song *et al.*, (2015) and Hong *et al.*, (2010) reported formation of cyclohexanone as one of the intermediate during the HDO reaction. In addition, (Hong *et al.*, 2010) reported formation of bicyclic compounds (Figure 2.5) resulting from ring coupling (condensation).

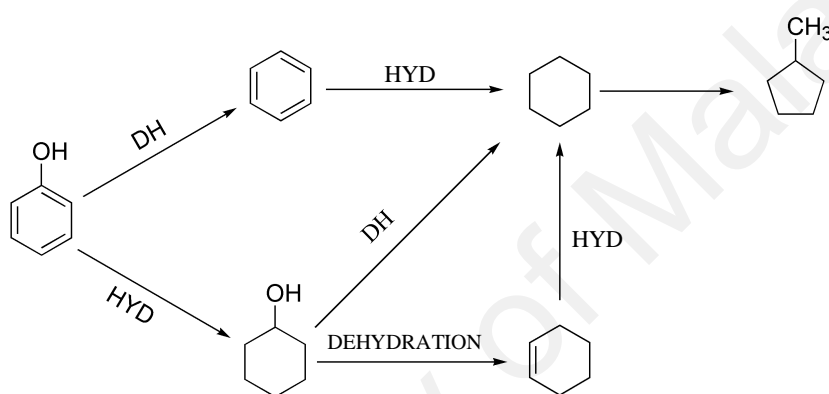


**Figure 2.4: Phenol HDO reaction pathways over Pd/HY catalyst**

[Adapted from Echeandia *et al.*, 2014]

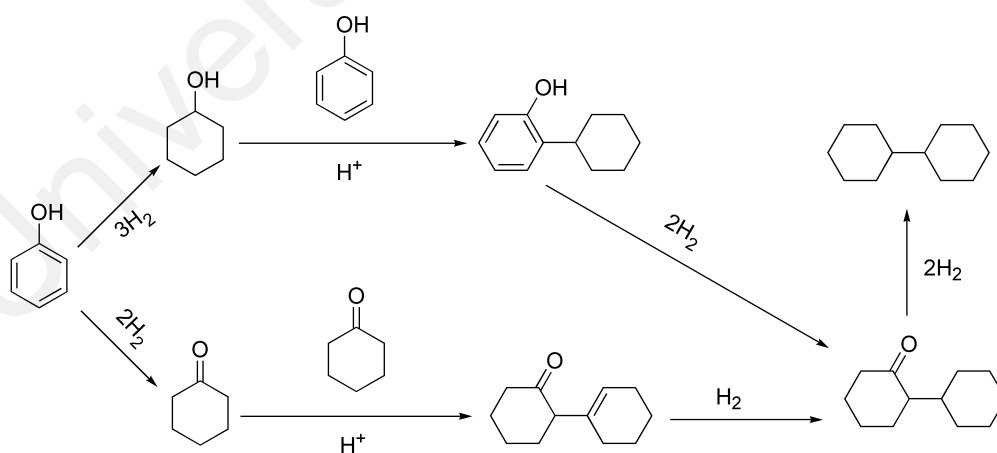


**Figure 2.5: Phenol HDO reaction pathways to bicyclic compounds over Pt/HY catalyst**

[Adapted from (Hong *et al.*, 2010)]

### 2.3.4 Dibenzofuran

Dibenzofuran (DBF) has a furan structure linking two aromatic rings via a C–C bond and C–O bond. It is considered as a bio-oil model compound with  $\beta$ -5 linkage with a molecular size of 0.67 nm. In biomass gasification, it is formed as an intermediate with a weight percent of 13.19% (Huelsman & Savage, 2012; Li *et al.*, 2008; Wang *et al.*, 2015). Like other bio-oil model compounds, the HDO of DBF and the products selectivity depends on the hydrogenating ability and acidity of the catalysts, and the process conditions used (Lee *et al.*, 2015; Wang *et al.*, 2014; Wang *et al.*, 2015; Wang *et al.*, 2013; Yuxin Wang *et al.*, 2011; Wang *et al.*, 2012). For example, Wang *et al.*, (2015) studied the influence of supports on the HDO of DBF over Pt supported on SiO<sub>2</sub>, Al<sub>2</sub>O<sub>3</sub>/SiO<sub>2</sub>, and ZrO<sub>2</sub>/SiO<sub>2</sub> catalysts. They reported that the HDO reactions proceeds via HYD route, and that the major product was bicyclohexyl over Pt on Al<sub>2</sub>O<sub>3</sub>/SiO<sub>2</sub>, and ZrO<sub>2</sub>/SiO<sub>2</sub> catalysts. In addition, they reported formation of cyclohexane over Pt/Al<sub>2</sub>O<sub>3</sub>/SiO<sub>2</sub>, and attributed its formation to the superior acidity of the catalyst. Figure 2.6 shows a detail reaction scheme of HDO of DBF.

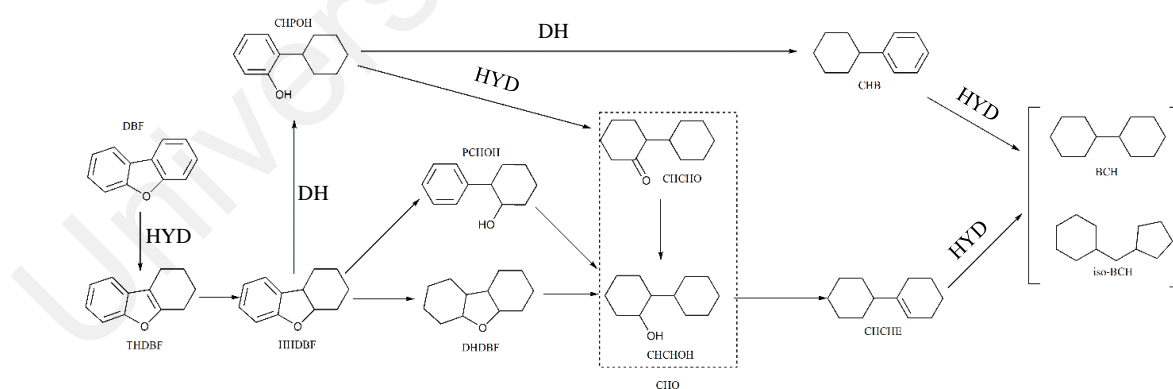


**Figure 2.6: HDO reaction pathways of DBF**

[Adapted from (Gbadamasi *et al.*, 2016; Wang *et al.*, 2015)]

### 2.3.5 Ketones, aldehydes, and acids

The chemical instability problem associated with bio-oils is because of the presence of high concentration of ketones and aldehydes. At high temperature during HDO, ketones and aldehydes undergo polymerization to form high molecular weight compounds (Bridgwater, 2012; Honkela *et al.*, 2010). To eliminate this challenge, a two-stage HDO process was studied where the first stage involves reaction temperature below 300 °C and consumes lesser hydrogen. The removal of oxygen from aldehydes, ketones, ethers and aliphatic alcohols take place during this stage. The second stage requires a temperature range of 300 – 450 °C and more hydrogen is consumed. During this second stage, oxygen removal from phenolics, furans, carboxylic acids, esters, etc. occurs (Bridgwater, 1994; Furimsky, 2000; He & Wang, 2012; Honkela *et al.*, 2010; Sharma & Bakhshi, 1991).

The HDO of ketones and aldehydes proceeds via three major mechanisms. The mechanisms involve transformation of the carbonyl group present into methyl group as shown in Figure 2.7 (He & Wang, 2012; Honkela *et al.*, 2010; Modak *et al.*, 2012; Procházková *et al.*, 2007; Wang *et al.*, 2005).

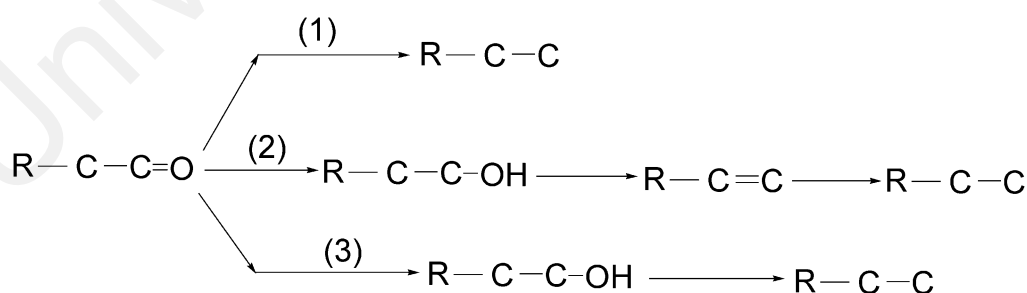


**Figure 2.7: HDO reaction pathways of carbonyl group into alkanes**

[R implies alkyl groups; Adapted from (He & Wang, 2012; Honkela *et al.*, 2010)]

1. DH of the C = O bond
2. HYD of the carbonyl group to form an alcohol, followed by dehydration to alkene and subsequently HYD to alkane
3. HYD of the carbonyl group to form an alcohol, followed by DH to alkane

The low pH (high acidity) of bio-oil is due to the presence of carboxylic acids such as acetic acids, and consequently making bio-oil to be corrosive (Bridgwater, 2011; Zhang *et al.*, 2007). (Elliott & Hart, 2009) studied the HDO of acetic acid as bio-oil model compound over Pd/C and Ru/C in a batch reactor. They reported that Ru/C is effective in hydrogenating acetic acid to ethanol while with Pd/C, there was successful HYD to ethanol at 300 °C.

## **2.4 Catalysts**

Catalysts are essential substances that play great role in the HDO of bio-oil and the model compounds. Active components like transition metal sulfides (TMS) catalysts, noble metal catalysts, non-noble transition metals, mixed oxides, and transition metal carbide, nitride and phosphide (TMC/N/P) have been studied for HDO processes. In addition, zeolites, Al<sub>2</sub>O<sub>3</sub>, SiO<sub>2</sub>, SBA-15, ZrO<sub>2</sub>, TiO<sub>2</sub>, etc. have all been studied as supports for the active components. However, the results obtained shows that there is need for more understanding of the catalysts reactivity and activity.

### **2.4.1 Transition metal sulfides (TMS)**

Transition metal sulfides (TMS) are the oldest catalysts studied in the HDO of bio-oil and its model compounds. This is due to their HYD and DH capabilities and the success of their usage in hydrodesulfurization (HDS) and hydrodenitrogenation (HDN) of fossil fuel (Honkela *et al.*, 2010; Ruddy *et al.*, 2014). Of keynote, the most studied sulfided catalysts are CoMo/Al<sub>2</sub>O<sub>3</sub> and NiMo/Al<sub>2</sub>O<sub>3</sub>, with Co and Ni acting as a promoter, Mo as the active component and Al<sub>2</sub>O<sub>3</sub> as the support (Bui *et al.*, 2011b; Krár *et al.*, 2011;

Romero *et al.*, 2010; Toba *et al.*, 2011). Ni/W/Al<sub>2</sub>O<sub>3</sub>, Ni/W/TiO<sub>2</sub> and ReS<sub>2</sub>/ZrO<sub>2</sub> are some of the other studied sulfided catalysts but found limited use in the literature (He & Wang, 2012; Hong *et al.*, 2014b; Ruddy *et al.*, 2014; Ruiz *et al.*, 2010; Toba *et al.*, 2011).

Studies have shown that these types of catalysts are only active in the sulfided form and vacancies generated due to loss of sulphur during HDO reactions are the active sites (Topsøe *et al.*, 1996). These sites (vacancies generated) are located at the edges of the MoS<sub>2</sub> or WS<sub>2</sub> phase, exhibiting Lewis acid properties, and can adsorb heteroatoms (Badawi *et al.*, 2013). The cleavage of C–O during the HDO reaction over these types of catalysts therefore takes place in these vacancies because of the Lewis acid properties (Badawi *et al.*, 2013; Şenol, 2007). In this type of catalysts, Ni-W-S, Ni-Mo-S and Co-Mo-S structures are formed with Co and Ni occupying the edges of the MoS<sub>2</sub> phases. The structures formed have the ability to mimic the noble metal based catalysts by donating d-electron(s) (Brorson *et al.*, 2007; Chianelli *et al.*, 2009). In addition to the Lewis acid characteristics, they exhibit Brønsted acid properties since activation of molecular hydrogen takes place at the edges to produce H<sup>+</sup> and SH<sup>-</sup> on the catalyst surface. The activated hydrogen can originate not only from molecular hydrogen, but also from alcohols, thiols, or water. In HDO reaction, the Brønsted acid properties is of great importance as SH<sup>-</sup> enhance deoxygenation while H<sup>+</sup> saturates multiple bonds to produce C–C bonds (Badawi *et al.*, 2013; He & Wang, 2012; Ratnasamy & Fripiat, 1970; Romero *et al.*, 2010; Ruddy *et al.*, 2014). The addition of promoters like Co and Ni do not increase the number of active sites. However, they improve the catalytic activity by creating weakness in the bond between molybdenum and sulphur (He & Wang, 2012; Popov *et al.*, 2010; Romero *et al.*, 2010; Travert *et al.*, 2002).

Romero *et al.*, (2010) studied the HDO of 2-ethylphenol in a fixed bed reactor as bio-oil model compound over sulfided CoMo/Al<sub>2</sub>O<sub>3</sub> and CoMo/Al<sub>2</sub>O<sub>3</sub> and proposed a

mechanism as shown in Figure 2.8. They reported that the removal of sulphur in the form of  $\text{H}_2\text{S}$  in the presence of  $\text{H}_2$  generate vacancies which act as the active sites. After formation of vacancies, heterolytic dissociation of  $\text{H}_2$  then led to the formation of one Mo–H and one S–H groups. The adsorption of 2-ethylphenol on the vacancies leads to the HYD of its benzene ring forming 2-ethylcyclohexanol. The 2-ethylcyclohexanol then undergoes dehydration on the acidic sites of the support and subsequent re-HYD to produce ethylcyclohexane.

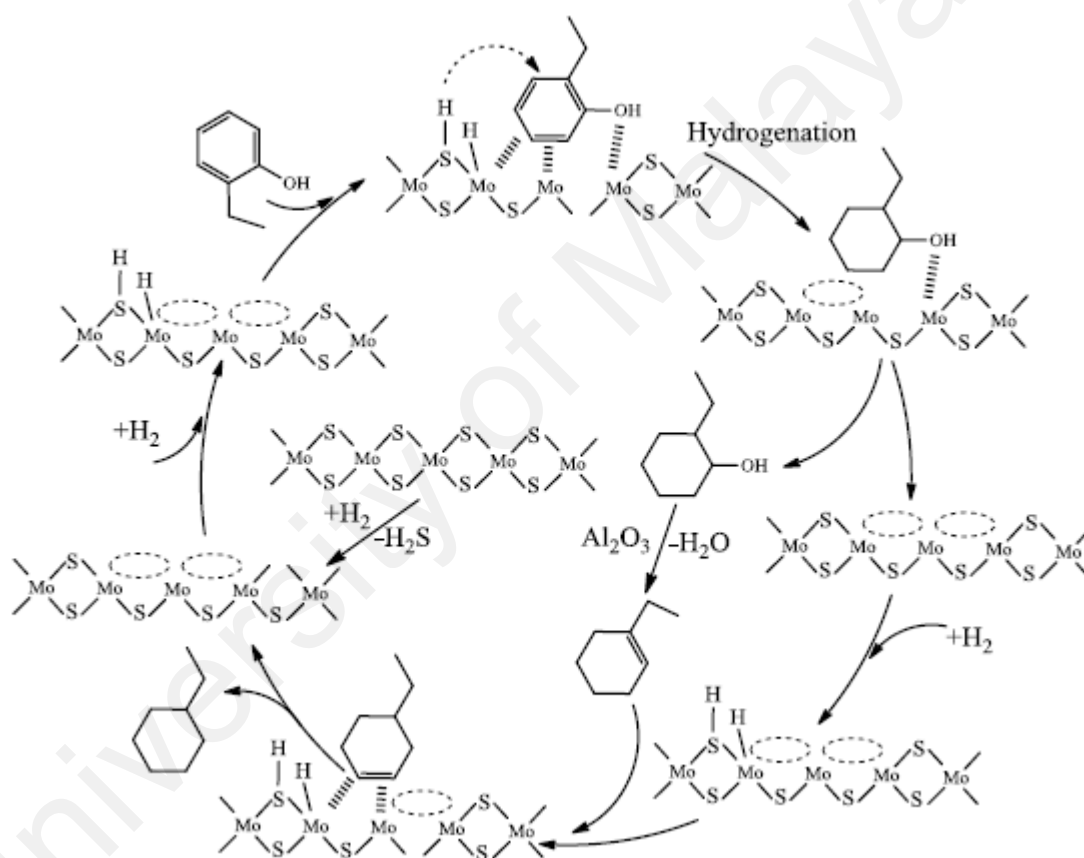


**Figure 2.8: Mechanism of 2-ethylphenol HDO over  $\text{MoS}_2$ -based catalyst**

[Adapted from (Romero *et al.*, 2010)]

#### 2.4.1.1 Challenges associated with the use of sulfided catalysts

Although the use of sulfided catalysts has produced high degree of HDO, however, the structures of the sulfided catalysts are not stable in the presence of sulphur free substrates. The loss of sulphur content during HDO reaction reduces the catalytic activity.

Consequently, there is need for continuous addition of sulphur to the system to maintain the catalysts activity (Furimsky, 2000; Furimsky & Massoth, 1999; Viljava *et al.*, 2000; Viljava *et al.*, 1999). In addition, there has been report of formation of sulphur containing intermediates, which are undesirable products (Gutierrez *et al.*, 2009; Şenol *et al.*, 2007).

Another challenge with the use of these sulfided catalysts is the presence of water and the affinity of its support ( $\text{Al}_2\text{O}_3$ ) for water. Water was formed as a by-product during HDO reaction and affects the activity of the sulfided catalyst by undergoing competitive adsorption for active sites (Laurent & Delmon, 1994). Although the water has low adsorption tendency for the sulfide phase, however, it binds strongly with the support and consequently inhibit the reaction to take place on the support. Another challenge is that the water vapour produce during HDO reaction causes  $\text{Al}_2\text{O}_3$  to undergo recrystallization to produce boehmite. In addition, it causes nickel sulfide phase to undergo partial oxidation to form nickel oxide and consequently a decrease in the catalyst activity (Bu *et al.*, 2012; Honkela *et al.*, 2010; Laurent & Delmon, 1994).

#### **2.4.2 Noble metal catalysts**

The ease of deactivation of TMS catalysts during HDO reaction due to the substrate nature and subsequent product contamination has resulted into call for alternative catalysts. Thus, supported noble metal based-catalysts have gain attention over time. The supported noble metal based-catalysts are very attractive because they do not require sulphur and consequently do not contaminate the products (Honkela *et al.*, 2010; Ruddy *et al.*, 2014). In addition, the efficient ability of noble metal in activating  $\text{H}_2$  under mild condition makes the supported noble metal catalyst very attractive (Ruddy *et al.*, 2014). Consequently, it is expected that the supported noble metal-based catalysts will exhibit higher catalytic activities than the TMS. The challenge of support stability associated with TMS is avoidable by not using  $\text{Al}_2\text{O}_3$  as a support for the noble metals (He & Wang,

2012; Honkela *et al.*, 2010). There have been reports on the use of noble metal such as Pd (Gutierrez *et al.*, 2009; Hong *et al.*, 2014a; Wang *et al.*, 2014; Zhao *et al.*, 2011), Pt (Gutierrez *et al.*, 2009; Wang *et al.*, 2014; Wang *et al.*, 2015), Ru (Lee *et al.*, 2012; Wang *et al.*, 2014; Wildschut *et al.*, 2009; Zhang *et al.*, 2014; Zhao *et al.*, 2011) and Rh (Gutierrez *et al.*, 2009; Lee *et al.*, 2012; Zhao *et al.*, 2011) as active component in HDO reaction and gives better catalytic activities when compared with TMS catalysts. For example, Wildschut *et al.*, (2009) studied the HDO of bio-oil over Ru/C and TMS (CoMo/Al<sub>2</sub>O<sub>3</sub> and NiMo/Al<sub>2</sub>O<sub>3</sub>) catalysts in a batch reactor at a temperature of 250 and 350 °C, and a pressure of 100 and 200 bar. Comparing the performances of the two catalysts, they reported that the Ru/C catalyst outperformed the TMS catalysts both in oil yield and degree of HDO. Table 2.5 presents a summary of some results of HDO of bio-oil model compounds over supported noble metal catalysts.

In HDO reaction over supported noble metal catalysts, activation of H<sub>2</sub> takes place on the noble metal sites. The support and the metal-support interface on the other hand are responsible for the transfer of activated H<sub>2</sub> (surface H\* species) to the reactant. The support and the metal-support interface adsorb and activate the substrate (oxy-compounds), and provide a platform for the spillover of the H\* species during HYD and subsequently leading to C–O cleavage. If the substrate is polar, the interaction with metal-support or support interface is via oxygen functionality. Recent studies show that HDO reaction over supported noble metal catalysts follows HYD–dehydration–HYD sequence and requires a HYD sites and an acidic sites (Boffa *et al.*, 1994; Boffa *et al.*, 1993; Lee *et al.*, 2012; Lin *et al.*, 2011; Mendes *et al.*, 2001; Pestman *et al.*, 1997).

**Table 2.5: Overview of results obtained for HDO of bio-oil model compounds over supported noble metal catalysts**

| Feed     | Reactor    | Catalysts   | t (h) | P (MPa) | T (°C) | Conversion (%) | Main product(s)                                       | Reference                     |
|----------|------------|---|-------|---------|--------|----------------|---|-------------------------------|
| Guaiacol | Batch      | Pd/C  | 4.0   | 13.8    | 300    | 99.0           | Cyclohexane   | (Elliott & Hart, 2009)        |
| Guaiacol | Batch      | Pd/WO <sub>x</sub> /Al <sub>2</sub> O <sub>3</sub>  | 2.5   | 7.0     | 300    | 100.0          | Cyclohexane   | (Hong <i>et al.</i> , 2014a)  |
| Guaiacol | Batch      | Ru/C  | 4.0   | 13.8    | 250    | 100.0          | Cyclohexane   | (Elliott & Hart, 2009)        |
| Guaiacol | Batch      | Rh/C  | 1.0   | 4.0     | 250    | 95.0           | 2-methoxycyclohexanol                                 | (Lee <i>et al.</i> , 2012)    |
| Phenol   | Batch      | Pd/C  | 0.5   | 5.0     | 250    | 100.0          | Cyclohexane   | (Zhao <i>et al.</i> , 2011)   |
| Phenol   | Batch      | Ru/HZSM-5   | 2.0   | 5.0     | 150    | 99.9           | Cyclohexanol  | (Zhang <i>et al.</i> , 2014)  |
| Phenol   | Continuous | Pt/HY   | -     | 4.0     | 200    | 100.0          | Cyclohexane   | (Hong <i>et al.</i> , 2010)   |
| Cresol   | Continuous | Pt/Al <sub>2</sub> O <sub>3</sub>                   | -     | 0.1     | 260    | 74.0           | Toluene, Methylcyclohexane                            | (Foster <i>et al.</i> , 2012) |
| Anisole  | Continuous | Pt/HBEA   | -     | 0.1     | 400    | 30.0           | Benzene, Toluene, Xylene                              | (Zhu <i>et al.</i> , 2011)    |
| DBF      | Batch      | Pt/MFI  | 3.0   | 4.0     | 250    | 100.0          | 1,1-bicyclohexyl,<br>(cyclopentylmethyl)- Cyclohexane | (Lee <i>et al.</i> , 2015)    |
| DBF      | Continuous | Pt/Al <sub>2</sub> O <sub>3</sub> /SiO <sub>2</sub> | -     | 3.0     | 280    | 95.0           | 1,1-bicyclohexyl                                      | (Wang <i>et al.</i> , 2015)   |
| DBF      | Continuous | Pd/SBA-15   | -     | 3.0     | 280    | 70.0           | 1,1-bicyclohexyl, Hexahydro<br>dibenzofuran           | (Wang <i>et al.</i> , 2014)   |

#### 2.4.2.1 Challenges associated with the use of supported noble metal catalysts

The use of supported noble metal catalysts in HDO of bio-oil and its model compound have proven to be a better catalyst than the TMS. However, their high costs make it difficult for any commercial (large-scale) usage. In addition to their high cost, noble metals are highly sensitive towards poisoning and consequently can lead to rapid deactivation (coking and sintering) (Dhandapani *et al.*, 1998; He & Wang, 2012; Honkela *et al.*, 2010; Ruddy *et al.*, 2014).

#### 2.4.3 Non-noble transition metal catalysts

In seeking solution to the challenges associated with the use of supported noble metal catalysts, there has been renewed interest in transition metals like Ni (Bykova *et al.*, 2014; Sankaranarayanan *et al.*, 2015; Yang *et al.*, 2014), Co (Olcese *et al.*, 2012; Sankaranarayanan *et al.*, 2015), Fe (Olcese *et al.*, 2012), and Cu (Bykova *et al.*, 2014) etc. Unlike the noble metals, they are cheap and readily available. These metals (Ni, Co, Fe, and Cu), just like the noble metals, can activate H<sub>2</sub> in HDO reaction but to a lesser degree. The metals have been studied as lone active component in HDO reaction and as bimetallic in order to improve the performance thermal resistance. In designing a catalyst using these metals (Ni, Co, Fe, and Cu), accurate choice of support is paramount since HDO reaction requires a bifunctional catalysts (Olcese *et al.*, 2012; Song *et al.*, 2015; Yang *et al.*, 2014).

There have been series of studies on the use of these metals (Ni, Co, Fe, and Cu) in the HDO of bio-oil model compounds and promising results have been achieved. For example Bykova *et al.*, (2012) studied the HDO of guaiacol over supported Ni-based catalysts in an autoclave reactor at 320 °C and 17 MPa. They reported the main products to be cyclohexane, benzene, 1-methylcyclohexane-1, 2-diol and cyclohexanone. In addition, they reported that the catalysts reactivity base on the degree of HDO follows the

order Ni/SiO<sub>2</sub> > Ni-Cu/Zr<sub>2</sub>O-SiO<sub>2</sub>-La<sub>2</sub>O<sub>3</sub> > Ni-Cu/ SiO<sub>2</sub> > Ni-Cu/ Al<sub>2</sub>O<sub>3</sub> > Ni-Cu/CeO<sub>2</sub>-ZrO<sub>2</sub>. Similarly, Olcese *et al.*, (2012) studied the HDO of guaiacol over Fe/SiO<sub>2</sub> catalyst in a fixed-bed reactor at atmospheric pressure and 350 – 450 °C. Toluene and benzene were identified to be the main products and proposed a reaction mechanism that is in agreement with the work of Popov *et al.*, (2010). In the mechanism (Figure 2.9), oxygen atoms from the substrate are adsorbed on the acidic sites of the support while the metallic site activates the H<sub>2</sub>. The activated H<sub>2</sub> are then spilled over to the adsorbed oxygen atoms and causes the cleavage of C-O bond. An oxy-compound like guaiacol, vanillin, etc. may have different adsorption sites.

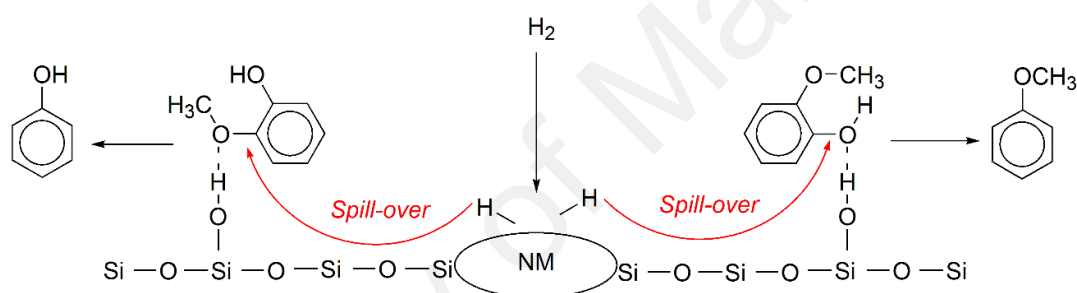


**Figure 2.9: Possible mechanism of guaiacol HDO over non-noble metal catalysts**

[NM implies non-noble metal; Adapted from (Olcese *et al.*, 2012; Popov *et al.*, 2010)]

In another report by Sankaranarayanan *et al.*, (2015), the effect of metal support interaction was investigated in the HDO of anisole over Ni and Co supported on Al-SBA-15. Also, Song *et al.*, (2015) studied the synergistic effects of Ni and support acidity for HDO of phenolics. Both reports agreed that the combine effect of support acidity and the metal HYD ability enhances the catalytic activity. However, strong metal support interaction (in the case of Co/Al-SBA-15) reduces the catalyst performance as it hinders the reduction of Co<sup>2+</sup> to Co<sup>0</sup> (Sankaranarayanan *et al.*, 2015). Table 2.6 presents a summary of recent HDO of bio-oil model compounds over supported non-noble transition metal catalysts.

**Table 2.6: Overview of some recent results for HDO of bio-oil model compounds over supported non-noble metal catalysts**

| Feed     | Reactor    | Catalysts   | t (h) | P (MPa) | T (°C) | Conversion (%) | Main product(s)      | Reference                               |
|----------|------------|---|-------|---------|--------|----------------|----------------------|---|
| Guaiacol | Continuous | Co/Al-MCM-41 & Ni/Al-MCM-41   | -     | 0.1     | 400    | 100.0          | Benzene, Phenol      | (Tran <i>et al.</i> , 2016)             |
| Guaiacol | Continuous | Fe/SiO <sub>2</sub>   | 2.5   | 0.1     | 400    | 100.0          | Benzene, Toluene     | (Olcese <i>et al.</i> , 2012)           |
| Guaiacol | Batch      | NiCu/SiO <sub>2</sub> -ZrO <sub>2</sub> -La <sub>2</sub> O <sub>3</sub> | 1.0   | 17.0    | 320    | 85.6           | Cyclohexane          | (Bykova <i>et al.</i> , 2012)           |
| Guaiacol | Batch      | Ni/SiO <sub>2</sub>   | 1.0   | 17.0    | 320    | 97.5           | Cyclohexane          | (Bykova <i>et al.</i> , 2012)           |
| Guaiacol | Batch      | NiCu/SiO <sub>2</sub> -ZrO <sub>2</sub>                                 | 1.0   | 17.0    | 320    | 95.0           | Cyclohexane, Benzene | (Bykova <i>et al.</i> , 2014)           |
| Guaiacol | Batch      | Ni/SiO <sub>2</sub> -ZrO <sub>2</sub>                                   | 8.0   | 5.0     | 300    | 100.0          | Cyclohexane          | (Zhang <i>et al.</i> , 2013)            |
| Guaiacol | Batch      | Ni/HZSM-5   | 2.0   | 3.0     | 200    | 18.0           | Phenol               | (Song <i>et al.</i> , 2015)             |
| Anisole  | Continuous | Ni/SBA-15   | -     | 0.3     | 290    | 100.0          | Cyclohexane, Hexane  | (Yang <i>et al.</i> , 2014)             |
| Anisole  | Batch      | Ni/HZSM-5   | 2.0   | 5.0     | 220    | 100.0          | Cyclohexane          | (Sankaranarayanan <i>et al.</i> , 2015) |
| Anisole  | Batch      | Co/Al-SBA-15  | 2.0   | 5.0     | 220    | 70.0           | Cyclohexane          | (Sankaranarayanan <i>et al.</i> , 2015) |
| Catechol | Batch      | Ni/HZSM-5   | 2.0   | 3.0     | 200    | 100.0          | Cyclohexane-1,2-diol | (Song <i>et al.</i> , 2015)             |

Studies on the use bimetallic catalysts for HDO of bio-oil and its model compounds have been reported. For example Xu *et al.*, (2010) reported the HDO of acetic acid as bio-oil model compound in an autoclave at 200 °C and 30 bar over MoNi/ $\gamma$  - Al<sub>2</sub>O<sub>3</sub>. They reported that the incorporation of Mo as a promoter into the catalyst system improve the performance by 200%. In addition, the addition of Mo enhances the dispersion of NiO, preventing formation of NiAl<sub>2</sub>O<sub>4</sub> and improve the catalyst stability. Similarly, there has been report on the use of Co–Mo–B and Ni–Mo–B as catalysts for HDO of phenol HDO (Alexander & Hargreaves, 2010; Wang *et al.*, 2009; Wang *et al.*, 2010; Wang *et al.*, 2011). The studies shows that the selectivity of the catalysts depend on the Ni/Mo and Co/Mo ratio. For example, Wang *et al.*, (2009) observed that with a Ni/Mo ratio of ~1 the main product is cyclohexanol while the main product is cyclohexane when Ni/Mo ratio is ½. In these types of catalysts, it was proposed that Ni and Mo act together with phenol being adsorb on the Brønsted acid Mo–OH sites while activation of H<sub>2</sub> is on the Ni sites (Hicks, 2011; Wang *et al.*, 2009). Further, the addition of promoters like Co and La to Ni–Mo–B enhances its activity and selectivity to cyclohexane (Wang *et al.*, 2010).

## 2.5 Catalyst supports

Catalyst supports plays an important role during the HDO reaction. The catalyst supports enhance active components dispersion and stabilization, and consequently reduce the total costs of the catalysts (Stakheev & Kustov, 1999). In addition, some catalyst supports also act as active component (in bifunctional catalysts) by providing acid (Brønsted and Lewis) sites on its surface (He & Wang, 2012). Since HDO reaction is a high temperature process that requires both active metal and acidic sites, thus, it is paramount to understand how different type of catalyst supports affect the HDO reaction.

### 2.5.1 Alumina

Alumina ( $\text{Al}_2\text{O}_3$ ) is the earliest studied catalyst support for HDO reaction because of its excellent performance in HDS and HDN reactions. In addition, its excellent strength and presence of Lewis acid sites initially makes it a good choice of catalyst support for HDO catalysts (Li *et al.*, 2011). However, the presence of high acidity led to rapid coke formation and consequently catalysts deactivation (Laurent & Delmon, 1994b; Popov *et al.*, 2010). In addition, another challenge associated with the use of  $\text{Al}_2\text{O}_3$  as support in HDO reaction is its instability in the presence of water, which is a by-product of HDO reaction. Also, water vapour produced during HDO reaction causes  $\text{Al}_2\text{O}_3$  to undergo recrystallization to produce boehmite ( $\text{AlO}(\text{OH})$ ). Boehmite ( $\text{AlO}(\text{OH})$ ) is an oxide that has the capacity to oxidized the active metal component of the catalysts into its oxides form while reaction ongoing and leads to rapid deactivation (Bu *et al.*, 2012; Honkela *et al.*, 2010; Laurent & Delmon, 1994a; Laurent & Delmon, 1994b).

These challenges associated with the use of  $\text{Al}_2\text{O}_3$  as catalysts support for HDO of bio-oil and its model compounds have led to the search for alternative supports. Supports such as metal oxides ( $\text{CeO}_2$ ,  $\text{TiO}_2$ ,  $\text{SiO}_2$  and  $\text{ZrO}_2$ ), zeolites, mesoporous silica (MCM-41, SBA-15), etc. are now being studied as alternative to the  $\text{Al}_2\text{O}_3$ . These new types of catalyst supports are resistant to high temperature and are stable in the presence of water.

### 2.5.2 Metal oxides

The use of metal oxides as support of catalysts designed for HDO of bio-oil and its model compounds have been studied extensively in recent times. For example, silica ( $\text{SiO}_2$ ) has been used as support to Ni and Co alone, and to sulfided NiMo/ $\text{SiO}_2$  and CoMo/ $\text{SiO}_2$  for HDO process. Although these catalysts are not as active as the corresponding sulfided  $\text{Al}_2\text{O}_3$ -based catalysts, however, the inert nature of  $\text{SiO}_2$  prevents it from forming strong interaction with the active components. As reported in literature,

SiO<sub>2</sub>-based catalysts show better selectivity to hydrocarbons as compared to Al<sub>2</sub>O<sub>3</sub>-based catalysts, and this is because the strong metal-interaction formed by the latter is detrimental to its activity. In addition, SiO<sub>2</sub> shows weak interaction with water and its affinity for coke formation is low as compared to Al<sub>2</sub>O<sub>3</sub>, thus, a good candidate for use as catalysts support for HDO of bio-oil.

Zirconia (ZrO<sub>2</sub>), ceria (CeO<sub>2</sub>) and titania (TiO<sub>2</sub>) are the other metal oxides that have been studied and reported in open literature for HDO reaction. ZrO<sub>2</sub> is considered a candidate for support in HDO catalysts due to its excellent textural and amphoteric properties, and its resistance to coke formation (Ardiyanti *et al.*, 2011; Bui *et al.*, 2011; Zhang *et al.*, 2013). Schimming *et al.*, (2015) and Yakovlev *et al.*, (2009) studied the HDO of guaiacol using CeO<sub>2</sub> and CeO<sub>2</sub>-ZrO<sub>2</sub> as the catalysts without the incorporation of any active metal. They reported that CeO<sub>2</sub> and CeO<sub>2</sub>-ZrO<sub>2</sub> have the potential to activate hydrogen and ability of generating oxygen vacancies just like the sulfided catalysts. Therefore, they concluded that CeO<sub>2</sub> and CeO<sub>2</sub>-ZrO<sub>2</sub> fulfil the necessary criteria of support for use in HDO catalysts. Several reports also exist in open literature on the use of TiO<sub>2</sub> as support for MoS<sub>2</sub> in HDS, which is a reaction similar to HDO. It was reported that TiO<sub>2</sub> enhances the dispersion of MoS<sub>2</sub>, sulfidability, ease of reduction and good morphology (Breysse *et al.*, 1991; Bui *et al.*, 2011).

In general, all these metal oxides possess weak acidity that can activate oxy-compound during HDO reactions. The acidity of these metal oxides follows the order Al<sub>2</sub>O<sub>3</sub> > TiO<sub>2</sub> > ZrO<sub>2</sub> > CeO<sub>2</sub> (He & Wang, 2012). However, these metal oxides are mostly microporous and possess relatively small surface areas, which in turn hamper their performances in HDO reactions.

### 2.5.3 Mesoporous silica

Mesoporous silica (MCM-41 and SBA-15), unlike the metal oxides, possess high surface areas that increases the total number of available active sites (Corma, 1997). In addition, the presence of mesopores enhances molecular diffusion of the substrates (Duan *et al.*, 2012), especially those of large molecules like benzaldehyde (Procházková *et al.*, 2007), dibenzofuran (Wang *et al.*, 2011) and triglycerides (Duan *et al.*, 2012).

MCM-41 is a mesoporous material that consists of cylindrical pores that are arranged in a regular pattern to form one-dimensional (1-D) system. Due to its 1-D system, it has low degree of cross-linkages of silicate units and not highly hydrothermally stable (Silaghi *et al.*, 2014). SBA-15 on the other hand consists of cylindrical pores that possess a two-dimensional (2-D) p6mm hexagonal symmetry (Zhao *et al.*, 1998). In addition, due to its 2-D system, it has very high degree cross-linkages of silicate units and is more hydrothermally stable than the MCM-41 (Li *et al.*, 2010; Zhao *et al.*, 1998).

## CHAPTER 3: RESEARCH METHODOLOGY

### 3.1 Materials

The list of chemicals and solvent used in this study are presented in Table 3.1, and all chemicals used received except where stated otherwise.

**Table 3.1: List of chemicals used in this study, their suppliers and purity**

| Chemicals   | Supplier                        | Purity (%) |
|---|---------------------------------|------------|
| Pluronic P123, EO <sub>20</sub> PO <sub>70</sub> EO <sub>20</sub> ,     | Sigma Aldrich                   | N/A        |
| Tetraethylorthosilicate (TEOS)  | Sigma Aldrich                   | ≥ 98       |
| Hydrochloric acid, HCl (ACS reagent, 37%)                               | Sigma Aldrich                   | N/A        |
| Nickel (II) nitrate hexahydrate, Ni(NO <sub>3</sub> ).6H <sub>2</sub> O | Friendemann Schmidt<br>Chemical | ≥ 97       |
| n-Heptane   | Merck                           | ≥ 99       |
| Guaiacol (2-methoxyphenol)  | Sigma Aldrich                   | ≥ 98       |
| Dibenzofuran (DBF)  | Merck                           | ≥ 97       |
| Aluminum isopropoxide (AIP)   | Sigma Aldrich                   | ≥ 98       |

N/A: Not applicable

### 3.2 Catalysts preparation

#### 3.2.1 Synthesis of SBA-15

The SBA-15 synthesis follows the method described by Zhao et al. (1998). In a typical synthesis, 8 g of pluronic P123 was added to 250 ml of 1.9 M HCl and stirred at 40 °C until it is totally dissolved. Subsequently, 16.2 g of TEOS was added and the mixture was stirred at 40 °C for 20 h. The resultant mixture was aged at 90 °C for 24 h in an oven. The solid product was then recovered by filtration and washed with deionized water (until filtrate pH = ~7) to remove excess HCl. After drying overnight at 90 °C, the solid was

grinded to powder form and calcined at 550 °C for 6 h with a heating rate of 1 °C /min, and labelled SBA-15. Figure 3.1 shows a detail flow diagram for the synthesis of the SBA-15.

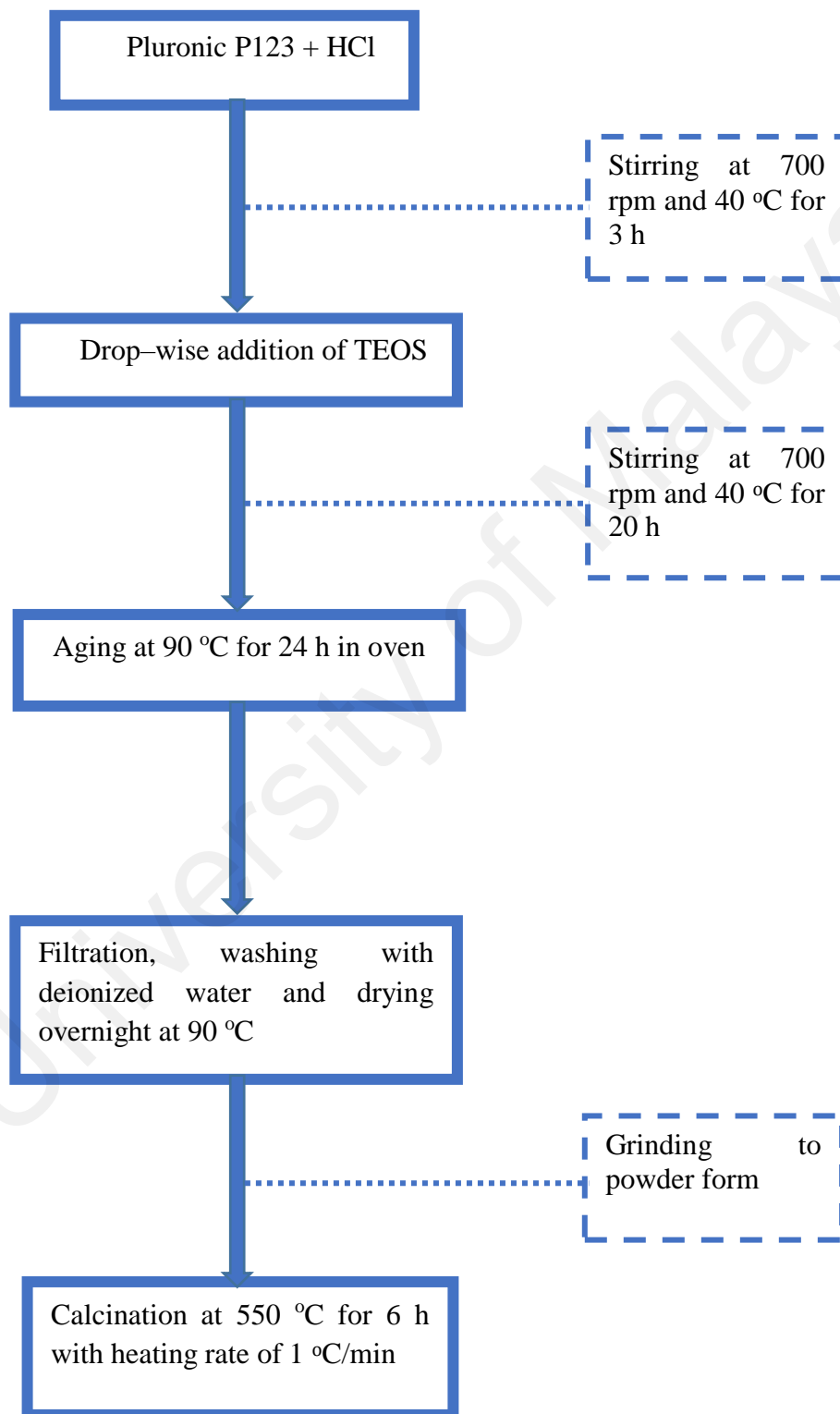


**Figure 3.1: Flow chart for the synthesis of SBA-15**

### 3.2.2 Synthesis of Al-SBA-15

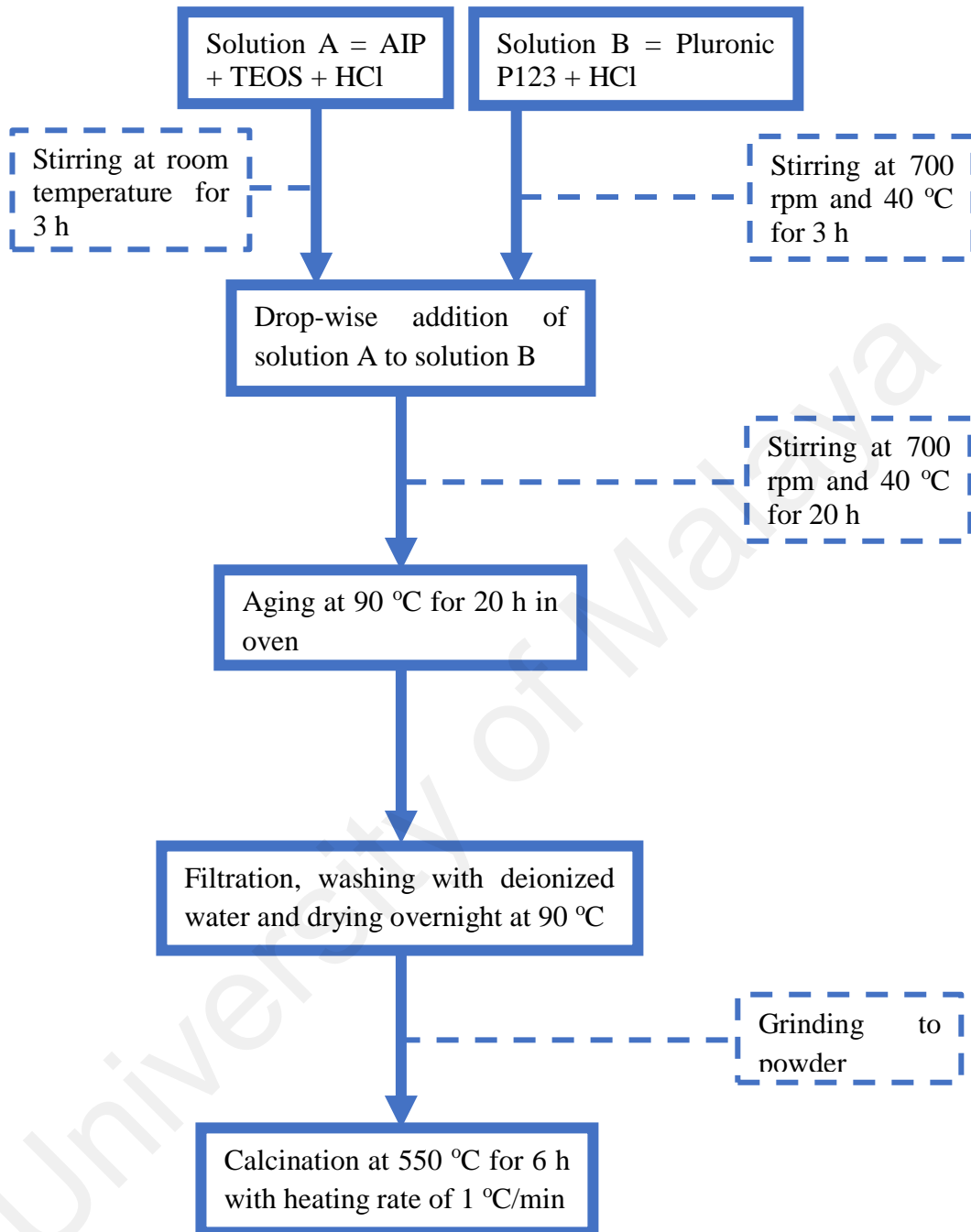


**Figure 3.2: Flow chart for the synthesis of Al-SBA-15**

The synthesis of Al-SBA-15 follows the procedure described by Yue et al. (1999). In a typical procedure, 17 g of TEOS and appropriate amount of AIP were added to 20 ml of HCl solution (pH = 1.5) with different mole ratios of Si/Al (50, 60, 70, and 80), and stirred at 40 °C for 3 h. The resultant solution was added to another solution that contains

dissolved 8 g of pluronic P123 in 300 ml of HCl (pH = 1.5) and stirred for 20 h at 40 °C. The resultant mixture was aged at 90 °C for 24 h in an oven. The solid product was recovered by filtration and washed with deionize water (until filtrate pH = ~7) to remove excess HCl. After drying overnight at 90 °C, the solid was grinded to powder form and calcined at 550 °C for 6 h at a heating rate of 1 °C /min. The obtained samples were labelled Al-SBA-15(n), where n represents the Si/Al mole ratio (50, 60, 70 and 80). Figure 3.2 shows flow diagram for the synthesis of the Al-SBA-15.

### **3.2.3 Synthesis of supported Ni-based catalysts**

The synthesis of the Ni/SBA-15 and Ni/Al-SBA-15(n) catalysts was done by wetness impregnation method using Ni(NO<sub>3</sub>).6H<sub>2</sub>O as Ni precursor. In a typical synthesis methodology, finely grinded powder of the support was dispersed in deionized water and a solution of Ni(NO<sub>3</sub>).6H<sub>2</sub>O containing 5 wt.% of Ni was added drop-wise. Evaporation of the excess water was carried out on a hot plate at ~65 °C under stirring conditions. The obtained sample was oven-dried at 90 °C for 12 h and finally calcined at 550 °C for 6 h with a heating rate of 1 °C /min in air. Figure 3.3 shows flow diagram for the Ni-supported catalysts synthesis.

## **3.3 Catalysts characterization**

### **3.3.1 X – Ray diffraction (XRD) analysis**

#### **3.3.1.1 Background**

X – Ray diffraction (XRD) analysis is a non-destructive technique that relies on the dual wave/particle nature of X-rays to obtain information about the structure of crystalline materials. The XRD technique helps in identifying and characterizing compounds based on their diffraction pattern. It is used for phase identification of a crystalline material and can provide information on unit cell dimensions. Identification of unknown samples is by

comparing its XRD pattern with known standards in the JCPDS database containing more than 287,000 reference patterns (Barbara & Christine, 2015).

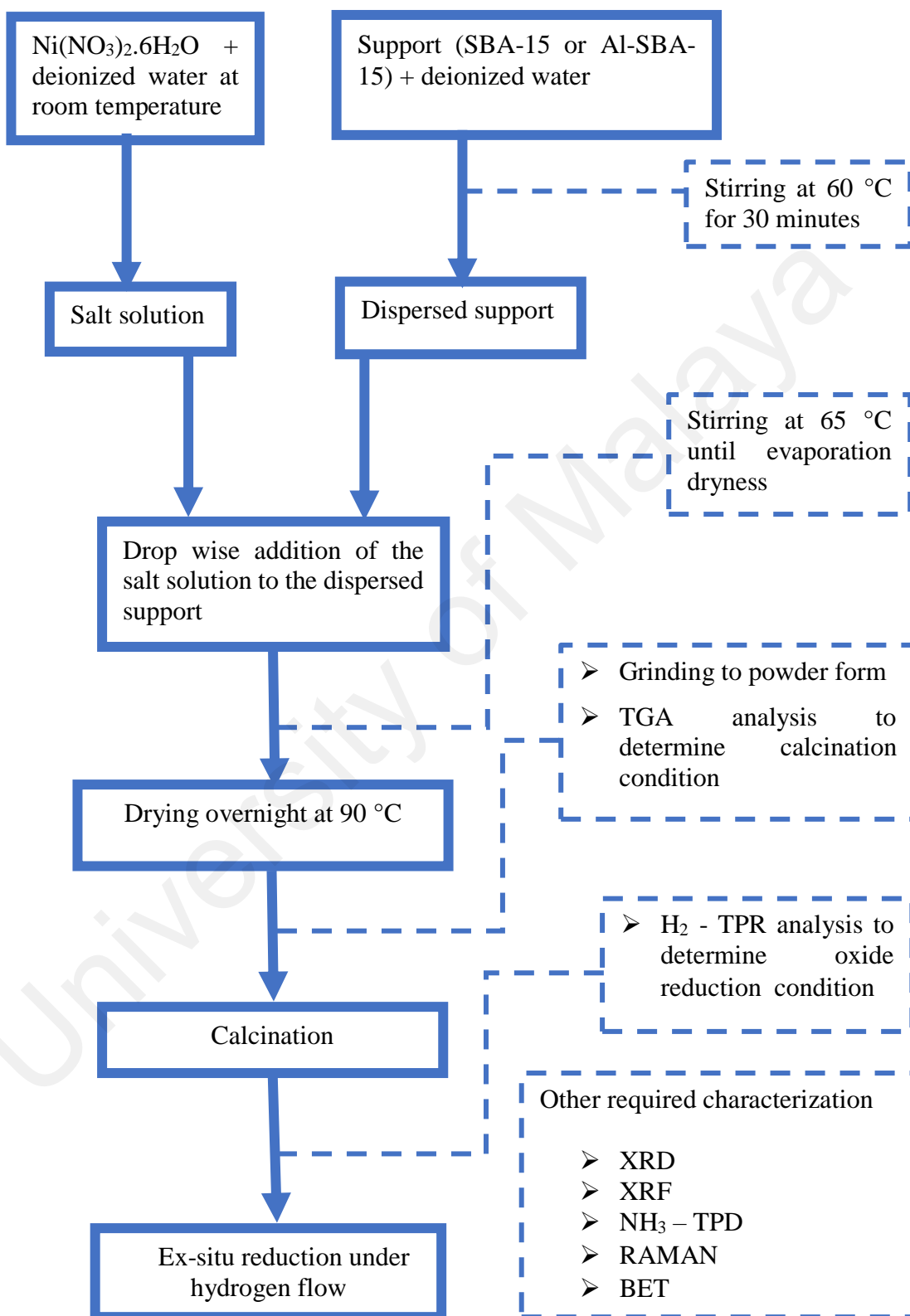


Figure 3.3: Flow chart for the catalysts synthesis

The X-ray diffraction is based on constructive interference of monochromatic X-rays and a crystalline sample. A cathode ray tube, filtered to produce monochromatic radiation, collimated to concentrate, and directed toward the sample, generates these X-rays. The interaction of the incident rays with the sample produces constructive interference (and a diffracted ray) when conditions satisfy Bragg's Law ( $n\lambda=2d \sin \theta$ ). This law relates the wavelength ( $\lambda$ ) of electromagnetic radiation to the diffraction angle ( $\theta$ ) and the lattice spacing ( $d$ ) in a crystalline sample. These diffracted X-rays are then detected, processed and counted. By scanning the sample through a range of  $2\theta$  angles, all possible diffraction directions of the lattice should be attained due to the random orientation of the powdered material. Conversion of the diffraction peaks to d-spacings allows identification of the material because each material has a set of unique d-spacings. Typically, this is achieved by comparison of d-spacings with standard reference patterns (BRUKER, 2016; Thermo Scientific, 2015).

### 3.3.1.2 Procedure

The XRD analysis was carried out using a PXRD PANalytical EMPYREAN (for small angle) and a BRUKER D8 advance XRD diffractometer (for wide-angle), equipped with Cu-K $\alpha$  ( $\lambda= 1.5406 \text{ \AA}$ ) radiation source operating at 40 kV and 40 mA. For each analysis, the samples were finely grinded and packed tightly in a sample holder. Prior to placing the sample holder (with the sample in it) in the diffractometer for analysis, the sample surface was smoothed with a glass slide. The data were recorded in the  $2\theta$  ranges of  $0.5 - 5^\circ$  with a step size of  $0.1^\circ \text{ s}^{-1}$  for small angle, and  $15 - 80^\circ$  with a step size of  $0.2^\circ \text{ s}^{-1}$  for wide-angle. The XRD patterns obtained were matched against the JCPDS standard reference patterns to confirm the identity of the samples. The average crystallite size of NiO in the synthesized catalysts was estimated using Scherrer equation from main diffractions of d(111), d(200) and d(220). Equation 3.1 was used to calculate the unit cell

parameter ( $a_0$ ) and Equation 3.2 was used to calculate the wall thickness using data from small angle XRD analysis.

$$a_0 = \frac{2d(100)}{\sqrt{3}} \dots \dots \dots \text{Equation 3.1}$$

$$\text{Wall thickness} = a_0 - \text{pore size} \dots \dots \dots \text{Equation 3.2}$$

Where  $d(100)$  is the  $d$  spacing for the peak indexed at plane (100) from small angle XRD analysis and pore size is the average pore size obtained from BJH analysis

### 3.3.2 X – Ray fluorescence (XRF) analysis

#### 3.3.2.1 Background

X-ray fluorescence (XRF) analysis is a non-destructive analytical technique used to determine the elemental composition of materials, be it liquids, solids or loose powders. It works on wavelength-dispersive spectroscopic principles that are similar to an electron microprobe. However, an XRF cannot generally make analyses at the small spot sizes (2-5 microns); therefore, it is used for bulk analyses of larger fractions of materials. XRF combines highest accuracy and precision with simple and fast sample preparation for the analysis of elements from Beryllium (Be) to Uranium (U) in the concentration range from 100% down to the sub-ppm-level (BRUKER, 2016; Thermo Scientific, 2015).

The XRF analysis is based on the behaviour of atoms when they interact with radiation. When materials are excited with high-energy (i.e. short wavelength) radiation like X-rays, they become ionized. If the energy of the radiation is enough to dislodge a tightly held inner electron, the atom becomes unstable and an outer electron replaces the missing inner electron. When this happens, there is a release of energy, which is due to a decrease in

the binding energy of the inner electron orbital. The emitted radiation is of lower energy than the primary incident X-rays and is termed fluorescent radiation. Because the energy of the emitted photon is characteristic of a transition between specific electron orbitals in a particular element, the resulting fluorescent X-rays can be used to detect the abundances of elements that are present in the sample (Karl & Andy, 2015; OXFORD Instruments, 2016).

### **3.3.2.2 Procedure**

The XRF analysis to determine the elemental composition of the catalysts was performed using a Bruker S4–Explorer X-ray Fluorescence. The machine was equipped with Spectra-plus V1.64 software for data acquisition and analysis, and x-ray source was operating at 1 kW. The analysis was done at ambient temperature using semi-quantitative method. Prior to analysis, the samples were grinded into a mortar and subsequently pressed to form pellet. The pellet in a 6  $\mu\text{m}$  Mylar film at the bottom was then transferred to the XRF analyzer. The data were recorded in the  $2\theta$  range of  $11^\circ$  to  $140^\circ$ .

### **3.3.3 BET and BJH analysis**

#### **3.3.3.1 Background**

BET analysis provides precise specific surface area evaluation of materials by nitrogen multilayer adsorption measured as a function of relative pressure using a fully automated analyzer. Adsorption results from relatively weak forces (van der Waals forces) between the adsorbate gas molecules and the adsorbent surface area of the test materials. The determination is done at the temperature of liquid nitrogen ( $-196^\circ\text{C}$ ). The technique encompasses external area and pore area evaluations to determine the total specific surface area in  $\text{m}^2/\text{g}$  yielding important information in studying the effects of surface porosity and particle size in many applications (James, 2006). BJH analysis on the other hand was employed to determine pore size and specific pore volume using adsorption and

desorption techniques. This technique characterizes pore size distribution independent of external area due to particle size of the sample. The BJH analysis also tells if a material is microporous, mesoporous or macroporous (Barrett *et al.*, 1951; James, 2006; Joyner *et al.*, 1951).

### **3.3.3.2 Procedure**

The BET and BJH analysis (N<sub>2</sub> adsorption–desorption measurements) were conducted on a Micrometrics TriStar II surface area and porosity analyzer at -196 °C using ASTM D3663–03 method. Before the analysis, all samples were degassed to remove physically adsorbed gases and vapours from the surface of the sample. This was achieved by heating 300 mg of the sample at 300 °C for 5 h in the analyzer sample cell. After degassing, the sample cell was made airtight and re-weighed to determine the actual weight of the sample. The sample cell was then connected to the analysis section of the analyzer, and cooled in liquid nitrogen. The surface area was calculated by multiple point BET method and the BJH method was applied to the desorption branch of the isotherms to determine the pore size distribution and pore volume of the sample.

### **3.3.4 Field Emission Scanning Electron Microscopy (FESEM) analysis**

#### **3.3.4.1 Background**

The Field Emission Scanning Electron Microscopy (FESEM) is an analytical equipment that provides topographical and elemental information at high magnifications. The FESEM produces images of a sample by scanning it with a focused beam of electrons. The electrons interact with atoms in the sample, producing various signals that contain information about the sample's surface topography and composition. The electron beam is scanned in a raster scan pattern, and the beam's position is combined with the detected signal to produce an image (Al-Obaidi, 2015; Danilatos *et al.*, 2015; Suga *et al.*, 2014). Scanning can be observe in low vacuum or high vacuum.

### **3.3.4.2 Procedure**

The FESEM images were taken on a FEI Quanta 200 electron microscope operating at 5 kV. Firstly, the samples were made conductive by dispersing on a carbon tape. The samples were then mounted on a sample holder and loaded into the FESEM chamber. Vacuum was created in the chamber by evacuating air prior to scanning. Scanning was done under low vacuum, spot size of 3  $\mu\text{m}$  and magnification range of 5,000 to 50,000.

### **3.3.5 Raman spectroscopy analysis**

#### **3.3.5.1 Background**

Raman spectroscopy is a spectroscopic technique that provides information about vibrational, rotational and other low frequency transitions in molecules. It is a technique that is based on inelastic scattering of monochromatic light, usually from a laser source. When monochromatic light is scattered from a molecule, most photons are elastically scattered. The scattered photons have the same energy (frequency) and, therefore, same wavelength, as the incident photons. However, a small fraction of the monochromatic light (approximately 1 in  $10^7$  photons) is scattered at optical frequencies different from (i.e. inelastic scattering), and usually lower than, the frequency of the incident photons. Photons of the laser light are absorbed by the sample and then re-emitted. Frequency of the re-emitted photons is shifted up or down in comparison with original monochromatic frequency, which is called the Raman Effect. Raman spectroscopy can be used for both qualitative and quantitative applications (Bumbrah & Sharma, 2015; Kaiser Optical Systems Inc, 2016; Princeton Instruments, 2016). The spectra are very specific, and chemical identifications can be performed by using search algorithms against digital databases.

### 3.3.5.2 Procedure

The Raman spectra were obtained at ambient temperature using Renishaw InVia Raman spectroscopy, equipped with a charge coupled device (CCD) detector. For the analysis, a 100%-20 mW power from 514 nm Ar laser was used. For each analysis, the sample was placed inside the spectrometer after it had been pressed into a self-supporting wafer. A monochromatic light (laser) is then shined on the sample and the resulting scattered rays were measured using the CCD detector. The measured data was subsequently saved and evaluated on a computer.

### 3.3.6 H<sub>2</sub>-Temperature-Programmed Reduction (H<sub>2</sub>-TPR) analysis

#### 3.3.6.1 Background

H<sub>2</sub>-Temperature-programmed reduction (H<sub>2</sub>-TPR) is a widely used tool for the characterization of metal oxides, mixed metal oxides, and metal oxides dispersed on a support. The H<sub>2</sub>-TPR method yields quantitative information of the reducibility of the oxide's surface. In addition, it determines the number of reducible species present on a catalyst surface and reveals the temperature at which the reduction of each species occurs. An important aspect of H<sub>2</sub>-TPR analysis is that the sample need not have any special characteristics other than containing reducible metals (Knözinger, 2008; Micromeritics, 2015; Reiche *et al.*, 2000).

The H<sub>2</sub>-TPR analysis begins by flowing an analysis gas (typically 5% to 20% hydrogen in an inert carrier gas such as nitrogen or argon) through the sample, usually at ambient temperature. While the gas is flowing, the temperature of the sample is increased linearly with time and a thermal conductivity detector (TCD) monitoring the consumption of hydrogen. Changes in the concentration of the gas mixture downstream from the reaction cell are determined. This information yields the volume of hydrogen uptake. H<sub>2</sub>-TPR ultimately yields a bulk reduction of the sample; the peak maxima in the H<sub>2</sub>-TPR

profile is an indication of the reducibility of the metal oxide phase (Gervasini, 2013; Reiche *et al.*, 2000).

### **3.3.6.2 Procedure**

The H<sub>2</sub>-TPR analysis of the catalysts were carried out using ThermoFinnigan TPDRO 1100 series equipped with a thermal conductivity detector (TCD). For each analysis, 61.7 mg of the catalyst was used. Prior to analysis, the catalysts were pre-treated in a TPDRO cell at 120 °C for 1 h under N<sub>2</sub> atmosphere to eliminate any volatile component. After pre-treatment, the TPR experiments were conducted by heating the sample at a rate of 10 °C /min between 200 and 600 °C under the flow of 5% H<sub>2</sub>/N<sub>2</sub> gas (20 ml/min). For each analysis, the sample was held at 600 °C for 1 h.

### **3.3.7 NH<sub>3</sub>-Temperature-Programmed Desorption (NH<sub>3</sub>-TPD) analysis**

#### **3.3.7.1 Background**

The NH<sub>3</sub>-TPD is one of the most widely used and flexible technique for characterizing the acid sites on oxide surface of catalysts. Determining the quantity and strength of the acid sites is crucial in understanding and predicting the performance of a catalyst.

The NH<sub>3</sub>-TPD analysis begins by saturating the sample with NH<sub>3</sub> (typically 5% to 20% NH<sub>3</sub> in helium): pulsing the NH<sub>3</sub> using the loop or continuously flowing NH<sub>3</sub>. The temperature of the sample is then increased linearly with time while helium is flowing. During the analysis, a built-in thermal conductivity detector (TCD) in the analyzer monitors the desorbed NH<sub>3</sub>.

#### **3.3.7.2 Procedure**

The NH<sub>3</sub>-TPD analysis of the catalysts were carried out using ThermoFinnigan TPDRO 1100 series equipped with a thermal conductivity detector (TCD). For each analysis, a 61.7 mg of the catalyst was used. The catalysts were first outgassed in the

TPDRO cell at 120 °C for 1 h in flowing helium. After outgassing, the system was allowed to cool to 50 °C. The catalysts were subsequently saturated with 10% NH<sub>3</sub>/He (20 ml/min) at 50 °C for 1 h under continuously flowing method. The system was then purged for 1 h with 100% helium to remove weakly physisorbed NH<sub>3</sub>. The TCD profiles of the chemisorbed NH<sub>3</sub> were obtained by heating the sample from 50 to 500 °C at a heating rate of 10 °C/min under the flow of helium.

### **3.4 Catalysts activity study**

#### **3.4.1 Catalysts activation**

The catalysts used in this study were activated (reduced) under hydrogen flow (50 ml/min) at 500 °C for 3 h. This was done in a pretreatment block (Cambridge Reactor Design) that has a maximum attainable temperature of 700 °C. The pretreatment block consists of two (2) units that can operate independently, and each unit consists of six (6) parallel glass reactors (making 12 in total). The pretreatment block is equipped with a temperature and pressure controller, and a cooling medium that uses compressed air. In addition, gas lines for hydrogen, compressed air and inert, and a switch valve for changing gas that flow through the reactors are connected to the pretreatment block.



**Figure 3.4: Pretreatment set-up for catalysts activation**

60 mg of the catalyst was weighed and loaded into the glass reactors, after which the upper part of the reactors were sealed by connecting a bulb. The sealed reactors were inserted into the pretreatment unit (Figure 3.4) and purged three (3) times with nitrogen after which the gas stream was switched to  $H_2$ . While  $H_2$  was flowing (50 ml/min), the reactors and its contents were heated to 500 °C at a rate of 5 °C/min. The system was maintained at 500 °C for 3 h, after which it was cooled to room temperature. After removing the reactors, they were turned upside down so that the reduced catalysts can move into the bulb. Sealing of the bulbs was with a torch in the encapsulation unit to produce the catalysts bulbs (Figure 3.5). It worth mentioning that the sealed reactor, after loading the catalyst, was weighed before and after reduction. The difference between the two weights gave the approximate weight of the catalysts that was used for the HDO reaction.

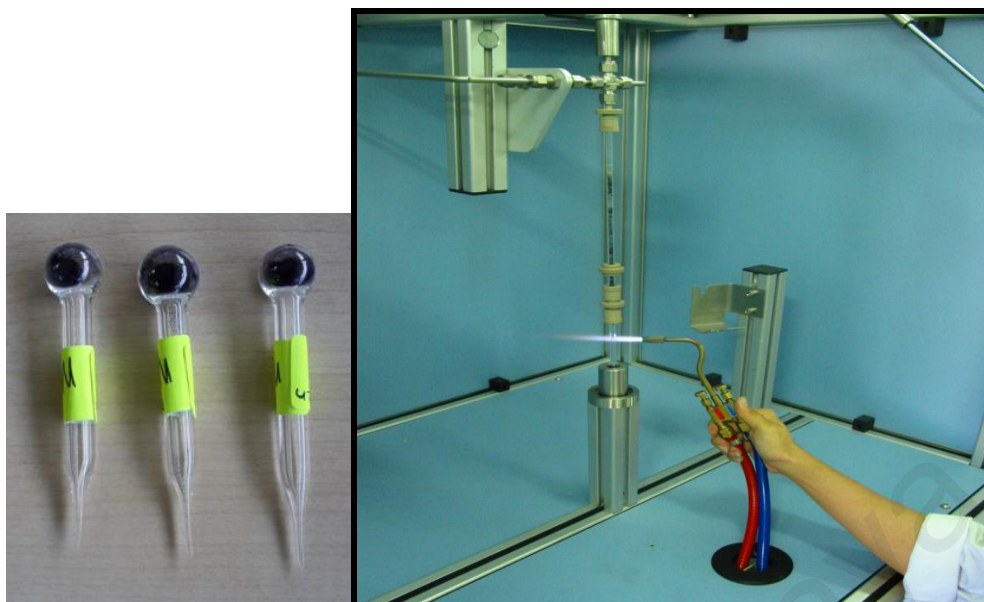


**Figure 3.5: Bulb sealing with a torch in the encapsulation unit and catalyst bulbs after sealing**

### 3.4.2 Reactor set-up

The catalysts performance tests were carried out in a workstation that contains multiple 100 ml stainless steel high-pressure batch reactors (Cambridge Reactor Design). The workstation comprises of 12 independent batch reactors (Figure 3.6) capable of operating at a maximum temperature and pressure of 300 °C and 30 MPa respectively. The reactors are equipped with a thermocouple, a mechanical stirrer (up to 1,500 rpm maximum speed), a pressure sensor, and a system for controlling temperature, stirring rate, and pressure. During the HDO reaction, the catalysts bulbs are usually mounted on the Polyether ether ketone (PEEK) holders that are connected to the mechanical stirrer. Upon starting the reaction, the mechanical stirrer breaks the catalyst bulb, and releases the catalyst into the reaction mixture. A recirculating cooling unit (Julabo, FC 600 model) that uses deionized water as cooling fluid was connected to the workstation for cooling the reactors after every reaction. The Julabo has a working temperature range of  $-20\text{ }^{\circ}\text{C}$  to  $+80\text{ }^{\circ}\text{C}$ , heating capacity of 1.2 kW and pump capacity flow rate of 20 l/min.

A hydrogen-dosing unit that receives supply from the main hydrogen cylinder is connected to each reactor. Subsequently, hydrogen is supplied to each reactor from the hydrogen-dosing unit through a check valve. In the case of drop in hydrogen pressure during the reaction (due to hydrogen consumption), the reactors are re-pressurized automatically from the hydrogen-dosing unit independently.



**Figure 3.6: A workstation that consist 12 independent batch reactors**

### **3.4.3 Hydrodeoxygenation reaction**

The HDO reaction was carried out using 3 wt.% substrate (DBF or guaiacol), 97 wt.% solvent (heptane) and approximately 50 mg of catalysts. For every reaction, 30 ml of solvent and substrate mixture was loaded into each reactor and sealed. The reactors were purge with nitrogen and subsequently filled with the same nitrogen to 11 MPa for leak check. After leak check, the reactors were de-pressurized and flushed with hydrogen. The reactors temperature was elevated to the reaction temperature (250 °C) after pressurized with H<sub>2</sub> to 1/3<sup>rd</sup> of reaction set pressure. The reactors were left to stabilize at the reaction temperature, and the pressure was elevated to 80% of the reaction pressure. The reactors

were left again for some minutes to stabilize, and subsequently, the remaining 20% pressure make-up was supplied from the hydrogen-doing units. The reactors were allowed to stabilize again, and subsequently, the stirrer (stirring speed = 1000 rpm) and timer starts automatically. The stirrer immediately causes the catalyst bulb to break, and released into the reaction mixture. After every reaction, the reactors were cooled to room temperature by circulating cold water from the Julabo, and subsequently de-pressurized. The liquid products were collected and analysed offline using GC-MS and GC-FID.

### **3.5 Product analysis**

#### **3.5.1 GC analysis**

The Analysis of the products was done by Agilent GC 6890N equipped with 5973 MSD and 30 m x 0.25 mm x 0.25  $\mu$ m HP-5ms capillary column. In addition, products quantification was conducted on an Agilent GC 6890N equipped with flame ionization detector and 30 m x 0.25 mm x 0.25  $\mu$ m HP-5ms capillary column. Prior to the analysis, the products were filtered using a micro filter to remove the catalysts.

To separate the products of the DBF HDO reaction, the GC oven temperature was held at 40 °C for 5.0 min, after which it was heated to 161 °C with a ramping of 15 °C/min. It was again held at 161 °C for 10.0 min, then heated to 170 °C at a rate of 15 °C/min and held for 10.0 min. Some of the chromatographs obtained for the analysis are shown in Appendix A.

To separate the products produced from guaiacol HDO reaction, the GC oven temperature was held at 40 °C for 2.0 min, after which it was heated to 60 °C at a ramping of 2 °C/min. It was again heated to 100 °C with a ramping of 5 °C, and subsequently heated to 200 °C with a ramping of 20 °C and held for 2.0 min. Some of the GC chromatographs obtained for the analysis are shown in Appendix A.

### 3.5.2 Conversion and selectivity calculation

All the conversions reported in this dissertation were calculated using Equation 3.3.

$$\text{Conversion (X)} = \frac{\text{Amount of substrate consumed}}{\text{Amount of substrate feed}} \times 100 \dots \dots \dots \text{Equation 3.3}$$

The HDO reactions of DBF and guaiacol led to the formation of more than one product. Therefore, the selectivity reported in this dissertation was calculated using Equation 3.4.

$$\text{Selectivity (S)} = \frac{n_i}{\sum n_i} \times 100 \dots \dots \dots \text{Equation 3.4}$$

Where  $n_i$  is the amount of a defined HDO product and  $\sum n_i$  is the total amount of the HDO products.

University of Malaya

## CHAPTER 4: RESULTS AND DISCUSSION

This chapter presents result of the research. The results for both the catalysts characterization and catalytic activity study are analyzed, discussed and compared to those in open literature.

### 4.1 Catalysts characterization

#### 4.1.1 Surface area and porosity measurement

The textural properties of the supports and corresponding supported Ni catalysts were investigated using N<sub>2</sub> adsorption-desorption analysis. The specific surface areas were calculated using the multiple points (P/P<sup>o</sup> ranging from 0.00005 to 0.9937) BET method. Similarly, the porosity (pore size and volume) was calculated by applying the BJH method to the desorption branch of the isotherm at P/P<sup>o</sup> = 0.99. Figure 4.1 to 4.5 shows the N<sub>2</sub> adsorption–desorption isotherms for the synthesized supports and the supported Ni catalysts, as well as the pore size distributions.

All the synthesized materials exhibited Type IV isotherms, which are characteristics of mesoporous materials according to IUPAC classification (Condon, 2006). In addition, the presence of pore sizes ranging from 38 – 53 Å, as it is evident from the pore size distribution further confirm the mesoporous nature of the synthesized materials. SBA-15 and Ni/SBA-15 samples exhibited H1 hysteresis loop (Figure 4.1a), while the Al-SBA-15 and Ni/Al-SBA-15 (Figure 4.2a to Figure 4.5a) samples exhibited H2 hysteresis loop (Condon, 2006).

The Type IV-H1 hysteresis loop exhibited by SBA-15 and Ni/SBA-15 is a typical adsorption for ordered mesoporous materials with 2D-hexagonal structure with well-defined cylindrical pore channels. Three distinct regions are evident from the adsorption isotherms shown in Figure 4.1a:

- i. Region (i) occurs at low relative pressure, with  $P/P^0$  ranging from 0 to 0.58. This region is considered the monolayer-multilayer adsorption region, and a moderate amount of nitrogen becomes physisorbed to the catalysts material (Li *et al.*, 2004; Zhao *et al.*, 1998),
- ii. Region (ii) occurs at intermediate relative pressure, with  $P/P^0$  ranging from 0.58 to 0.77. In this region, a well-defined step occurs and this corresponds to the capillary condensation of  $N_2$ , indicative of uniform pores (Li *et al.*, 2004; Zhao *et al.*, 1998),
- iii. Region (iii) occurs at high relative pressure, with  $P/P^0$  ranging from 0.77 to 1.0. In this region, multilayer adsorption takes place on the outer surfaces of the catalysts materials, and after which desorption of nitrogen starts (Li *et al.*, 2004; Zhao *et al.*, 1998).

As evident from the obtained hysteresis loop (Figure 4.1a), the impregnation of Ni into the SBA-15 does not alter its original structure. However, there was a decrease in the total surface area and the pore volume (Figure 4.1) after Ni incorporation.

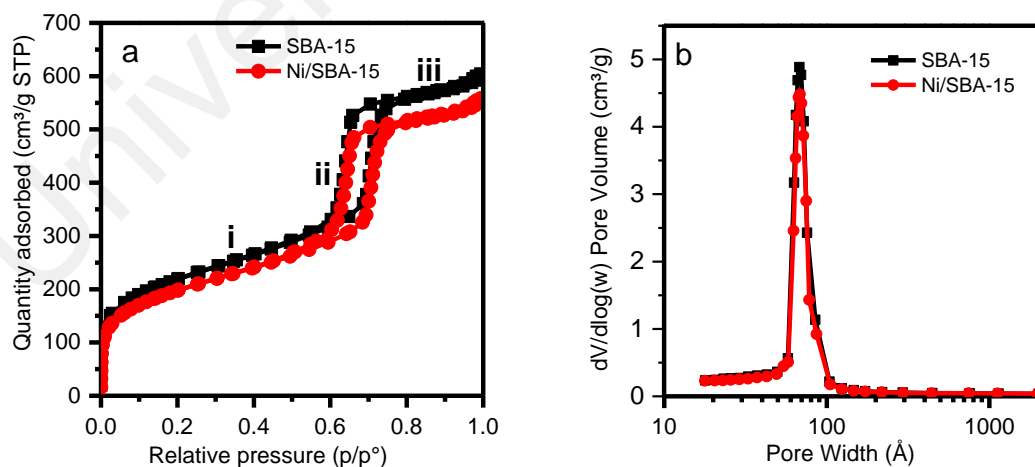


**Figure 4.1: (a)  $N_2$  adsorption-desorption isotherms (b) pore size distribution of SBA-15 and Ni/SBA-15**

In contrast to the SBA-15, the Al-SBA-15 and Ni/Al-SBA-15 exhibited the Type IV-H2 hysteresis loop with capillary condensation at relative pressure ranging from 0.47 to 0.92. The Type IV-H2 hysteresis loop exhibited by the Al-SBA-15 and Ni/Al-SBA-15 (Figure 4.2a to Figure 4.5a) catalysts reveals the presence of pores blockage in the synthesized Al-SBA-15 supports. This observation indicates that the incorporation of Al<sup>3+</sup> into the SBA-15 matrix altered its textural properties. The impregnation of Ni into the Al-SBA-15 materials does not affect its structure, however, there was a decrease in the total surface area and pore volume. This is due to partial deposition of Ni on the surface and in the pores of the Al-SBA-15.

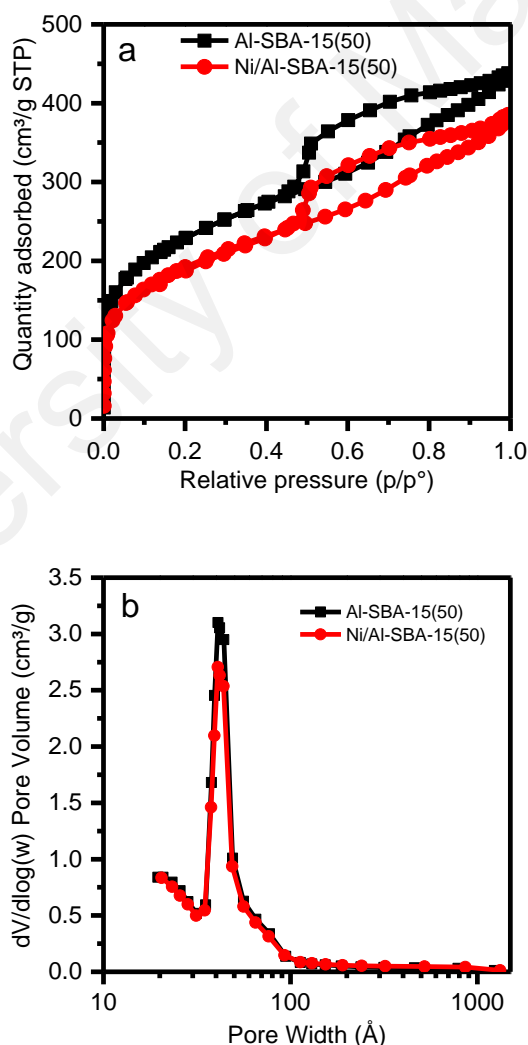


**Figure 4.2:** (a) N<sub>2</sub> adsorption-desorption isotherms (b) pore size distribution of Al-SBA-15(50) and Ni/ Al-SBA-15(50)

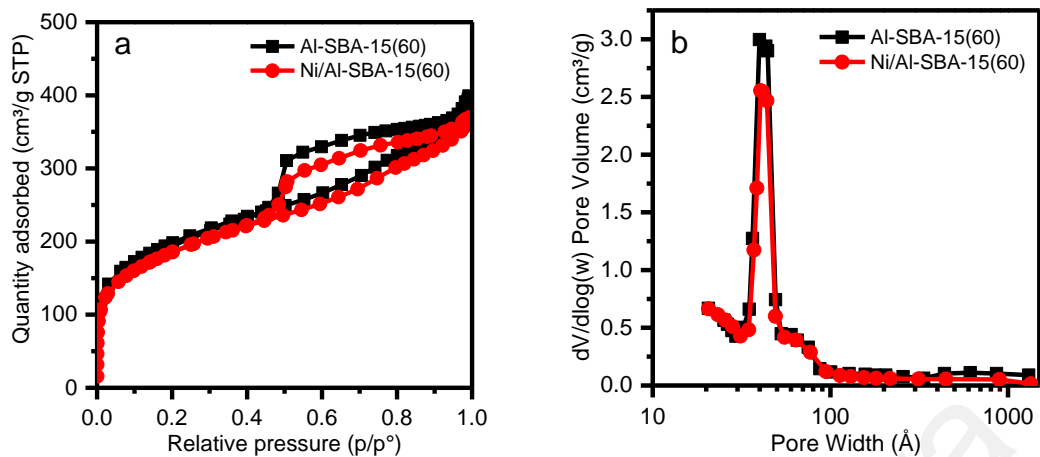


**Figure 4.3: (a) N<sub>2</sub> adsorption-desorption isotherms (b) pore size distribution of Al-SBA-15(60) and Ni/ Al-SBA-15(60)**

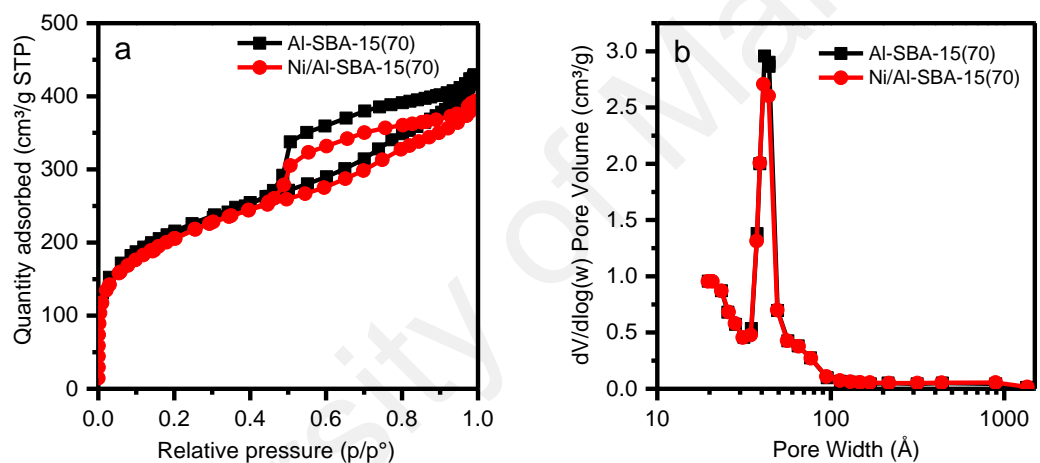


**Figure 4.4: (a) N<sub>2</sub> adsorption-desorption isotherms (b) pore size distribution of Al-SBA-15(70) and Ni/ Al-SBA-15(70)**

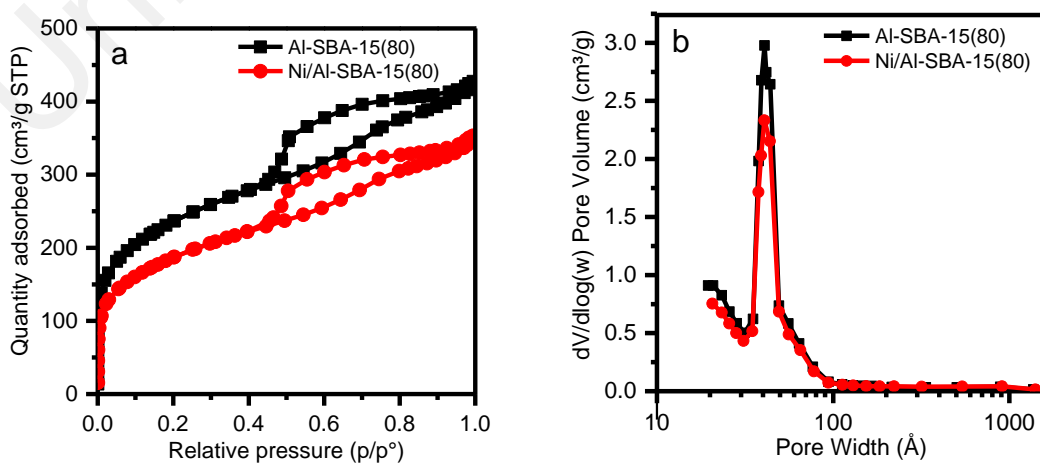


**Figure 4.5: (a) N<sub>2</sub> adsorption-desorption isotherms (b) pore size distribution of Al-SBA-15(80) and Ni/ Al-SBA-15(80)**

**Table 4.1: Textural properties of the synthesized catalysts**

| Sample           | BET surface area (m <sup>2</sup> /g) | Mesopore Volume (cm <sup>3</sup> /g) | Micropore Volume (cm <sup>3</sup> /g) | Average pore size (Å) |
|------------------|--------------------------------------|--------------------------------------|---------------------------------------|-----------------------|
| SBA-15           | 783                                  | 0.9183                               | 0.0643                                | 53                    |
| Ni/SBA-15        | 711                                  | 0.8622                               | 0.0427                                | 52                    |
| Al-SBA-15(50)    | 821                                  | 0.6117                               | 0.0557                                | 40                    |
| Ni/Al-SBA-15(50) | 694                                  | 0.5737                               | 0.0359                                | 39                    |
| Al-SBA-15(60)    | 707                                  | 0.5703                               | 0.0666                                | 41                    |
| Ni/Al-SBA-15(60) | 665                                  | 0.5154                               | 0.0471                                | 41                    |
| Al-SBA-15(70)    | 769                                  | 0.6131                               | 0.0644                                | 40                    |
| Ni/Al-SBA-15(70) | 740                                  | 0.5533                               | 0.0458                                | 39                    |
| Al-SBA-15(80)    | 846                                  | 0.5749                               | 0.0666                                | 39                    |
| Ni/Al-SBA-15(80) | 672                                  | 0.4859                               | 0.0400                                | 38                    |

Table 4.1 present the surface areas, pore sizes and pore volumes, of the supports and the corresponding supported Ni catalysts. The obtained results show that SBA-15 has high surface area (783 m<sup>2</sup>/g) and moderate pore diameter (53 Å). Interestingly, the incorporation of Al<sup>3+</sup> into the SBA-15 matrix leads to improved surface areas. The increase in surface area is an indication that the incorporated Al<sup>3+</sup> ions have successfully replaced some of the Si<sup>4+</sup> ions to aluminosilicate (Al-SBA-15). In addition, there is expectation of lattice expansion in Al-SBA-15 because Al<sup>3+</sup> has bigger ionic radii than Si<sup>4+</sup> (Al<sup>3+</sup> = 0.039 nm; Si<sup>4+</sup> = 0.026 nm) and consequently an increase in surface area. Both surface area and pore volume showed a V-shaped trend as the Al<sup>3+</sup> amount increases, while the pore size decreased slightly, though not linear. Among the synthesized Al-SBA-15 supports, Al-SBA-15(80) has the highest surface area (846 m<sup>2</sup>/g), while Al-SBA-

15(60) has the least surface area (707 m<sup>2</sup>/g). Similarly, the synthesized Ni/SBA-15 and Ni/Al-SBA-15 catalysts exhibited high surface areas (665–740 m<sup>2</sup>/g) which could play a favourable role in HDO of DBF and guaiacol, because they increase the number of available active sites. In addition, owing to mesoporous nature of the catalysts (pore sizes in the range of 39–52 Å) the DBF and guaiacol molecules can be easily accessed into the active sites within the catalyst pores. Comparing the surface areas and pore volumes of each catalyst with its support, it is evident that there is a decrease in the surface areas and pore volumes after Ni incorporation. This is due to micropores filling by the NiO nanoparticles, and subsequent loss of mesopores area that coincides with shrinkage of average pore sizes. Evidence of the pore sizes shrinkage is clear from the downshift in the unimodal BJH pore sizes distributions (Figure 4.1 to Figure 4.5).

#### 4.1.2 Morphological properties

Field Emission Electron Microscope (FESEM) was used to study the morphology of the synthesized supports. In addition, with the aid of the FESEM images, effect of Al<sup>3+</sup> incorporation into the SBA-15 was evaluated. The FESEM images were obtained under low vacuum and at a magnification of 10,000. Figure 4.6 shows the FESEM images of the synthesized SBA-15 and Al-SBA-15.

Figure 4.6a reveal that the synthesized SBA-15 contains many rod-like (cylindrical) structures with relatively uniform length of ~1–2 μm between each joints and ~300–500 nm external diameter that are aggregated into wheat-like macrostructures. This is in agreement with the result obtained from the BET isotherm (Figure 4.1a), which shows that the synthesized SBA-15 is an ordered mesoporous materials with 2D-hexagonal structure with well-defined cylindrical pore channels.

On the other hand, the original rod-like morphology of SBA-15 changes to a separate sub-unit (i.e. rice-like units) when Al<sup>3+</sup> is incorporated into the SBA-15 matrix (Figure 4.6b to 4.6e). The obtained rice-like units for the Al-SBA-15 are of ~400–900 nm in

length and ~180–350 nm in diameter. Comparing the morphologies of SBA-15 and Al-SBA-15, it is evident that there is a lesser degree of uniformity in Al-SBA-15, indicating the possible distortion caused by the incorporation of  $\text{Al}^{3+}$  into the SBA-15 matrix. This is in agreement with the BET hysteresis loop obtained for the synthesized Al-SBA-15 (Figure 4.2 to 4.5), and they both (BET and FESEM) confirm structural modification caused by  $\text{Al}^{3+}$  incorporation.

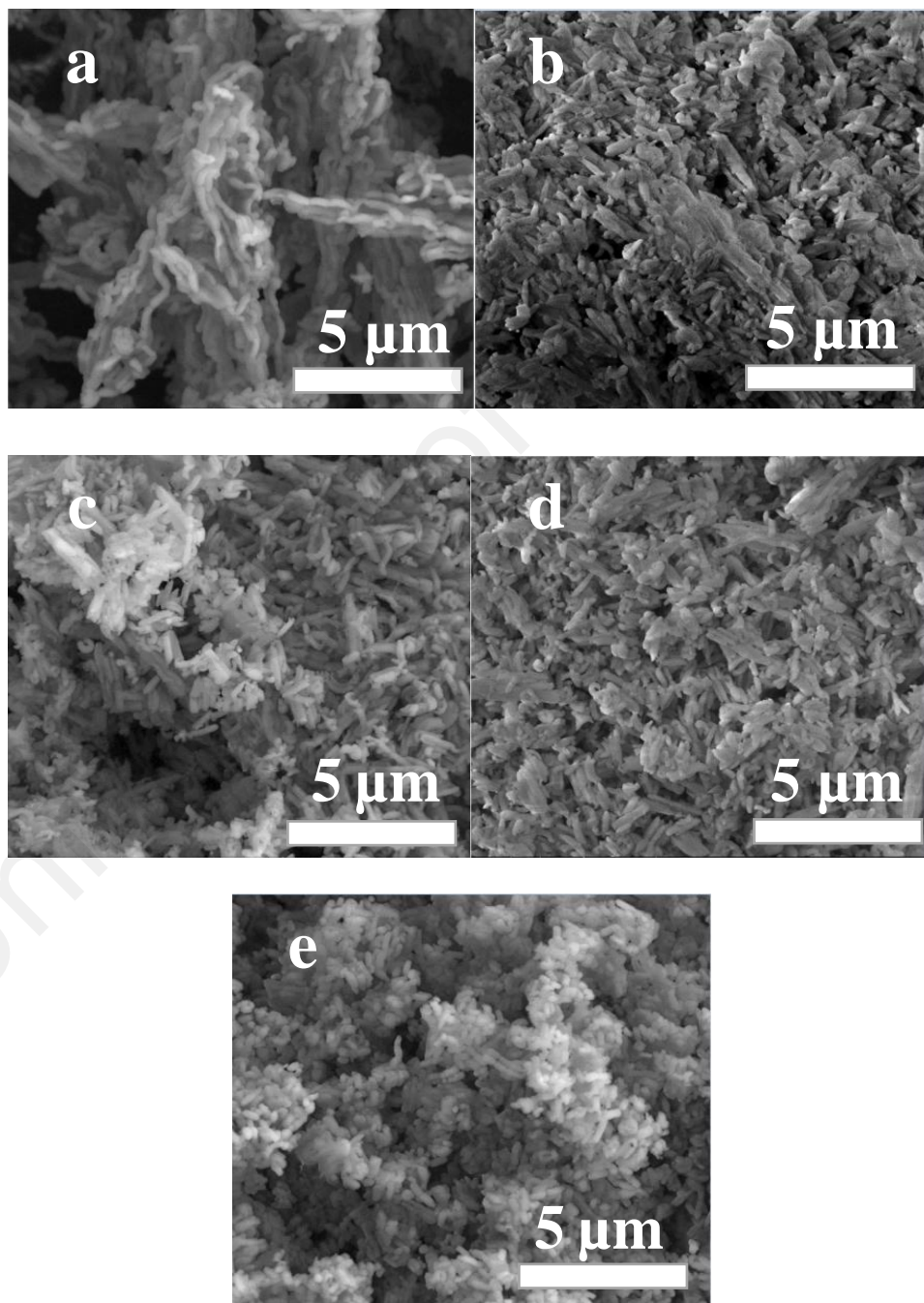


**Figure 4.6: FESEM images of (a) SBA-15 (b) Al-SBA-15(50) (c) Al-SBA-15(60) (d) Al-SBA-15(70) (e) Al-SBA-15(80); magnification = x 10,000**

### 4.1.3 Powder XRD analysis

The crystalline structures and phases of the synthesized supports and the corresponding supported catalysts were studied using powder XRD technique. Figure 4.7 and Figure 4.8 shows the XRD patterns of the supports and the corresponding supported Ni catalysts. In addition, Table 4.2 and Table 4.3 presents the summary of both the small angle and wide angle XRD analysis respectively. For the record, it is worth mentioning that XRD analysis were carried out on calcined catalysts, and consequently, nickel is expected to exist in oxide form (i.e. NiO). Also, the XRD analyzer used has a detection limit of ~2 wt.% for composite samples.

The small angle diffraction pattern (Figure 4.7a) of the synthesized SBA-15 reveal the presence of an ordered mesoporous structure. This is evident by the presence of three distinct peaks that can be indexed as (100), (110) and (200) diffraction peaks associated with a two-dimensional P6mm hexagonal symmetry (Zhao *et al.*, 1998) and, this confirm the structure obtained from the FESEM image of the SBA-15. The intense (100) peak reflects a  $d$  spacing of 92.1 (Å), which correspond to a large unit cell parameter ( $a_0$ ) of 106.35(Å) and a wall thickness of 53.35 (Å). In addition to the SBA-15, Figure 4.7a also shows the small angle XRD patterns for the synthesized Al-SBA-15. All the synthesized Al-SBA-15 shows a clear diffraction peak at  $2\theta = 0.96^\circ$  and indexed as (100). The intensity of the (100) diffraction peak of the synthesized Al-SBA-15 decreases with an increase in the incorporated  $Al^{3+}$  amount (i.e. decrease in Si/Al mole ratio). Also, the diffraction peaks indexed at (110) and (200) decrease as  $Al^{3+}$  is being incorporated into the SBA-15 matrix and becomes difficult to observe for the Al-SBA-15(50). This results reveal that the synthesized Al-SBA-15 still possess a two-dimensional p6mm hexagonal symmetry. However, the incorporation of  $Al^{3+}$  into the SBA-15 results into partial distortion of the original SBA-15 structure and, this also confirm the FESEM images obtained for the synthesized Al-SBA-15. These results are consistent with those

previously reported for SBA-15 and Al-SBA-15 prepared from same materials and using the same method (Ochoa-Hernández *et al.*, 2013). All the synthesized Al-SBA-15 have a large unit cell parameter (110.59 – 111.67 Å) and wall thickness ranging from 69.76 – 72.67 Å. The unit cell parameter and wall thickness decreases with an increase in Al<sup>3+</sup> incorporated into the SBA-15 matrix and Table 4.2 presents a summary of this results.

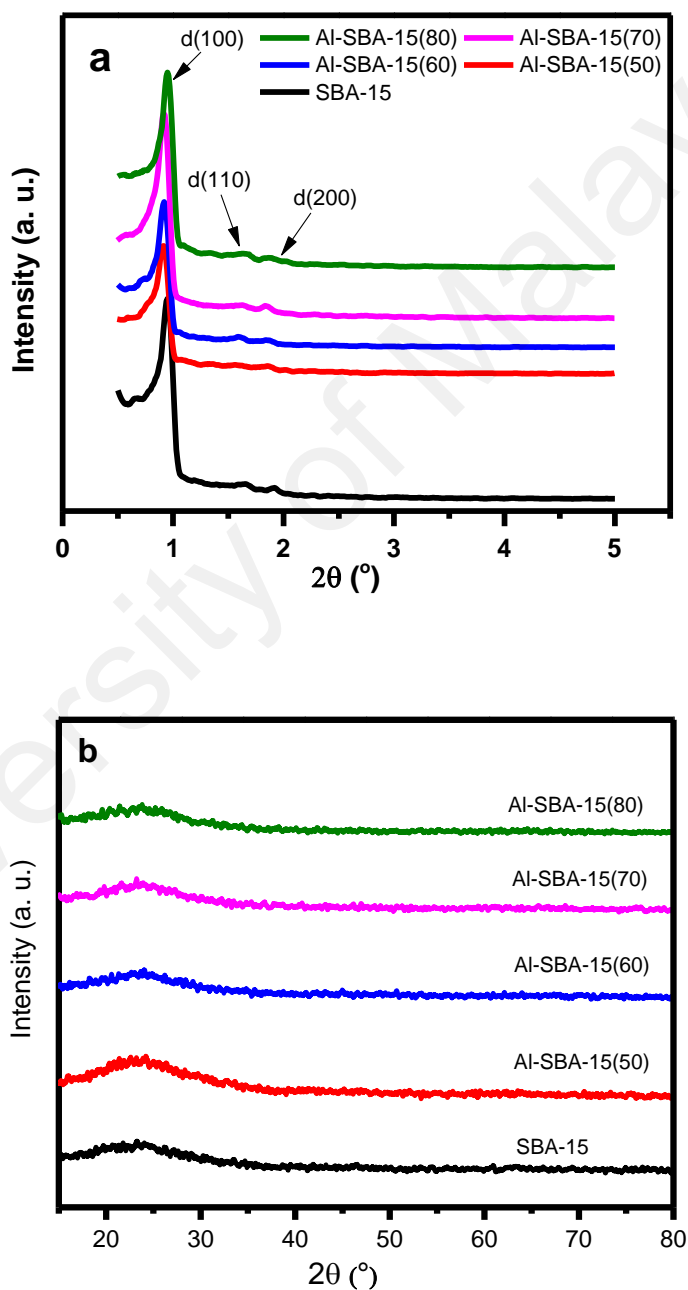


**Figure 4.7:** (a) Small angle and (b) wide angle XRD analysis of the synthesized supports

Figure 4.7(b) shows the wide-angle XRD patterns for all the synthesized supports (SBA-15 and Al-SBA-15). A broad peak is observable for all the supports with  $2\theta$  ranging from  $20^\circ$  to  $23^\circ$ . These broad peaks are characteristics features attributable to the presence of amorphous mesostructured silica. Comparing the XRD pattern of the SBA-15 with that of the Al-SBA-15, there was no formation of new peak. The absence of extra peaks formation for the Al-SBA-15 supports is not an indication that there was no structural change, as this is already confirmed from both the BET of FESEM results. However, the absence of extra peaks for the Al-SBA-15 is an indication that the quantity of  $\text{Al}^{3+}$  incorporated into the SBA-15 is below the XRD analyzer detection limit.

**Table 4.2: Summary of extract from small angle XRD analysis**

| Sample           | $d_{100}$ (Å) | Intensity (counts) | $a_0$ (Å) | Wall thickness (Å) |
|------------------|---------------|--------------------|-----------|--------------------|
| SBA-15           | 92.10         | 998                | 106.35    | 53.35              |
| Ni/SBA-15        | 91.84         | 854                | 106.05    | 54.05              |
| Al-SBA-15(50)    | 95.77         | 625                | 110.59    | 70.59              |
| Ni/Al-SBA-15(50) | 95.11         | 210                | 109.82    | 70.82              |
| Al-SBA-15(60)    | 95.92         | 702                | 110.76    | 69.76              |
| Ni/Al-SBA-15(60) | 95.39         | 303                | 110.15    | 69.15              |
| Al-SBA-15(70)    | 96.11         | 905                | 110.98    | 70.98              |
| Ni/Al-SBA-15(70) | 96.67         | 400                | 110.47    | 71.47              |
| Al-SBA-15(80)    | 96.71         | 970                | 111.67    | 72.67              |
| Ni/Al-SBA-15(80) | 95.98         | 615                | 110.83    | 72.83              |

Figure 4.8a presents the small angle XRD patterns of the synthesized catalysts. The pattern for Ni/SBA-15 reveals the presence of three peaks that are indexed as (100), (110) and (200) diffraction peaks associated with a two-dimensional P6mm hexagonal symmetry (Zhao *et al.*, 1998). The pattern reveals that the original shape of the synthesized SBA-15 is conserved even after the impregnation of nickel and this is in agreement with the hysteresis loop obtained from the BET analysis of SBA-15 and Ni/SBA-15. Though the impregnation of nickel into the SBA-15 did not denatured its original shape, however, there was a decrease in the intensity of the (100) diffraction peak. In addition, the  $d$  spacing and unit cell parameter equally decreased, but there was an increase in the wall thickness after impregnating nickel. The decrease in the peak intensity and unit cell parameter, and increase in the wall thickness are due to partial coverage caused by nickel impregnation. Table 4.2 presents summary of extracts from the small angle XRD analysis. Figure 4.8a also presents the small angle XRD patterns for the Ni/Al-SBA-15 catalysts. Noticeably, after the impregnation of nickel into the Al-SBA-15 to form Ni/Al-SBA-15 there was a decrease in the intensity (counts) of peak (100) for all the Ni/Al-SBA-15 catalysts. Imp  rator-Clerc *et al.*, (2000) observed an increase in the intensity of peak (100) when they studied the ‘existence of a microporous corona around the mesopores of silica-based SBA-15 materials templated by triblock copolymers’. They attributed the increase in the intensity to increase in pore diameter when the SBA-15 was hydrothermally treated and similar result was reported by Bhangre *et al.*, (2011). However, in the present study, as evident from the BET analysis, there was a slight decrease in the pore diameter (sizes) after nickel was impregnated. This could be the reason for the decrease in intensity of the peak (100). Similarly, there was a decrease in the  $d$  spacing of the peaks indexed at (100) and the unit cell parameters of the catalysts when compared with the corresponding supports. However, for all the catalysts (Ni/SBA-15 and Ni/Al-SBA-15) there was an increase in the wall thickness and this is a desired

property, since high wall thickness will make the catalysts highly stable (thermally and hydrothermally). These observations are consistent with the work of Sankaranarayanan et al. (2015), when they deposited transition metals on SBA-15 for hydrodeoxygenation of anisole in a batch reactor.

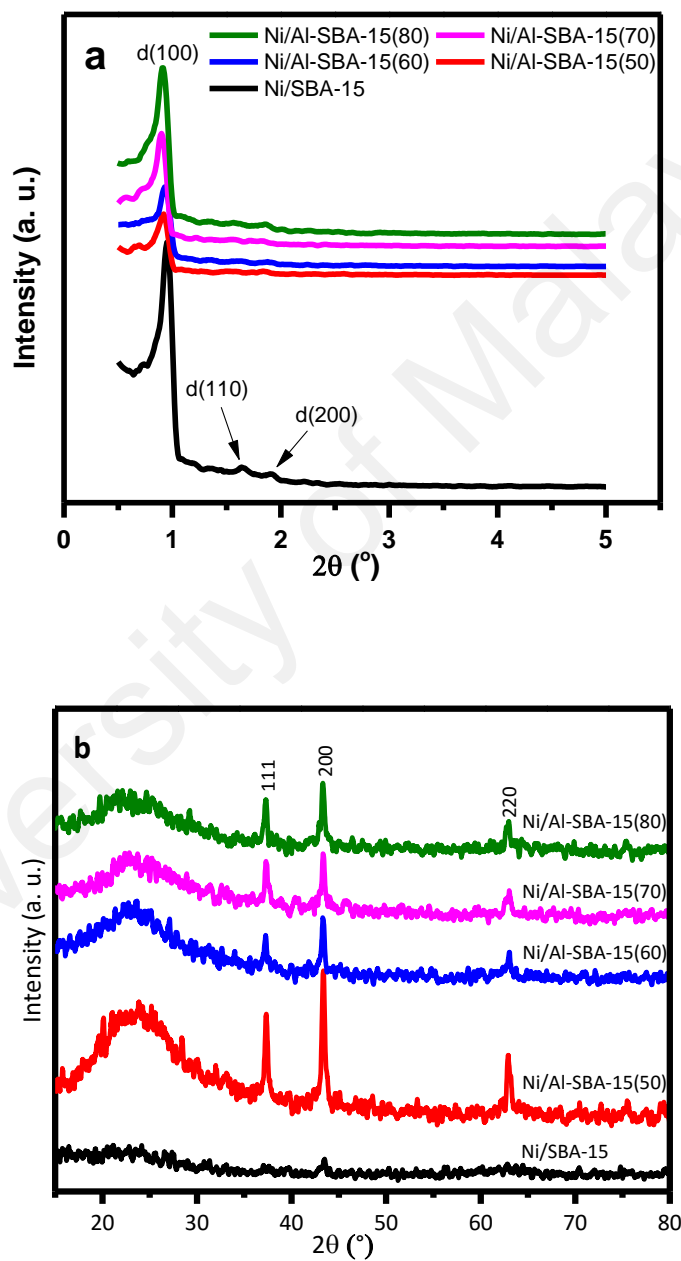


**Figure 4.8:** (a) Small angle and (b) wide angle XRD analysis of the synthesized catalysts

**Table 4.3: Summary of extract from wide-angle XRD analysis**

| Catalyst         | Main peaks, $2\theta$ ( $^{\circ}$ ) | Phases | NiO crystallite size (nm) |
|------------------|--------------------------------------|--------|---------------------------|
| Ni/SBA-15        | 43.37                                | 200    | 9.5                       |
| Ni/Al-SBA-15(50) | 37.32                                | 111    | 21.3                      |
|                  | 43.37                                | 200    |                           |
|                  | 63.00                                | 220    |                           |
| Ni/Al-SBA-15(60) | 37.32                                | 111    | 16.0                      |
|                  | 43.37                                | 200    |                           |
|                  | 63.00                                | 220    |                           |
| Ni/Al-SBA-15(70) | 37.32                                | 111    | 19.8                      |
|                  | 43.37                                | 200    |                           |
|                  | 63.00                                | 220    |                           |
| Ni/Al-SBA-15(80) | 37.32                                | 111    | 20.2                      |
|                  | 43.37                                | 200    |                           |
|                  | 63.00                                | 220    |                           |

Figure 4.8(b) present the wide angle XRD patterns for Ni/SBA-15 and Ni/Al-SBA-15 catalysts. Prominent peaks were observable at  $2\theta$  values of  $\sim 37.32$ ,  $43.37$  and  $63^{\circ}$  for all the Ni/Al-SBA-15 catalysts. These peaks correspond to the (111), (200) and (220) crystallographic planes of face-centered cubic structured NiO, respectively (JCPDS 01-

075-0197). The results are clear indication that the NiO present in the Ni/Al-SBA-15 catalysts are crystalline. This is a desired property, as it shows that the synthesized catalysts will be stable during the course of the HDO reactions. On the other hand, the Ni/SBA-15 catalyst shows only one small peak at  $2\theta = 43.37^\circ$ , which correspond to the (200) reflection of NiO (JCPDS 01-075-0197). This observation indicates that abundant NiO are present inside the pores of SBA-15 owing to its larger average pore size than the Al-SBA-15, thus absence of remaining XRD peaks as found in the Ni/Al-SBA-15 catalysts. The H<sub>2</sub>-TPR analysis will further substantiate this claim. In addition, the average NiO crystallite sizes of the catalysts were calculated using the Scherrer equation and results are shown in Table 4.3 (column 4).

#### 4.1.4 Elemental composition determination

The measurement of Ni amount present in each of the catalyst was determined using the XRF analysis. This is an important analysis, as it reveals the actual amount of Ni present in the catalyst. Theoretically, the Ni amount loaded into each catalyst was 5 wt.% of the catalyst. The use of high metal loading is likely to lead to agglomeration and less dispersion (Ma'amor, 2005), therefore the choice of 5 wt.% Ni for this studies.

Table 4.4 presents the theoretical and experimental Ni composition of each catalyst as determined by XRF. The results showed there was variation in the experimental and theoretical amount of Ni. The analysis shows that all the catalysts contains higher nickel amount than the theoretical amount, and this can be attributed to possible losses of supports during synthesis or instrument sensitivity. Ni/Al-SBA-15(50) has the least Ni loading of 5.28 wt.% while Ni/Al-SBA-15(80) has the highest loading of 6.60 wt.%. Since all the supports are mesoporous and have high surface area, it is expected with this result, Ni/Al-SBA-15(50) will have the highest Ni dispersion.

**Table 4.4: Amount of Ni metal present in the catalysts**

| Catalyst         | Weight of Ni metal (wt.%) |              |
|------------------|---------------------------|--------------|
|                  | Theoretical               | Experimental |
| Ni/SBA-15        | 5.00                      | 5.64         |
| Ni/Al-SBA-15(50) | 5.00                      | 5.28         |
| Ni/Al-SBA-15(60) | 5.00                      | 6.04         |
| Ni/Al-SBA-15(70) | 5.00                      | 6.09         |
| Ni/Al-SBA-15(80) | 5.00                      | 6.60         |

#### 4.1.5 Raman spectroscopy analysis

The vibrational mode of the synthesized supports and the corresponding catalysts were studied using the Raman spectroscopy method. Unlike BET and BJH, FESEM and XRD analysis, the Raman spectroscopy reveals information on the intrinsic properties of the materials. This analysis reveals the internal structural modification to the SBA-15 due to the incorporation of Al<sup>3+</sup> and impregnation of Ni.

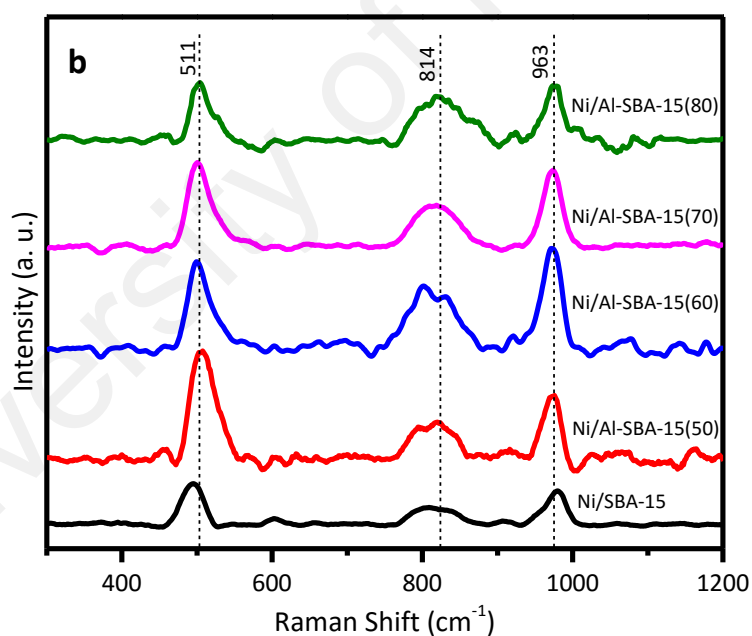
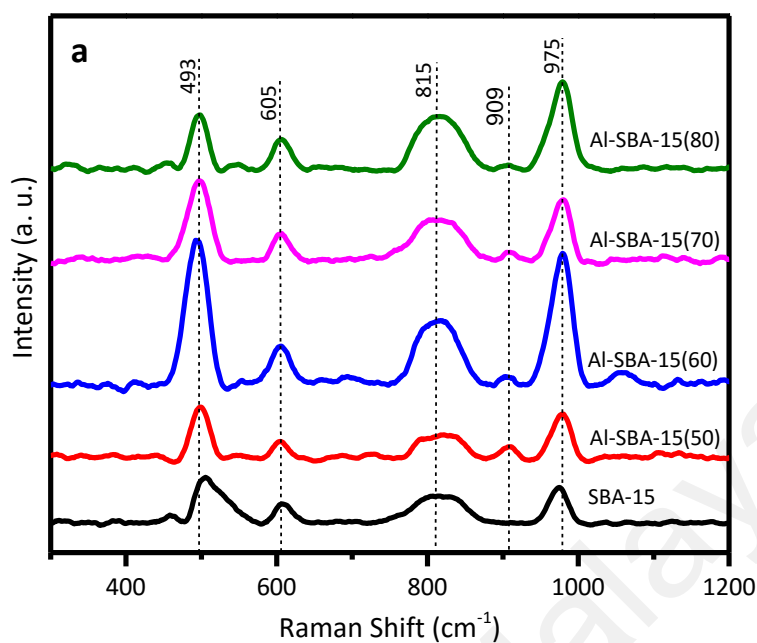


**Figure 4.9: Raman spectra of the synthesized (a) SBA-15 and Al-SBA-15 supports, and (b) Ni/SBA-15 and Ni/Al-SBA-15(n) catalysts**

Figure 4.9 shows Raman spectra of the supports and the corresponding supported Ni catalysts in the range of 300-1200  $\text{cm}^{-1}$ . The SBA-15 and Al-SBA-15 supports exhibit Raman features at 493, 605, 815 and 975  $\text{cm}^{-1}$  (Figure 4.9(a)). The band at 975  $\text{cm}^{-1}$  indicates Si-OH stretching of the surface silanols group, while the broadband at 815  $\text{cm}^{-1}$

is due to symmetric stretching mode of the siloxane linkages (Gao *et al.*, 1998b). The bands at 493 and 605  $\text{cm}^{-1}$  are assigned to D1 and D2 defect modes, which are attributed to four-membered and three-membered siloxane rings produced by the condensation of surface hydroxyls, respectively (Gao *et al.*, 1998b). An extra Raman band at  $\sim 909 \text{ cm}^{-1}$  was observed for all the Al-SBA-15 and the intensity increases gradually with increase in  $\text{Al}^{3+}$  loading (i.e. decrease in Si/Al mole ratio). This band, which was also observed in the Raman of  $\text{TiO}_2/\text{SiO}_2$  and  $\text{V}_2\text{O}_5/\text{SiO}_2$ , is a characteristic of  $\text{Si}(\text{O}^-)_2$  functionality (Gao *et al.*, 1998a; Gao *et al.*, 1998b). This Raman shift ( $909 \text{ cm}^{-1}$ ) can be assigned to perturbed silica vibration, which is an indication of the formation of Al–O–Si bonds (Gao *et al.*, 1998a; Gao *et al.*, 1998b). These results reveals that the incorporation of  $\text{Al}^{3+}$  into the SBA-15 matrix breaks some the Si–O–Si siloxane bridges for the formation of Al–O–Si bridging bonds. However, XRD experiments cannot detect the presence of the Al–O–Si (even at Si/Al mole ratio = 50), suggesting that the Al–O–Si bridges are below the detection sensitivity of the XRD analyzer. This observation demonstrates that Raman spectroscopy is extremely sensitive to the formation of Al–O–Si bridges.

**Table 4.5: Raman band assignment for the synthesized supports and catalysts**

| Raman band position ( $\text{cm}^{-1}$ ) |             | Assignment  |
|--|-------------|---|
| Literature                               | Obtained    |   |
| (485 – 510) <sup>a, b</sup>              | 493 and 511 | D1, four membered siloxane rings  |
| (600 – 610) <sup>a, b</sup>              | 605         | D2, three membered siloxane rings   |
| (800 – 815) <sup>a, b, c</sup>           | 814 and 815 | Symmetric siloxane stretching mode  |
| (900 – 915) <sup>a</sup>                 | 909         | $\text{Si}(\text{O}^-)_2$ functionality that result into formation of Al–O–Si bonds |
| (960 – 976) <sup>a, b, c</sup>           | 963 and 975 | Stretching of surface Si–OH groups  |

<sup>a</sup> (Gao *et al.*, 1998a; Gao *et al.*, 1998b)

<sup>b</sup> (Borodko *et al.*, 2005)

<sup>c</sup> (Scarano *et al.*, 1993)

The impregnation of nickel onto the supports, as shown in Figure 4.9(b), led to the collapse of the D2 band. The collapse of the D2 band at  $605\text{ cm}^{-1}$  is attributed to a decrease in concentration of reactive Si-O at the surface caused by nickel incorporation (Borodko *et al.*, 2005). In addition, the D1 band blue shift from  $493$  to  $511\text{ cm}^{-1}$  when compared with the supports. This blue shift may be due to shortening of some Si-O bond lengths caused by possible acidity generated by impregnating Ni species (Fang *et al.*, 2005) and since bond length is inversely related to Raman vibration frequency (Hardcastle & Wachs, 1991). In addition, comparing Figure 4.9(a) and Figure 4.9(b), it is evident that the intensity of the surface silanols (Si-OH) group also decreases with the impregnation of Ni specie. Table 4.5 present a summary of all the observable Raman bands and their corresponding assignments.

#### 4.1.6 H<sub>2</sub>-TPR analysis

All the Ni supported catalysts in this study were synthesized with the sole aim of investigating their performance in HDO reaction. As mentioned in Section 2.2.2, one of the key reactions that take place during HDO is hydrogenation reaction catalyzed by transition metals. It is a general rule of thumb that transition metals catalysts are only active at zero oxidation state for hydrogenation reaction. Consequently, the reducibility of NiO to Ni metal (i.e. Ni<sup>2+</sup> to Ni<sup>0</sup>) is paramount. H<sub>2</sub>-TPR analysis reveals information on the reducibility of the synthesized catalysts and the minimum temperature for catalysts activation (reduction). In addition, information on the strength of interaction between the Ni metal and the corresponding support (SBA-15 or Al-SBA-15), as well as possible dispersion are revealed.

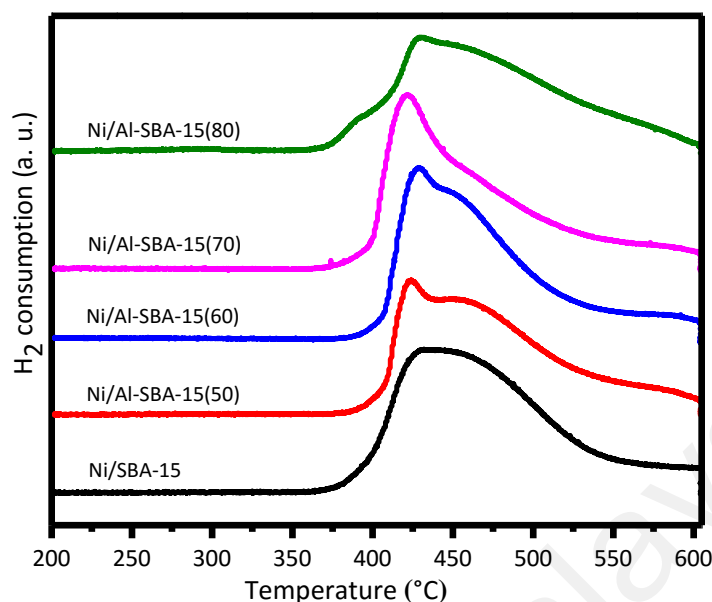


**Figure 4.10: TPR profiles of all the synthesized catalysts**

Figure 4.10 presents the H<sub>2</sub>-TPR profiles of the supported Ni catalysts. The Ni/SBA-15 catalyst shows a broad peak in the range of 375 – 525 °C and a centroid at 433 °C. This broad peak correspond to the reduction of Ni<sup>2+</sup> (NiO) impregnated into the SBA-15 to Ni<sup>0</sup> in the presence of hydrogen gas. The presence of this broad high temperature reduction peak in the TPR profile of Ni/SBA-15 is attributed to highly dispersed NiO particles present inside the pores of the SBA-15 and possible strong metal-support interaction as well (Li & Chen, 1995; Liu *et al.*, 2008; Takahashi *et al.*, 2001). The presence of NiO nanoparticles inside the pores of the SBA-15 makes it difficult for reduction at lower temperature. This result justifies why there was absence of prominent NiO peaks in the wide-angle XRD profile of Ni/SBA-15 (Figure 4.8(b)).

In the case of the Ni/Al-SBA-15 catalysts, two broad peaks in the range of 422–430 and 465–475 °C were observed for the reduction of nickel from Ni<sup>2+</sup> to Ni<sup>0</sup>. In addition to these two peaks, the Ni/Al-SBA-15(80) catalyst has an extra shoulder peak at 391 °C. As reported by Chary *et al.* (2006), this shoulder peak at 391 °C is attributed to the

reduction of free NiO species deposited mainly on the Al-SBA-15 surface without any form of interaction and it is easy to reduce. The observed sharp peaks in the region of 422–430 °C for all the Ni/Al-SBA-15 catalysts can be assigned to the reduction of homogeneous smaller particles of NiO within the pores of the Al-SBA-15. This is possible because the supports (i.e. Al-SBA-15) are mesopores as evident from the BET and BJH analysis. The presence of extra peaks at higher temperatures (465–475 °C) for all the Ni/Al-SBA-15 catalysts indicates the existence of strong metal-support interactions and, consequently difficulty in reduction. The incorporation of Al<sup>3+</sup> into the SBA-15 matrix enhances the interaction between nickel and the support, in line with the literature reports (Klimova *et al.*, 2003; Lindo *et al.*, 2010; Ochoa-Hernández *et al.*, 2013).

Based on the TPR data, 500 °C was chosen for the activation of the catalysts used in the HDO of dibenzofuran and guaiacol.

#### 4.1.7 NH<sub>3</sub>-TPD analysis

Acidic property is a key property desired for any HDO catalysts, since the reaction is catalyzed by both metallic and acidic sites. It is desirable to have a catalyst(s) with weak acidity (strong acidity leads to formation of light HC via cracking) and sufficient acid sites. NH<sub>3</sub>-TPD is an analytical technique that reveals information on the catalysts acidic strength (weak, medium or strong) and the number of acidic sites. Ammonia is a suitable probe molecule for this technique because of its small size and high basicity, which allows it to interact with most of the acidic sites. Thus, the total amount of ammonia desorbed at particular temperature corresponds to the number of acidic sites, while the temperature range in which the ammonia is desorbed is an indicator of the strength of the acidic sites. Figure 4.11 presents the NH<sub>3</sub>-TPD profiles and Table 4.6 presents a summary of the total acidity of all the synthesized catalysts.

As shown in Figure 4.11, a sharp peak was obtained at ~121 °C for Ni/SBA-15 and Ni/Al-SBA-15(80), and 126 °C for Ni/Al-SBA-15(50), Ni/Al-SBA-15(60), and Ni/Al-SBA-15(70). These results indicate that all the synthesized catalysts exhibit abundance weak acidic sites (Wang *et al.*, 2015; Yang *et al.*, 2014). Considering the fact that SBA-15 is almost inert, the peak obtained for Ni/SBA-15 could be associated with acidic sites created by the incorporation of Ni metal into the silica matrix (Fang *et al.*, 2005). This partly explains the high temperature reduction profile obtained during the H<sub>2</sub>-TPR analysis of Ni/SBA-15.

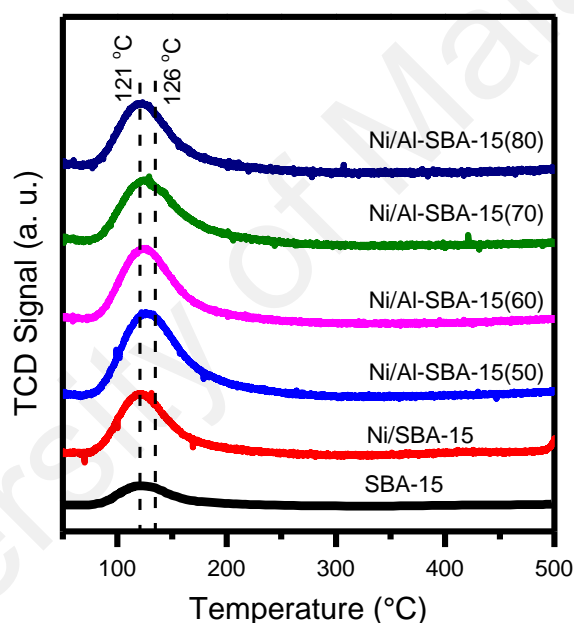


**Figure 4.11: NH<sub>3</sub>-TPD profiles of the synthesized catalysts**

As evident from Table 4.6, the acidity of the catalysts increases with the decrease of Si/Al mole ratio. This observation indicates that the amount of incorporated Al<sup>3+</sup> species into the SBA-15 matrix and subsequent interactions between Ni and Al-SBA-15 influences the acidity of the catalyst. Among the synthesized catalysts, the Ni/Al-SBA-15(50) catalyst has highest amount of acidic sites, and expected to influence its performance in HDO reaction of DBF and guaiacol.

**Table 4.6: Summary of total acidity**

| Catalyst         | Total acidity (mmol/g) |
|------------------|------------------------|
| SBA-15           | 0.371                  |
| Ni/SBA-15        | 0.803                  |
| Ni/Al-SBA-15(50) | 1.351                  |
| Ni/Al-SBA-15(60) | 1.056                  |
| Ni/Al-SBA-15(70) | 0.922                  |
| Ni/Al-SBA-15(80) | 0.919                  |

## 4.2 Catalytic activity results

### 4.2.1 HDO of DBF

**Table 4.7: Conversion of DBF over the synthesized catalysts at 250 °C and 2 h**

| s/n | Catalysts        | Conversion (%) |
|-----|------------------|----------------|
| 1   | Ni/SBA-15        | 97.97 ± 0.96   |
| 2   | Ni/Al-SBA-15(50) | 100.00         |
| 3   | Ni/Al-SBA-15(60) | 100.00         |
| 4   | Ni/Al-SBA-15(70) | 100.00         |
| 5   | Ni/Al-SBA-15(80) | 99.31 ± 0.52   |

The HDO of DBF was performed using supported Ni catalysts at 250 °C and 10 MPa of pure H<sub>2</sub> for 2 h. The main products in HDO of DBF reaction over the Ni catalysts are bicyclohexyl (BCH), cyclohexyl-cyclohexene (CHCHE) and cyclohexyl-benzene (CHB). In addition, various oxygenated products are possible in this reaction, which include tetrahydro-dibenzofuran (THDBF), hexahydro-dibenzofuran (HHDBF),

dodecahydro-dibenzofuran (DHDBF), cyclohexyl-phenol (CHPOH), phenyl-cyclohexanol (PCHOH), cyclohexyl cyclohexanone (CHCHO) and cyclohexyl-cyclohexanol (CHCHOH). Also, there is a possibility for the formation of cyclopentylmethyl-cyclohexane (iso-BCH), which is an isomer of BCH. Table 4.6 presents the obtained conversion results for HDO of DBF over the Ni-based catalysts. The Ni/SBA-15 and Ni/Al-SBA-15(80) catalysts show 97.97 and 99.31% DBF conversions, respectively, while a 100% DBF conversion was found for the remaining Ni based catalysts. These high DBF conversions for all the synthesized catalysts are attributed to their high BET surface area (Table 4.1), mesoporosity (Table 4.1), good reducible nature (Figure 4.10), and presence of acidic sites (Figure 4.11 and Table 4.6). However, highest selectivity towards hydrodeoxygenated products (Figure 4.12) was found for the Ni/Al-SBA-15(50) catalysts containing lowest Si/Al mole ratio. The acidic strength of the catalysts is a key factor for the observed differences in the products selectivity. As reported by Rana *et al.* (2000), the acidity of catalyst promotes hydrogenation and cracking. Also, the presence of acid sites in a catalyst enhances dehydration and isomerization that could co-operatively function with metal catalyzed hydrogenation, and in turn promote HDO reaction (Xinghua *et al.*, 2010). The selectivity for total hydrocarbons (sum of BCH, iso-BCH, CHCHE and CHB) was found to be 73% for Ni/Al-SBA-15(50) and the selectivity of BCH, a non-aromatic product, was about 57%. These findings are of great importance in the production of biofuels because the regulations are restricting the use of aromatics in fuels.

Figure 4.12 shows products distribution in HDO of DBF obtained over supported Ni catalysts. It was found that the selectivity of HDO products (sum of BCH, iso-BCH, CHCHE and CHB) increases with the increase in the acidity of the catalysts (Figure 4.11 and Table 4.6), with BCH being the dominant product. On the other hand, the selectivity of non-HDO products (sum of CHCHO, CHCHOH, DHDBF, HHDBF PCHOH,

CHPOH, and THDBF) decreased sharply with the increase of the catalyst acidity (Table 4.6). Further, the isomerization ability of the catalysts was increased with the increase of the catalyst acidity. As shown in Figure 4.12, the formation of iso-BCH, which is a useful component of biofuel, gradually increased to 6.08% for Ni/Al-SBA-15(50) catalyst. These results show that the Ni/Al-SBA-15(50) catalyst (with lowest Si/Al mole ratio and highest acidity) proved to be the most efficient catalyst for HDO of DBF among the tested catalysts. In the case of Ni/SBA-15, the dominant products were oxygenated compounds, which accounted for 91.26% of the product distribution. Similarly, CHO (sum of CHCHO and CHCHOH) accounted for 41.67% of the products, indicating that the dehydration ability of Ni/SBA-15 is weak because of its less acidity compared to that of remaining Ni/Al-SBA-15 catalysts (Figure 4.11 and Table 4.6). These results imply that the presence of bifunctional sites (active metal species and sufficient acid sites) within the catalyst structure is of great importance for efficient HDO of DBF. Although direct comparisons with previous studies is quite difficult because of diversity in reactor type and reaction conditions used, however, the results of the present study show that Ni-based catalysts exhibited comparable performances in HDO of DBF reaction to those (e.g., Pd, Pt and Ru catalysts) reported in literature (Cecilia *et al.*, 2013; Lee *et al.*, 2015; Wang *et al.*, 2015; Wang *et al.*, 2013; Yuxin Wang *et al.*, 2011). As well, it must be noted that the price advantage of Ni over Pt, Pd, and Ru obviously highlights the significance of the present study in HDO of DBF reaction.

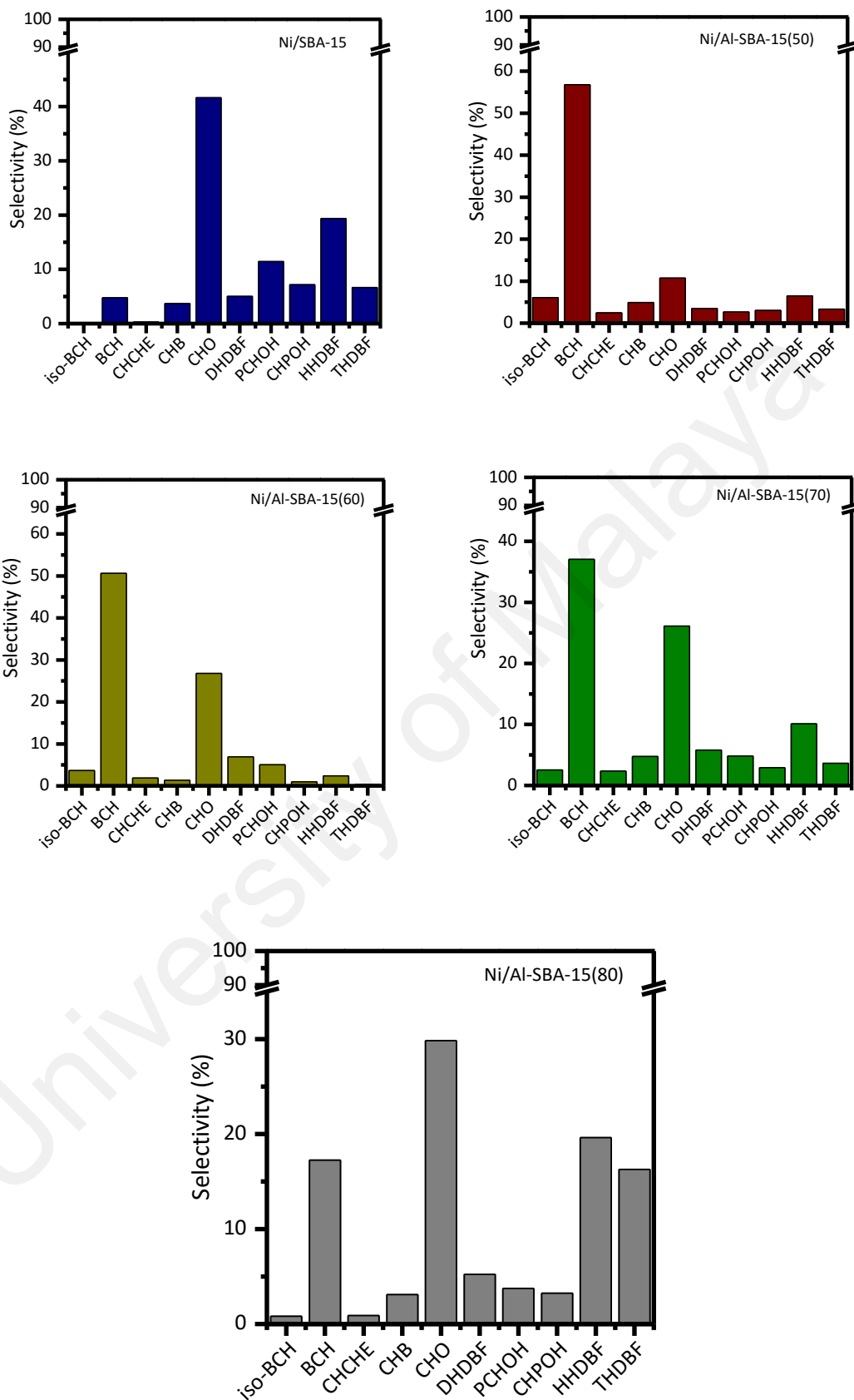


Figure 4.12: Products distribution obtained over supported Ni catalysts at 250 °C and 2 h

#### 4.2.1.1 Effect of reaction temperature on HDO of DBF

The effect of reaction temperature (240, 250 and 260 °C) on HDO of DBF and product distribution was investigated using all the Ni catalysts and the obtained results are summarized in Table 4.8. Evidently, the reaction temperature has a pronounced effect on DBF conversion and products selectivity: the conversion of DBF increases with the increase in the temperature. Remarkably, all the catalysts showed a 100% DBF conversion at 260 °C except the Ni/SBA-15 catalyst, which exhibited a 99.33% DBF conversion. In all cases, numbers of products formed remain the same except for Ni/Al-SBA-15(50) catalyst, which has zero quantity of CHB at 260 °C and Ni/SBA-15 with zero quantity of iso-BCH at 240 and 250 °C. For all the catalysts, BCH was the main product at all temperatures. Although, the selectivity of Ni/Al-SBA-15(80) and Ni/SBA-15 catalysts towards BCH was low at 240 °C, there was a remarkable increment in BCH selectivity as the temperature increases to 260 °C. This observation reveals the significance of the temperature in the HDO of DBF reaction to obtain higher selectivity of the desired products.

Figure 4.13 shows the comparison of HDO ability of the catalysts at 260 °C and 2 h. Clearly, the Ni/Al-SBA-15(50) catalyst, with a degree of HDO of 84%, is the most effective catalyst amongst all the catalysts. Since all the catalysts have the same Ni loading, the superior performance of Ni/Al-SBA-15(50) catalyst is due to its higher acid content

**Table 4.8: Products distribution in HDO of DBF at 2 h and varying temperature over the synthesized catalysts**

| Temperature | Catalysts        | X <sub>DBF</sub> | S <sub>iso-BCH</sub> | S <sub>BCH</sub> | S <sub>CHCHE</sub> | S <sub>CHB</sub> | S <sub>CHO</sub> | S <sub>DHDBF</sub> | S <sub>PCHOH</sub> | S <sub>CHPOH</sub> | S <sub>HHDBF</sub> | S <sub>THDBF</sub> | %HDO  |
|-------------|------------------|------------------|----------------------|------------------|--------------------|------------------|------------------|--------------------|--------------------|--------------------|--------------------|--------------------|-------|
| 240 °C      | Ni/SBA-15        | 97.21            | 0                    | 3.51             | 0.32               | 3.56             | 34.03            | 5.41               | 9.53               | 6.09               | 23.32              | 14.23              | 7.39  |
|             | Ni/Al-SBA-15(50) | 100.00           | 5.30                 | 51.77            | 2.86               | 1.72             | 15.70            | 4.49               | 3.26               | 4.38               | 7.02               | 3.49               | 61.66 |
|             | Ni/Al-SBA-15(60) | 100.00           | 4.82                 | 39.87            | 5.89               | 9.72             | 9.10             | 3.82               | 1.48               | 4.25               | 12.12              | 8.92               | 60.30 |
|             | Ni/Al-SBA-15(70) | 98.27            | 0.29                 | 10.31            | 1.26               | 2.44             | 30.38            | 5.27               | 5.34               | 5.72               | 22.82              | 16.18              | 14.29 |
|             | Ni/Al-SBA-15(80) | 98.16            | 0.37                 | 10.93            | 0.97               | 3.19             | 25.11            | 5.10               | 6.00               | 5.98               | 22.38              | 19.97              | 15.46 |
| 250 °C      | Ni/SBA-15        | 97.97            | 0                    | 4.77             | 0.29               | 3.69             | 41.63            | 5.01               | 11.43              | 7.17               | 19.37              | 6.66               | 8.74  |
|             | Ni/Al-SBA-15(50) | 100.00           | 6.08                 | 56.78            | 2.46               | 4.93             | 10.73            | 3.48               | 2.67               | 3.03               | 6.49               | 3.34               | 70.26 |
|             | Ni/Al-SBA-15(60) | 100.00           | 3.65                 | 50.63            | 1.88               | 1.35             | 26.78            | 6.92               | 5.04               | 0.97               | 2.39               | 0.38               | 57.52 |
|             | Ni/Al-SBA-15(70) | 100.00           | 2.54                 | 37.04            | 2.35               | 4.74             | 26.12            | 5.79               | 4.82               | 2.90               | 10.09              | 3.62               | 46.67 |
|             | Ni/Al-SBA-15(80) | 99.31            | 0.81                 | 17.26            | 0.88               | 3.10             | 29.83            | 5.24               | 3.75               | 3.25               | 19.63              | 16.27              | 22.04 |
| 260 °C      | Ni/SBA-15        | 99.33            | 0.79                 | 25.80            | 1.31               | 4.13             | 37.07            | 7.34               | 14.38              | 1.78               | 6.00               | 1.40               | 32.02 |
|             | Ni/Al-SBA-15(50) | 100.00           | 8.20                 | 74.71            | 1.52               | 0.00             | 6.13             | 1.69               | 3.67               | 0.92               | 2.26               | 0.89               | 84.43 |
|             | Ni/Al-SBA-15(60) | 100.00           | 5.47                 | 59.35            | 1.45               | 2.16             | 19.00            | 5.88               | 4.16               | 0.44               | 1.44               | 0.66               | 68.43 |
|             | Ni/Al-SBA-15(70) | 100.00           | 2.74                 | 41.88            | 1.99               | 4.42             | 23.88            | 5.09               | 3.60               | 2.30               | 9.40               | 4.70               | 51.03 |
|             | Ni/Al-SBA-15(80) | 100.00           | 2.27                 | 42.35            | 1.71               | 1.06             | 32.73            | 8.33               | 7.55               | 0.88               | 2.27               | 0.86               | 47.38 |

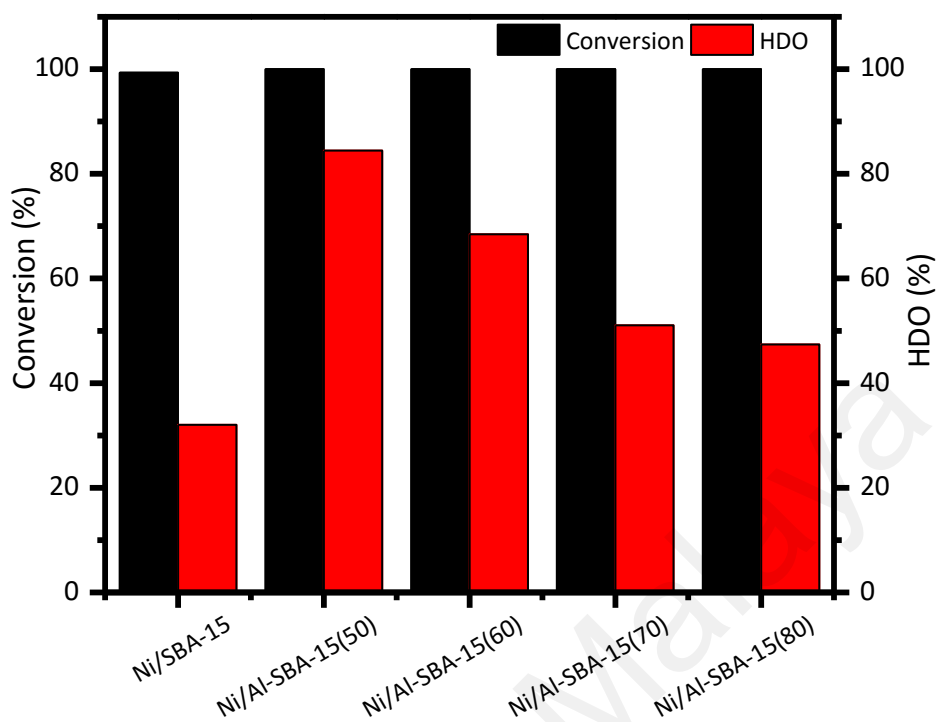


**Figure 4.13: DBF conversion and degree of deoxygenation (HDO) over synthesized catalysts at 260 °C and 2 h**

#### 4.2.1.2 Effect of reaction time on HDO of DBF

The effect of reaction time on degree of HDO and product selectivity was investigated using the Ni/Al-SBA-15(50) catalyst at 260 °C and the results are shown in Figure 4.14. Under these reaction conditions, 100% DBF conversion was obtained in all cases (Figure 4.14(a)). It was found that the selectivity of BCH increases with reaction time to an excess of 87% (Figure 4.14(b)). Similarly, the selectivity of iso-BCH increased to an excess of 9.3% after 5 h (Figure 4.14(b)). In addition, the degree of HDO increases with the increase of the reaction time and a deoxygenation degree of 96.3% was obtained at 5 h (Figure 4.14(a)). With the increase of reaction time from 3 to 5 h, the main hydrocarbons formed were BCH and iso-BCH, which indicates that total HDO was achieved as reaction time increases up to 5 h.

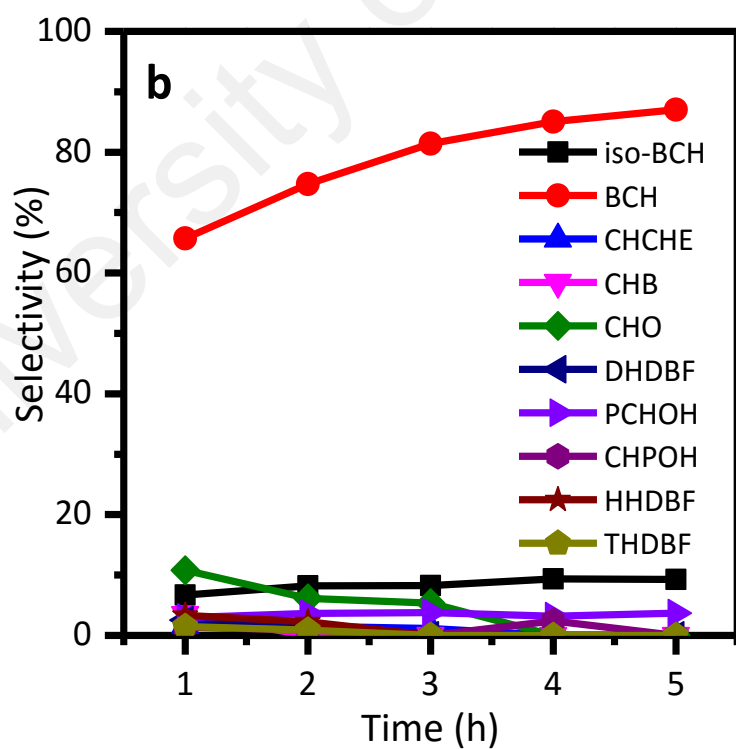
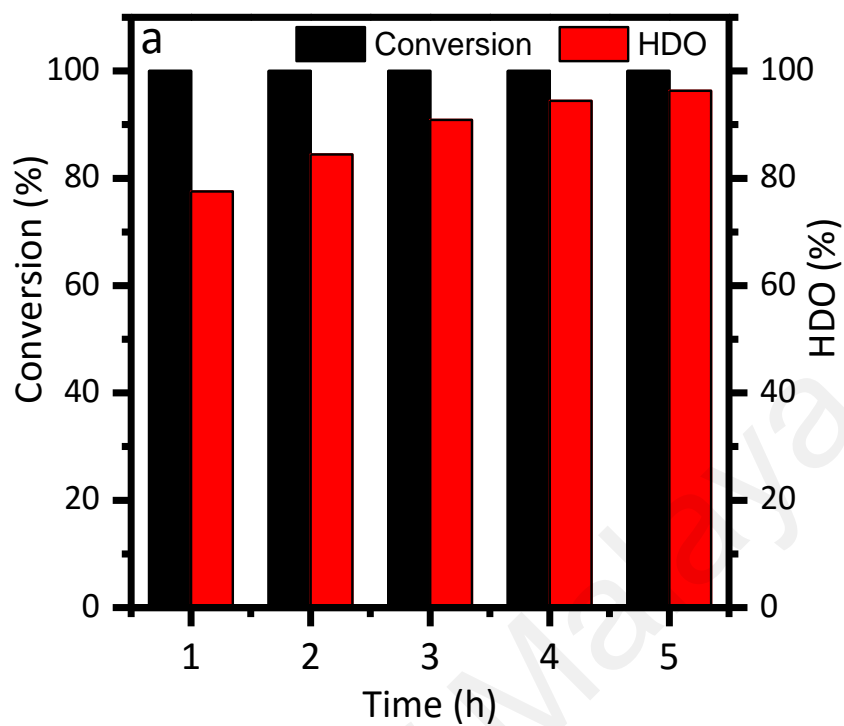
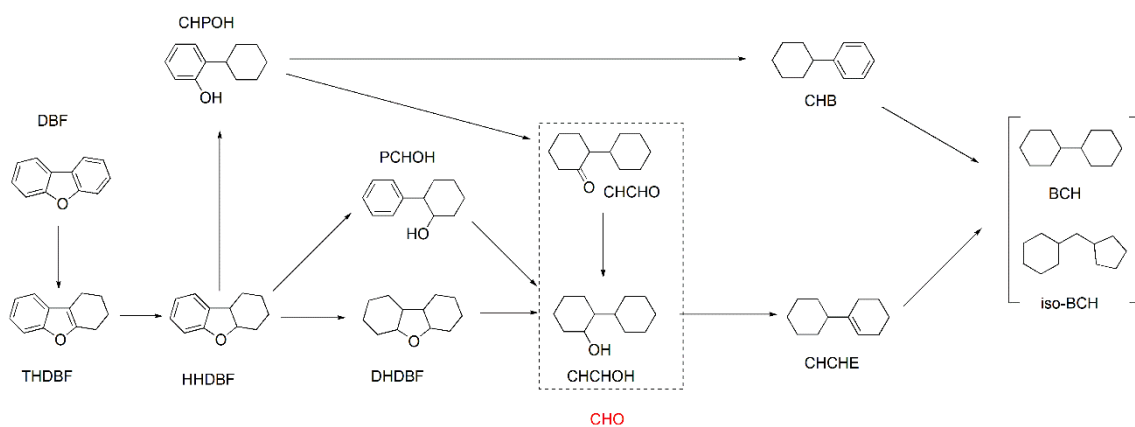


Figure 4.14: Effect of reaction time on (a) DBF conversion and selectivity, and (b) product selectivity

#### 4.2.1.3 Possible reaction pathways in HDO of DBF

Possible reaction products in the HDO of DBF over the synthesized Ni/SBA-15 and Ni/Al-SBA-15 catalysts are shown in Figure 4.15. As shown in Figure 4.15, the HDO of DBF reaction involves partial and total hydrogenation of one of the benzene rings on the nickel metal surface to form THDBF, HHDBF, and DHDBF. This assertion is consistent with the reports of Massoth *et al.* (2006) and Resasco (2011), which proposed that aromatic rings are partially or wholly hydrogenated initially to produce an intermediate that converts  $sp^2$  C-O bond to  $sp^3$  C-O bond. The later bond is easier to cleave on a metal or dehydration on acid sites. Subsequently, hydrogenolysis of the  $sp^3$  C-O bond of HHDBF and DHDBF produces CHPOH and CHCHOH, respectively. Direct hydrogenolysis of  $sp^2$  C-O bond without breaking the aromaticity is energetically unfavourable because of stability created when the out of plane O-lone pair orbital gets delocalized. However, cleavage from both  $sp^2$  C-O bond and  $sp^3$  C-O bond in HHDBF is possible because of the reaction conditions. As a result, direct hydrogenolysis of  $sp^2$  C-O bond in HHDBF produces PCHOH. Similarly, hydrogenation of CHPOH produces CHCHO, while hydrogenation of PCHOH and CHCHO results into the formation of CHCHOH. Certainly, hydrogenolysis of CHPOH gives CHB, while the dehydration of CHCHOH on the catalyst acidic sites produces CHCHE. The subsequent hydrogenation of CHB and CHCHE forms BCH and its isomer (iso-BCH).



**Figure 4.15: Proposed reaction scheme of DBF HDO over the synthesized catalysts**

#### 4.2.2 HDO of guaiacol

Guaiacol contains adjacent hydroxyl ( $-\text{OH}$ ) and methoxy ( $-\text{OCH}_3$ ) functional groups. It is a typical phenolic model compound obtained from thermal conversion of lignocellulosic biomass. Based on the results obtained for the HDO of DBF, Ni/Al-SBA-15(50) being the most effective catalysts, was chosen to study the HDO of guaiacol. For further justification, HDO of guaiacol was equally studied over Ni/SBA-15 for proper comparison. Figure 4.16 presents the conversion of guaiacol over these catalysts (Ni/SBA-15 and Ni/Al-SBA-15(50)) at 250 °C, 5 MPa and 3 h, and the corresponding degree of hydrodeoxygenation. A conversion of ~89% and ~74.97% degree of hydrodeoxygenation were obtained for the Ni/Al-SBA-15(50) catalyst. As expected, a lesser conversion (~78%) and degree of hydrodeoxygenation (~59.33%) were obtained for the Ni/SBA-15. As explained in Section 4.2.1, this high activity exhibited by the Ni/Al-SBA-15(50) is due to its higher acidity. These results further confirm the significance of presence of sufficient number of acidic sites.

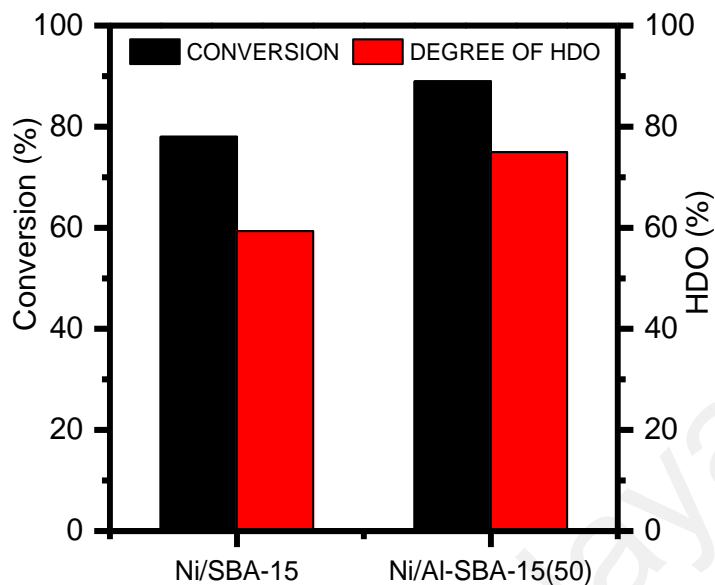


**Figure 4.16: Guaiacol and degree of HDO at 250 °C and 2 h of reaction**

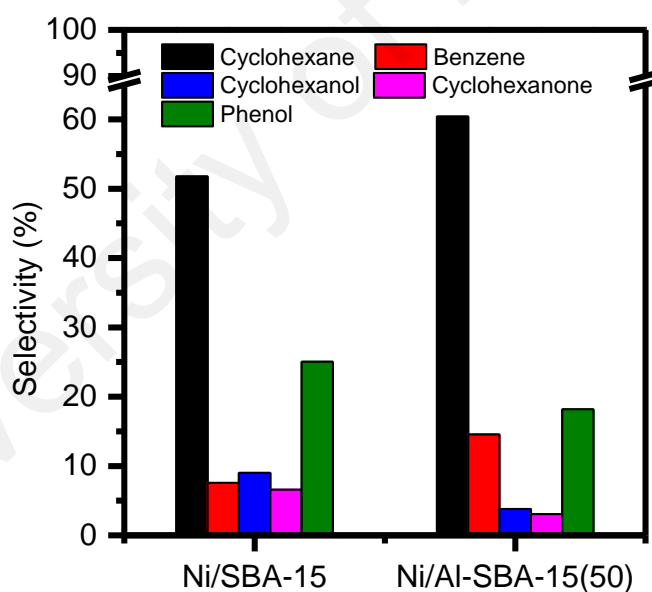


**Figure 4.17: Products distribution from HDO of guaiacol at 250 °C and 2 h of reaction**

In Section 2.3.1, a detail structural analysis of guaiacol was described in relation to the bond dissociation energies (BDE) of its C–O bonds. It would be expected that guaiacol DME to form catechol should be favoured over DMO to phenol based on the BDE. However, the products obtained in this study (Figure 4.17) suggest otherwise as there was

no catechol detection in the product analysis. The products obtained include cyclohexane, benzene, phenol, cyclohexanol and cyclohexanone. The result is a clear indication that these catalysts (Ni/SBA-15 and Ni/Al-SBA-15(50)) favour the DMO reaction route over DME. This is in agreement with the work of Bykova *et al.* (2014), and Song *et al.* (2015), and in all these reports, Ni-based catalysts were used. This preference for DMO over DME is speculated to be due to steric hindrance, i.e. the C<sub>(SP<sup>2</sup>)</sub>-OMe bond approaches the Ni surface more easily.

In open literature, there have been reports on the HDO of guaiacol over different types of catalysts in recent time. For example, Bui *et al.* (2011b) studied the HDO of guaiacol in a batch reactor at 300 °C and 4 MPa over sulfided CoMo catalysts supported on  $\gamma$ -Al<sub>2</sub>O<sub>3</sub> and ZrO<sub>2</sub>. Although 100% conversion was reported, however, the dominant products were oxygenated compounds like cresol and phenol. In addition, the selectivity for HDO products was not more than 30% and benzene was the dominant among the HDO products. However, in this present work, the selectivity for total of hydrocarbons (i.e. degree of HDO (Figure 4.16)) was the dominant products over both catalysts and is in excess of 74.97% for Ni/Al-SBA-15(50) catalyst. Among these hydrocarbons (cyclohexane and benzene), the dominant product is cyclohexane (Figure 4.17) and the selectivity was 60.4% over Ni/Al-SBA-15(50) catalyst. These results are of great important for the production of bio-fuels from biomass because current regulations are restricting aromatics content in fuel.

#### **4.2.2.1 Effect of reaction temperature on HDO of guaiacol**

The effect of reaction temperature (240, 250 and 260 °C) on HDO of guaiacol and product distribution was investigated over Ni/Al-SBA-15(50) at 5 MPa of H<sub>2</sub> pressure and 3 h of reaction. Figure 4.18 and Figure 4.19 present the obtained results. Evidently,

the reaction temperature has a pronounced effect on guaiacol conversion and products selectivity. The conversion and degree of HDO increases from ~83% and ~72% to ~98% and 89% as the temperature increases from 240 to 260 °C respectively (Figure 4.18). In all cases, the dominant product was cyclohexane and it attained a selectivity of ~73% at 260 °C. At 260 °C, there was absence of phenol, and this indicates that the phenol has either undergone direct hydrogenolysis to benzene or hydrogenation of its benzene ring to form cyclohexanol or cyclohexanone. Both direct hydrogenolysis and hydrogenation are reactions that are highly favoured in the presence of high temperature (Hong *et al.*, 2014a). This observation reveals the significance of temperature in guaiacol HDO reaction to obtain higher selectivity of the desired products.

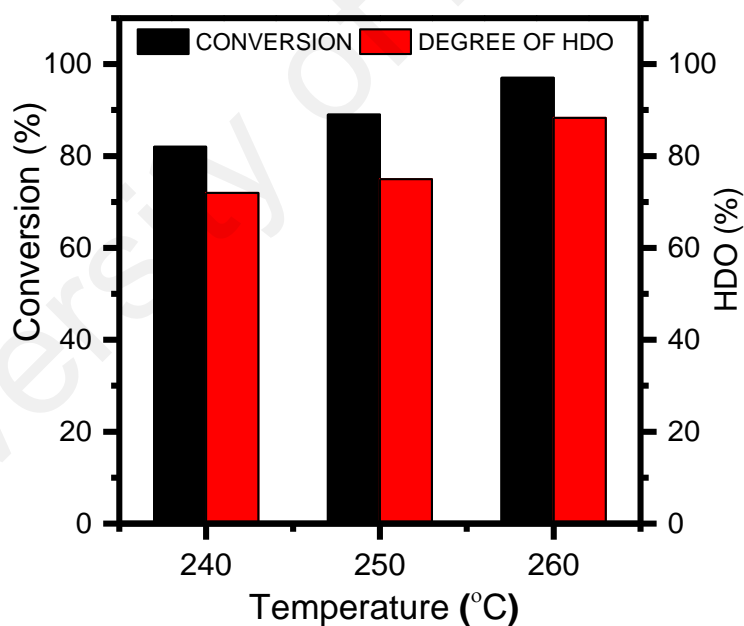


**Figure 4.18: Guaiacol conversion and degree of HDO as a function of temperature at 5 MPa and 3 h of reaction**

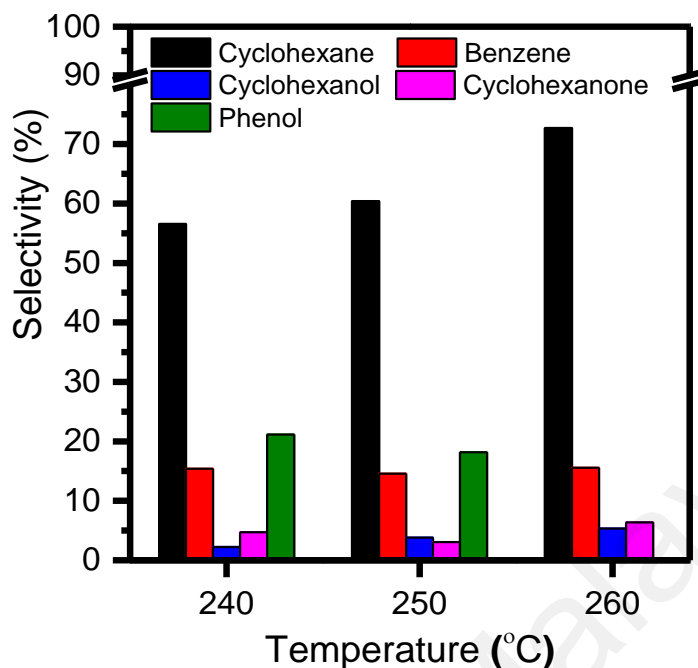
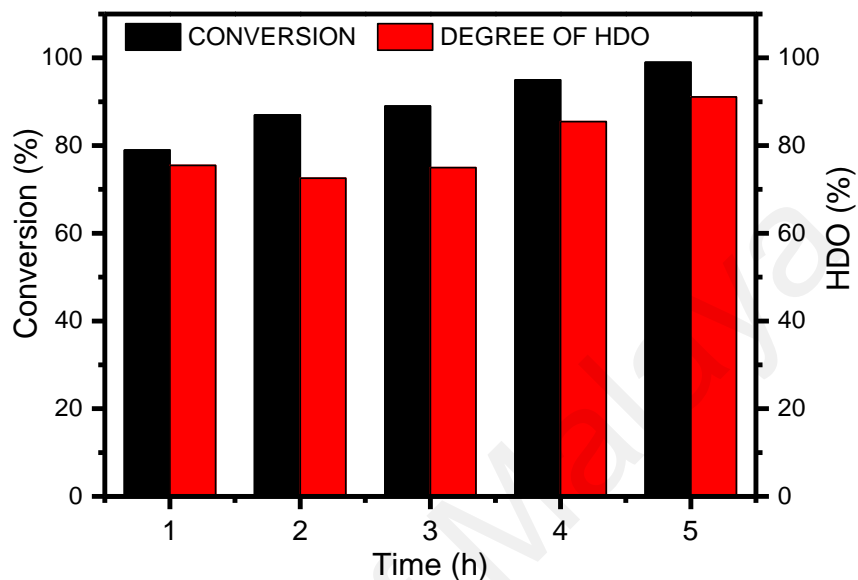


**Figure 4.19: product selectivity obtained over Ni/Al-SBA-15(50) as a function of temperature at 5MPa and 3 h of reaction**

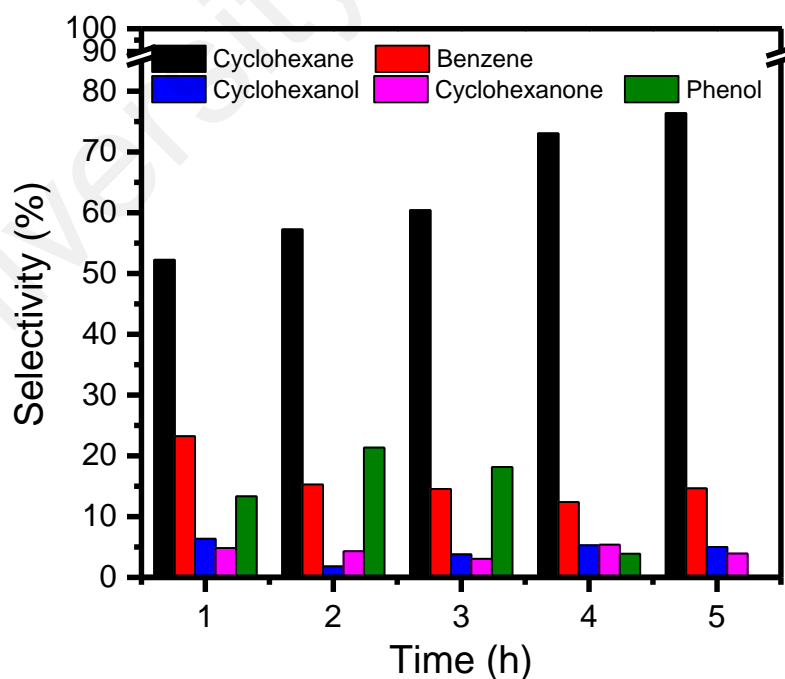
#### 4.2.2.2 Reaction pathways and effect of reaction time on HDO of guaiacol

Figure 4.19 and 4.20 presents the variation of conversion, degree of HDO and products selectivity as a function of time over Ni/Al-SBA-15(50) catalyst at 5 MPa and 250 °C. The conversion, degree of HDO and products selectivity as a function of time reported in this section are analysis of separate batch reaction since *in situ* sampling was not possible. Guaiacol conversion increases from ~79% to ~99% in the range of 1–5 h, similarly, the degree of HDO also increase from ~75% to ~92% within the same range (Figure 4.20). At the beginning of the reaction, the selectivity of cyclohexane was ~52% and benzene was ~24%. However, as the reaction proceeds from 1–5 h, the selectivity of cyclohexane gradually increased and attained a value of ~76%. Comparing Figure 4.20 and Figure 4.21, it is evident that conversion and cyclohexane selectivity are linearly related, while

phenol on the other hand is inversely related as it diminishes with time. The continuous increase in the catalyst performance with time is a clear indication of the catalyst stability.



**Figure 4.20: Guaiacol conversion and degree of HDO as a function of reaction time at 5 MPa and 250 °C**



**Figure 4.21: Product selectivity obtained over Ni/Al-SBA-15(50) as a function of reaction time at 5 MPa and 250 °C**

The HDO of guaiacol over the synthesized Ni/SBA-15 and Ni/Al-SBA-15 (50) catalysts goes through DMO reaction route as shown in the proposed reaction pathway (Figure 4.22). Briefly, DMO of the methoxy ( $-\text{OCH}_3$ ) group of guaiacol takes place first to produce phenol. The produced phenol subsequently undergoes both direct hydrogenolysis and hydrogenation competitively to produce benzene and cyclohexanone respectively. This assertion is consistent with the report of Echeandia et al. (2014), which proposed competitive hydrogenation and hydrogenolysis of phenol over Pd/HY and sulfided NiMo/Al<sub>2</sub>O<sub>3</sub> catalysts. Further hydrogenation of the produced benzene ring forms cyclohexane. Similarly, further hydrogenation of cyclohexanone produces cyclohexanol, and subsequently undergoes dehydration to produce cyclohexane.

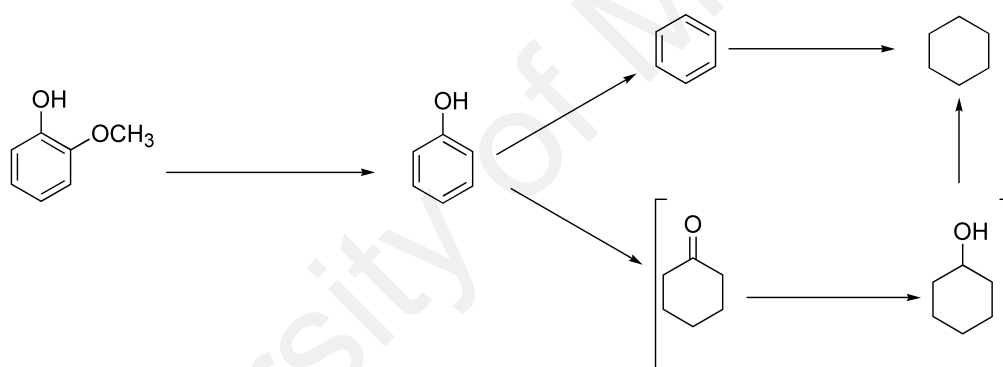


**Figure 4.22: Proposed reaction scheme of guaiacol HDO over Ni/SBA-15 and Ni/Al-SBA-15(50)**

## CHAPTER 5: CONCLUSION AND RECOMMENDATIONS

### 5.1 Conclusion

Bio-oil obtained from biomass is considered a suitable candidate that possesses the potential of mitigating petro-fuel because it is renewable and sustainable. This looks more interesting because in addition, it is eco-friendly, as it does not release any greenhouse gas to the environment. However, the cost of its post-production upgrading has not been friendly, as the upgrading technique requires high hydrogen pressure and high temperature. In addition, most catalysts that have been investigated in recent time have been the noble metal-based catalyst and consequently increase the production cost. Accordingly, proper understanding of the reaction chemistry that takes place during the upgrading procedure will definitely lead to the development of cost effective catalysts. As a result, mesoporous solid acid catalyst(s) that consists of non-noble transition metal was developed and synthesized. In addition, the applicability of the synthesized catalyst(s) was investigated for the HDO of DBF and guaiacol as bio-oil model compounds to fuel grade hydrocarbons in a batch reactor.

In synthesizing the mesoporous catalyst(s) (Ni/Al-SBA-15), firstly Al-SBA-15 (with different Si/Al mole ratio) and SBA-15 was synthesized via a one-pot synthesis method. Subsequently, Ni (5 wt.%) was impregnated into the SBA-15 and Al-SBA-15 to obtain the Ni/SBA-15 and Ni/Al-SBA-15 catalysts. These catalysts were systematically characterized using N<sub>2</sub>-sorption method, XRD, XRF, RAMAN, FESEM, H<sub>2</sub>-TPR and NH<sub>3</sub>-TPD techniques.

The characterization results revealed that the synthesized catalysts possess high surface areas, mesoporous and crystalline structures, and varying acidity properties. For example, Ni/SBA-15 has a surface area of 711 m<sup>2</sup>/g while the Ni/Al-SBA-15 catalysts have a surface area ranging from 665 – 740 m<sup>2</sup>/g. In addition, all the catalysts have

average pore sizes in the range 38 – 52 Å. Although the incorporation of Al<sup>3+</sup> into the SBA-15 matrix altered the morphology as revealed by the BET hysteresis loops and the FESEM images, however, the desired properties were the high surface areas and mesoporous structures. The XRD patterns reveal that the synthesized catalysts are crystalline, which is desired property as it gives the catalysts stability. In addition, the XRF analyses confirm the successful impregnation of Ni (though more than the calculated amount) into the supports to form the catalysts. The NH<sub>3</sub>-TPD analyses confirm the acidity properties of the catalysts and that all the catalysts contain weak acids sites. It reveals that the catalysts acidity is inversely related to the Si/Al mole ratio (i.e. acidity increases with a decrease in the Si/Al mole ratio).

Investigation of the catalysts performance tests in HDO of DBF and guaiacol confirmed that bifunctional catalysts (containing both hydrogenation and acidic sites) are required for HDO reactions. The HDO of DBF reveals that Ni/Al-SBA-15(50) is the best performing catalyst among the synthesized catalysts, and this is due to its superior acidity. DBF conversion at all time over Ni/Al-SBA-15(50) was 100% and the major product was bicyclohexyl. The highest bicyclohexyl selectivity was ~87% and ~96% degree of total hydrodeoxygenation. These were achieved at a reaction condition of 5h, 260 °C and 10 MPa H<sub>2</sub> pressure and this is a clear indication of the stability of the catalyst.

Similarly, the HDO of guaiacol was investigated using Ni/Al-SBA-15(50) because of its superiority in the HDO of DBF. The HDO reaction of guaiacol proceeded via demethoxylation (DMO) reaction and the major product was cyclohexane. The highest conversion ~99% was achieved at 250 °C, 5 h and 5 MPa, and the corresponding degree of HDO was 92%. Cyclohexane was the dominant product with a maximum selectivity of 76%, while benzene is the other HDO product obtained.

The performances of the synthesized catalysts have answered some important challenges associated with upgrading bio-oil model compounds, such as operating temperature (since temperature used in reports available in open literature is 300 °C and above). In addition, the price advantage of Ni over noble metal-based catalysts offers a prospect of lowering the financial upgrading cost of bio-oil model. It is plausible because despite the choice of Ni-based catalysts, the results obtained are comparable with those obtained with noble metals.

## **5.2 Recommendations for future work**

Though this work articulately reported a compelling advancement of knowledge in the development of catalysts for upgrading bio-oil model compounds, however, there is need for further studies on these achievements. These include:

- i. Catalysts deactivation mechanism studies and possibility of leaching.
- ii. There is need to investigate the applicability of the synthesized catalysts in HDO of real bio-oil and not just only the model compounds.

## REFERENCES

- Adjaye, J. D., & Bakhshi, N. N. (1995). Production of hydrocarbons by catalytic upgrading of a fast pyrolysis bio-oil. Part I: Conversion over various catalysts. *Fuel Processing Technology*, 45(3), 161-183. doi:[http://dx.doi.org/10.1016/0378-3820\(95\)00034-5](http://dx.doi.org/10.1016/0378-3820(95)00034-5)
- Al-Obaidi, H. N. (2015). Beam analysis of scanning electron microscope according to the mirror effect phenomenon. *Journal of Electrostatics*, 74, 102-107. doi:<http://dx.doi.org/10.1016/j.elstat.2015.01.004>
- Alexander, A.-M., & Hargreaves, J. S. J. (2010). Alternative catalytic materials: carbides, nitrides, phosphides and amorphous boron alloys. *Chemical Society Reviews*, 39(11), 4388-4401. doi:10.1039/B916787K
- Ardiyanti, A. R., Gutierrez, A., Honkela, M. L., Krause, A. O. I., & Heeres, H. J. (2011). Hydrotreatment of wood-based pyrolysis oil using zirconia-supported mono- and bimetallic (Pt, Pd, Rh) catalysts. *Applied Catalysis A: General*, 407(1-2), 56-66. doi:<http://dx.doi.org/10.1016/j.apcata.2011.08.024>
- Badawi, M., Paul, J.-F., Payen, E., Romero, Y., Richard, F., Brunet, S., Popov, A., Kondratieva, E., Gilson, J.-P., Mariey, L., Travert, A., & Maugé, F. (2013). Hydrodeoxygenation of Phenolic Compounds by Sulfided (Co)Mo/Al<sub>2</sub>O<sub>3</sub> Catalysts, a Combined Experimental and Theoretical Study. *Oil Gas Sci. Technol. – Rev. IFP Energies nouvelles*, 68(5), 829-840. Retrieved from <http://dx.doi.org/10.2516/ogst/2012041>
- Baldauf, W., Balfanz, U., & Rupp, M. (1994). Upgrading of flash pyrolysis oil and utilization in refineries. *Biomass and Bioenergy*, 7(1-6), 237-244. doi:[http://dx.doi.org/10.1016/0961-9534\(94\)00065-2](http://dx.doi.org/10.1016/0961-9534(94)00065-2)
- Barbara, L. D., & Christine, M. C. (2015). X-ray Powder Diffraction (XRD). Retrieved from [http://serc.carleton.edu/research\\_education/geochemsheets/techniques/XRD.html](http://serc.carleton.edu/research_education/geochemsheets/techniques/XRD.html)
- Barrett, E. P., Joyner, L. G., & Halenda, P. P. (1951). The Determination of Pore Volume and Area Distributions in Porous Substances. I. Computations from Nitrogen Isotherms. *Journal of the American Chemical Society*, 73(1), 373-380. doi:10.1021/ja01145a126
- Bertero, M., & Sedran, U. (2013). Conversion of pine sawdust bio-oil (raw and thermally processed) over equilibrium FCC catalysts. *Bioresource Technology*, 135, 644-651. doi:<http://dx.doi.org/10.1016/j.biortech.2012.11.070>
- Bhange, P., Bhange, D. S., Pradhan, S., & Ramaswamy, V. (2011). Direct synthesis of well-ordered mesoporous Al-SBA-15 and its correlation with the catalytic activity. *Applied Catalysis A: General*, 400(1-2), 176-184. doi:<http://dx.doi.org/10.1016/j.apcata.2011.04.031>
- Boffa, A., Lin, C., Bell, A. T., & Somorjai, G. A. (1994). Promotion of CO and CO<sub>2</sub> Hydrogenation over Rh by Metal Oxides: The Influence of Oxide Lewis Acidity

and Reducibility. *Journal of Catalysis*, 149(1), 149-158. doi:<http://dx.doi.org/10.1006/jcat.1994.1280>

Boffa, A. B., Bell, A. T., & Somorjai, G. A. (1993). Vanadium Oxide Deposited on an Rh Foil: CO and CO<sub>2</sub> Hydrogenation Reactivity. *Journal of Catalysis*, 139(2), 602-610. doi:<http://dx.doi.org/10.1006/jcat.1993.1053>

Borodko, Y., Ager, J. W., Marti, G. E., Song, H., Niesz, K., & Somorjai, G. A. (2005). Structure Sensitivity of Vibrational Spectra of Mesoporous Silica SBA-15 and Pt/SBA-15. *The Journal of Physical Chemistry B*, 109(37), 17386-17390. doi:10.1021/jp051801x

Breysse, M., Portefaix, J. L., & Vrinat, M. (1991). Support effects on hydrotreating catalysts. *Catalysis Today*, 10(4), 489-505. doi:[http://dx.doi.org/10.1016/0920-5861\(91\)80035-8](http://dx.doi.org/10.1016/0920-5861(91)80035-8)

Bridgwater, A. V. (1994). Catalysis in thermal biomass conversion. *Applied Catalysis A: General*, 116(1-2), 5-47. doi:[http://dx.doi.org/10.1016/0926-860X\(94\)80278-5](http://dx.doi.org/10.1016/0926-860X(94)80278-5)

Bridgwater, A. V. (1996). Production of high grade fuels and chemicals from catalytic pyrolysis of biomass. *Catalysis Today*, 29(1-4), 285-295. doi:[http://dx.doi.org/10.1016/0920-5861\(95\)00294-4](http://dx.doi.org/10.1016/0920-5861(95)00294-4)

Bridgwater, A. V. (2010). Chapter 7 Fast Pyrolysis of Biomass for Energy and Fuels *Thermochemical Conversion of Biomass to Liquid Fuels and Chemicals* (pp. 146-191): The Royal Society of Chemistry.

Bridgwater, A. V. (2011). Upgrading Fast Pyrolysis Liquids *Thermochemical Processing of Biomass* (pp. 157-199): John Wiley & Sons, Ltd.

Bridgwater, A. V. (2012). Upgrading biomass fast pyrolysis liquids. *Environmental Progress & Sustainable Energy*, 31(2), 261-268. doi:10.1002/ep.11635

Bridgwater, A. V., & Cottam, M. L. (1992). Opportunities for biomass pyrolysis liquids production and upgrading. *Energy & Fuels*, 6(2), 113-120. doi:10.1021/ef00032a001

Brorson, M., Carlsson, A., & Topsøe, H. (2007). The morphology of MoS<sub>2</sub>, WS<sub>2</sub>, Co-Mo-S, Ni-Mo-S and Ni-W-S nanoclusters in hydrodesulfurization catalysts revealed by HAADF-STEM. *Catalysis Today*, 123(1-4), 31-36. doi:<http://dx.doi.org/10.1016/j.cattod.2007.01.073>

BRUKER. (2016). X-ray Fluorescence (XRF). Retrieved from <https://www.bruker.com/products/x-ray-diffraction-and-elemental-analysis/x-ray-fluorescence.html?gclid=CJLbwJrzg8sCFQ-raQod-F8GIA>

Bu, Q., Lei, H., Zacher, A. H., Wang, L., Ren, S., Liang, J., Wei, Y., Liu, Y., Tang, J., Zhang, Q., & Ruan, R. (2012). A review of catalytic hydrodeoxygenation of lignin-derived phenols from biomass pyrolysis. *Bioresource Technology*, 124, 470-477. doi:<http://dx.doi.org/10.1016/j.biortech.2012.08.089>

- Bui, P., Cecilia, J. A., Oyama, S. T., Takagaki, A., Infantes-Molina, A., Zhao, H., Li, D., Rodríguez-Castellón, E., & Jiménez López, A. (2012). Studies of the synthesis of transition metal phosphides and their activity in the hydrodeoxygenation of a biofuel model compound. *Journal of Catalysis*, 294, 184-198. doi:<http://dx.doi.org/10.1016/j.jcat.2012.07.021>
- Bui, V. N., Laurenti, D., Afanasiev, P., & Geantet, C. (2011a). Hydrodeoxygenation of guaiacol with CoMo catalysts. Part I: Promoting effect of cobalt on HDO selectivity and activity. *Applied Catalysis B: Environmental*, 101(3-4), 239-245. doi:<http://dx.doi.org/10.1016/j.apcatb.2010.10.025>
- Bui, V. N., Laurenti, D., Delichère, P., & Geantet, C. (2011b). Hydrodeoxygenation of guaiacol: Part II: Support effect for CoMoS catalysts on HDO activity and selectivity. *Applied Catalysis B: Environmental*, 101(3-4), 246-255. doi:<http://dx.doi.org/10.1016/j.apcatb.2010.10.031>
- Bui, V. N., Toussaint, G., Laurenti, D., Mirodatos, C., & Geantet, C. (2009). Co-processing of pyrolysis bio oils and gas oil for new generation of bio-fuels: Hydrodeoxygenation of guaiacol and SRGO mixed feed. *Catalysis Today*, 143(1-2), 172-178. doi:<http://dx.doi.org/10.1016/j.cattod.2008.11.024>
- Bumbrah, G. S., & Sharma, R. M. (2015). Raman spectroscopy – Basic principle, instrumentation and selected applications for the characterization of drugs of abuse. *Egyptian Journal of Forensic Sciences*. doi:<http://dx.doi.org/10.1016/j.ejfs.2015.06.001>
- Bykova, M. V., Ermakov, D. Y., Kaichev, V. V., Bulavchenko, O. A., Saraev, A. A., Lebedev, M. Y., & Yakovlev, V. A. (2012). Ni-based sol-gel catalysts as promising systems for crude bio-oil upgrading: Guaiacol hydrodeoxygenation study. *Applied Catalysis B: Environmental*, 113-114, 296-307. doi:<http://dx.doi.org/10.1016/j.apcatb.2011.11.051>
- Bykova, M. V., Ermakov, D. Y., Khromova, S. A., Smirnov, A. A., Lebedev, M. Y., & Yakovlev, V. A. (2014). Stabilized Ni-based catalysts for bio-oil hydrotreatment: Reactivity studies using guaiacol. *Catalysis Today*, 220-222, 21-31. doi:<http://dx.doi.org/10.1016/j.cattod.2013.10.023>
- Cecilia, J. A., Infantes-Molina, A., Rodríguez-Castellón, E., Jiménez-López, A., & Oyama, S. T. (2013). Oxygen-removal of dibenzofuran as a model compound in biomass derived bio-oil on nickel phosphide catalysts: Role of phosphorus. *Applied Catalysis B: Environmental*, 136-137, 140-149. doi:<http://dx.doi.org/10.1016/j.apcatb.2013.01.047>
- Chary, K. V. R., Rao, P. V. R., & Vishwanathan, V. (2006). Synthesis and high performance of ceria supported nickel catalysts for hydrodechlorination reaction. *Catalysis Communications*, 7(12), 974-978. doi:<http://dx.doi.org/10.1016/j.catcom.2006.04.013>
- Chianelli, R. R., Berhault, G., & Torres, B. (2009). Unsupported transition metal sulfide catalysts: 100 years of science and application. *Catalysis Today*, 147(3-4), 275-286. doi:<http://dx.doi.org/10.1016/j.cattod.2008.09.041>

- Chiaromonti, D., Bonini, M., Fratini, E., Tondi, G., Gartner, K., Bridgwater, A. V., Grimm, H. P., Soldaini, I., Webster, A., & Baglioni, P. (2003). Development of emulsions from biomass pyrolysis liquid and diesel and their use in engines—Part 2: tests in diesel engines. *Biomass and Bioenergy*, 25(1), 101-111. doi:[http://dx.doi.org/10.1016/S0961-9534\(02\)00184-8](http://dx.doi.org/10.1016/S0961-9534(02)00184-8)
- Condon, J., B. (2006). *Surface Area and Porosity Determinations By Physisorption: Measurements and Theory* (1st ed.). Amsterdam, Netherlands: Elsevier.
- Corma, A. (1997). From Microporous to Mesoporous Molecular Sieve Materials and Their Use in Catalysis. *Chemical Reviews*, 97(6), 2373-2420. doi:10.1021/cr960406n
- Czernik, S., & Bridgwater, A. V. (2004). Overview of Applications of Biomass Fast Pyrolysis Oil. *Energy & Fuels*, 18(2), 590-598. doi:10.1021/ef034067u
- Danilatos, G., Kollia, M., & Dracopoulos, V. (2015). Transmission environmental scanning electron microscope with scintillation gaseous detection device. *Ultramicroscopy*, 150, 44-53. doi:<http://dx.doi.org/10.1016/j.ultramic.2014.11.010>
- Debdoubi, A., El amarti, A., Colacio, E., Blesa, M. J., & Hajjaj, L. H. (2006). The effect of heating rate on yields and compositions of oil products from esparto pyrolysis. *International Journal of Energy Research*, 30(15), 1243-1250. doi:10.1002/er.1215
- Demirbas, A. (2007). The influence of temperature on the yields of compounds existing in bio-oils obtained from biomass samples via pyrolysis. *Fuel Processing Technology*, 88(6), 591-597. doi:<http://dx.doi.org/10.1016/j.fuproc.2007.01.010>
- Deutsch, K. L., & Shanks, B. H. (2012). Hydrodeoxygenation of lignin model compounds over a copper chromite catalyst. *Applied Catalysis A: General*, 447-448, 144-150. doi:<http://dx.doi.org/10.1016/j.apcata.2012.09.047>
- Dhandapani, B., St. Clair, T., & Oyama, S. T. (1998). Simultaneous hydrodesulfurization, hydrodeoxygenation, and hydrogenation with molybdenum carbide. *Applied Catalysis A: General*, 168(2), 219-228. doi:[http://dx.doi.org/10.1016/S0926-860X\(97\)00342-6](http://dx.doi.org/10.1016/S0926-860X(97)00342-6)
- Duan, J., Han, J., Sun, H., Chen, P., Lou, H., & Zheng, X. (2012). Diesel-like hydrocarbons obtained by direct hydrodeoxygenation of sunflower oil over Pd/Al-SBA-15 catalysts. *Catalysis Communications*, 17, 76-80. doi:<http://dx.doi.org/10.1016/j.catcom.2011.10.009>
- Echeandia, S., Pawelec, B., Barrio, V. L., Arias, P. L., Cambra, J. F., Loricera, C. V., & Fierro, J. L. G. (2014). Enhancement of phenol hydrodeoxygenation over Pd catalysts supported on mixed HY zeolite and Al<sub>2</sub>O<sub>3</sub>. An approach to O-removal from bio-oils. *Fuel*, 117, Part B, 1061-1073. doi:<http://dx.doi.org/10.1016/j.fuel.2013.10.011>
- Elliott, D. C., & Hart, T. R. (2009). Catalytic Hydroprocessing of Chemical Models for Bio-oil. *Energy & Fuels*, 23(2), 631-637. doi:10.1021/ef8007773

- Elliott, D. C., Hart, T. R., Neuenschwander, G. G., Rotness, L. J., & Zacher, A. H. (2009). Catalytic hydroprocessing of biomass fast pyrolysis bio-oil to produce hydrocarbon products. *Environmental Progress & Sustainable Energy*, 28(3), 441-449. doi:10.1002/ep.10384
- Fang, K., Ren, J., & Sun, Y. (2005). Effect of nickel precursors on the performance of Ni/AlMCM-41 catalysts for n-dodecane hydroconversion. *Journal of Molecular Catalysis A: Chemical*, 229(1-2), 51-58. doi:<http://dx.doi.org/10.1016/j.molcata.2004.10.055>
- Foster, A., Do, P. M., & Lobo, R. (2012). The Synergy of the Support Acid Function and the Metal Function in the Catalytic Hydrodeoxygenation of m-Cresol. *Topics in Catalysis*, 55(3-4), 118-128. doi:10.1007/s11244-012-9781-7
- Furimsky, E. (2000). Catalytic hydrodeoxygenation. *Applied Catalysis A: General*, 199(2), 147-190. doi:[http://dx.doi.org/10.1016/S0926-860X\(99\)00555-4](http://dx.doi.org/10.1016/S0926-860X(99)00555-4)
- Furimsky, E., & Massoth, F. E. (1999). Deactivation of hydroprocessing catalysts. *Catalysis Today*, 52(4), 381-495. doi:[http://dx.doi.org/10.1016/S0920-5861\(99\)00096-6](http://dx.doi.org/10.1016/S0920-5861(99)00096-6)
- Gao, X., Bare, S. R., Fierro, J. L. G., Banares, M. A., & Wachs, I. E. (1998a). Preparation and in-Situ Spectroscopic Characterization of Molecularly Dispersed Titanium Oxide on Silica. *The Journal of Physical Chemistry B*, 102(29), 5653-5666. doi:10.1021/jp981423e
- Gao, X., Bare, S. R., Weckhuysen, B. M., & Wachs, I. E. (1998b). In Situ Spectroscopic Investigation of Molecular Structures of Highly Dispersed Vanadium Oxide on Silica under Various Conditions. *The Journal of Physical Chemistry B*, 102(52), 10842-10852. doi:10.1021/jp9826367
- Gbadamasi, S., Ali, T. H., Voon, L. H., Atta, A. Y., Sudarsanam, P., Bhargava, S. K., & Abd Hamid, S. B. (2016). Promising Ni/Al-SBA-15 catalysts for hydrodeoxygenation of dibenzofuran into fuel grade hydrocarbons: synergetic effect of Ni and Al-SBA-15 support. *RSC Advances*, 6(31), 25992-26002. doi:10.1039/C5RA27526A
- Gervasini, A. (2013). Temperature Programmed Reduction/Oxidation (TPR/TPO) Methods. In A. Auroux (Ed.), *Calorimetry and Thermal Methods in Catalysis* (pp. 175-195). Berlin, Heidelberg: Springer Berlin Heidelberg.
- González-Borja, M. Á., & Resasco, D. E. (2011). Anisole and Guaiacol Hydrodeoxygenation over Monolithic Pt-Sn Catalysts. *Energy & Fuels*, 25(9), 4155-4162. doi:10.1021/ef200728r
- Gutierrez, A., Kaila, R. K., Honkela, M. L., Slioor, R., & Krause, A. O. I. (2009). Hydrodeoxygenation of guaiacol on noble metal catalysts. *Catalysis Today*, 147(3-4), 239-246. doi:<http://dx.doi.org/10.1016/j.cattod.2008.10.037>
- Hahn-Hägerdal, B., Galbe, M., Gorwa-Grauslund, M. F., Lidén, G., & Zacchi, G. (2006). Bio-ethanol – the fuel of tomorrow from the residues of today. *Trends in*

- Hansen, A. C., Zhang, Q., & Lyne, P. W. L. (2005). Ethanol–diesel fuel blends — a review. *Bioresource Technology*, 96(3), 277-285. doi:<http://dx.doi.org/10.1016/j.biortech.2004.04.007>
- Hardcastle, F. D., & Wachs, I. E. (1991). Determination of vanadium-oxygen bond distances and bond orders by Raman spectroscopy. *The Journal of Physical Chemistry*, 95(13), 5031-5041. doi:10.1021/j100166a025
- He, Z., & Wang, X. (2012). Hydrodeoxygenation of model compounds and catalytic systems for pyrolysis bio-oils upgrading. *Catalysis for Sustainable Energy*, 1. doi:10.2478/cse-2012-0004
- Hicks, J. C. (2011). Advances in C–O Bond Transformations in Lignin-Derived Compounds for Biofuels Production. *The Journal of Physical Chemistry Letters*, 2(18), 2280-2287. doi:10.1021/jz2007885
- Hong, D.-Y., Miller, S. J., Agrawal, P. K., & Jones, C. W. (2010). Hydrodeoxygenation and coupling of aqueous phenolics over bifunctional zeolite-supported metal catalysts. *Chemical Communications*, 46(7), 1038-1040. doi:10.1039/B918209H
- Hong, Y. K., Lee, D. W., Eom, H.-J., & Lee, K.-Y. (2014a). The catalytic activity of Pd/WOx/ $\gamma$ -Al<sub>2</sub>O<sub>3</sub> for hydrodeoxygenation of guaiacol. *Applied Catalysis B: Environmental*, 150–151, 438-445. doi:<http://dx.doi.org/10.1016/j.apcatb.2013.12.045>
- Hong, Y. K., Lee, D. W., Eom, H.-J., & Lee, K.-Y. (2014b). The catalytic activity of Sulfided Ni/W/TiO<sub>2</sub> (anatase) for the hydrodeoxygenation of Guaiacol. *Journal of Molecular Catalysis A: Chemical*, 392, 241-246. doi:<http://dx.doi.org/10.1016/j.molcata.2014.05.025>
- Honkela, M. L., Viljava, T.-R., Gutierrez, A., & Krause, A. O. I. (2010). Chapter 11 Hydrotreating for Bio-Oil Upgrading *Thermochemical Conversion of Biomass to Liquid Fuels and Chemicals* (pp. 288-306): The Royal Society of Chemistry.
- Huelsman, C. M., & Savage, P. E. (2012). Intermediates and kinetics for phenol gasification in supercritical water. *Physical Chemistry Chemical Physics*, 14(8), 2900-2910. doi:10.1039/C2CP23910H
- Huuska, M., & Rintala, J. (1985). Effect of catalyst acidity on the hydrogenolysis of anisole. *Journal of Catalysis*, 94(1), 230-238. doi:[http://dx.doi.org/10.1016/0021-9517\(85\)90099-5](http://dx.doi.org/10.1016/0021-9517(85)90099-5)
- Ikura, M., Stanciulescu, M., & Hogan, E. (2003). Emulsification of pyrolysis derived bio-oil in diesel fuel. *Biomass and Bioenergy*, 24(3), 221-232. doi:[http://dx.doi.org/10.1016/S0961-9534\(02\)00131-9](http://dx.doi.org/10.1016/S0961-9534(02)00131-9)
- Imp  rator-Clerc, M., Davidson, P., & Davidson, A. (2000). Existence of a Microporous Corona around the Mesopores of Silica-Based SBA-15 Materials Templated by

Triblock Copolymers. *Journal of the American Chemical Society*, 122(48), 11925-11933. doi:10.1021/ja002245h

Jacobson, K., Maheria, K. C., & Kumar Dalai, A. (2013). Bio-oil valorization: A review. *Renewable and Sustainable Energy Reviews*, 23, 91-106. doi:<http://dx.doi.org/10.1016/j.rser.2013.02.036>

James, B. C. (2006). *Surface Area and Porosity Determinations by Physisorption: Measurements and Theory* (1st ed. ed.). Amsterdam, Netherlands: ELSEVIER.

Joyner, L. G., Barrett, E. P., & Skold, R. (1951). The Determination of Pore Volume and Area Distributions in Porous Substances. II. Comparison between Nitrogen Isotherm and Mercury Porosimeter Methods. *Journal of the American Chemical Society*, 73(7), 3155-3158. doi:10.1021/ja01151a046

Kaiser Optical Systems Inc. (2016). Raman Spectroscopy - A Tutorial. Retrieved from [http://www.kosi.com/na\\_en/products/raman-spectroscopy/raman-technical-resources/raman-tutorial.php](http://www.kosi.com/na_en/products/raman-spectroscopy/raman-technical-resources/raman-tutorial.php)

Karl, W., & Andy, B. (2015, 20/08/2015). X-Ray Fluorescence (XRF). Retrieved from [http://serc.carleton.edu/research\\_education/geochemsheets/techniques/XRF.html](http://serc.carleton.edu/research_education/geochemsheets/techniques/XRF.html)

Katikaneni, S. P. R., Adjaye, J. D., & Bakhshi, N. N. (1995). Performance of Aluminophosphate Molecular Sieve Catalysts for the Production of Hydrocarbons from Wood-Derived and Vegetable Oils. *Energy & Fuels*, 9(6), 1065-1078. doi:10.1021/ef00054a021

Klimova, T., Calderón, M., & Ramírez, J. (2003). Ni and Mo interaction with Al-containing MCM-41 support and its effect on the catalytic behavior in DBT hydrodesulfurization. *Applied Catalysis A: General*, 240(1-2), 29-40. doi:[http://dx.doi.org/10.1016/S0926-860X\(02\)00417-9](http://dx.doi.org/10.1016/S0926-860X(02)00417-9)

Knözinger, H. (2008). Temperature-Programmed Reduction and Oxidation *Handbook of Heterogeneous Catalysis*: Wiley-VCH Verlag GmbH & Co. KGaA.

Krár, M., Kasza, T., Kovács, S., Kalló, D., & Hancsók, J. (2011). Bio gas oils with improved low temperature properties. *Fuel Processing Technology*, 92(5), 886-892. doi:<http://dx.doi.org/10.1016/j.fuproc.2010.12.007>

Laurent, E., & Delmon, B. (1994a). Influence of water in the deactivation of a sulfided NiMo $\gamma$ -Al<sub>2</sub>O<sub>3</sub> catalyst during hydrodeoxygenation. *Journal of Catalysis*, 146(1), 281-291. doi:[http://dx.doi.org/10.1016/0021-9517\(94\)90032-9](http://dx.doi.org/10.1016/0021-9517(94)90032-9)

Laurent, E., & Delmon, B. (1994b). Study of the hydrodeoxygenation of carbonyl, carboxylic and guaiacyl groups over sulfided CoMo/ $\gamma$ -Al<sub>2</sub>O<sub>3</sub> and NiMo/ $\gamma$ -Al<sub>2</sub>O<sub>3</sub> catalyst: II. Influence of water, ammonia and hydrogen sulfide. *Applied Catalysis A: General*, 109(1), 97-115. doi:[http://dx.doi.org/10.1016/0926-860X\(94\)85005-4](http://dx.doi.org/10.1016/0926-860X(94)85005-4)

Lee, C. R., Yoon, J. S., Suh, Y.-W., Choi, J.-W., Ha, J.-M., Suh, D. J., & Park, Y.-K. (2012). Catalytic roles of metals and supports on hydrodeoxygenation of lignin

monomer guaiacol. *Catalysis Communications*, 17, 54-58.  
doi:<http://dx.doi.org/10.1016/j.catcom.2011.10.011>

Lee, H. W., Jun, B. R., Kim, H., Kim, D. H., Jeon, J.-K., Park, S. H., Ko, C. H., Kim, T.-W., & Park, Y.-K. (2015). Catalytic hydrodeoxygenation of 2-methoxy phenol and dibenzofuran over Pt/mesoporous zeolites. *Energy*, 81, 33-40.  
doi:<http://dx.doi.org/10.1016/j.energy.2014.11.058>

Li, C., & Chen, Y.-W. (1995). Temperature-programmed-reduction studies of nickel oxide/alumina catalysts: effects of the preparation method. *Thermochimica Acta*, 256(2), 457-465. doi:[http://dx.doi.org/10.1016/0040-6031\(94\)02177-P](http://dx.doi.org/10.1016/0040-6031(94)02177-P)

Li, K., Wang, R., & Chen, J. (2011). Hydrodeoxygenation of Anisole over Silica-Supported Ni<sub>2</sub>P, MoP, and NiMoP Catalysts. *Energy & Fuels*, 25(3), 854-863.  
doi:10.1021/ef101258j

Li, Q., Wu, Z., Tu, B., Park, S. S., Ha, C.-S., & Zhao, D. (2010). Highly hydrothermal stability of ordered mesoporous aluminosilicates Al-SBA-15 with high Si/Al ratio. *Microporous and Mesoporous Materials*, 135(1-3), 95-104.  
doi:<http://dx.doi.org/10.1016/j.micromeso.2010.06.016>

Li, X., Li, Z., & Luo, L. a. (2008). Adsorption Kinetics of Dibenzofuran in Activated Carbon Packed Bed\*. *Chinese Journal of Chemical Engineering*, 16(2), 203-208.  
doi:[http://dx.doi.org/10.1016/S1004-9541\(08\)60063-4](http://dx.doi.org/10.1016/S1004-9541(08)60063-4)

Li, Y., Zhang, W., Zhang, L., Yang, Q., Wei, Z., Feng, Z., & Li, C. (2004). Direct synthesis of Al-SBA-15 mesoporous materials via hydrolysis-controlled approach. *The Journal of Physical Chemistry B*, 108(28), 9739-9744.

Lin, Y.-C., Li, C.-L., Wan, H.-P., Lee, H.-T., & Liu, C.-F. (2011). Catalytic Hydrodeoxygenation of Guaiacol on Rh-Based and Sulfided CoMo and NiMo Catalysts. *Energy & Fuels*, 25(3), 890-896. doi:10.1021/ef101521z

Lindo, M., Vizcaíno, A. J., Calles, J. A., & Carrero, A. (2010). Ethanol steam reforming on Ni/Al-SBA-15 catalysts: Effect of the aluminium content. *International Journal of Hydrogen Energy*, 35(11), 5895-5901.  
doi:<http://dx.doi.org/10.1016/j.ijhydene.2009.12.120>

Liu, H., Wang, H., Shen, J., Sun, Y., & Liu, Z. (2008). Preparation, characterization and activities of the nano-sized Ni/SBA-15 catalyst for producing CO<sub>x</sub>-free hydrogen from ammonia. *Applied Catalysis A: General*, 337(2), 138-147.  
doi:<http://dx.doi.org/10.1016/j.apcata.2007.12.006>

Ma'amor, A. (2005). *Application of combinatorial technology: Catalytic hydrogenolysis of fatty esters*. (Masters), University of Malaya, Kuala Lumpur, Malaysia.

Massoth, F. E., Politzer, P., Concha, M. C., Murray, J. S., Jakowski, J., & Simons, J. (2006). Catalytic Hydrodeoxygenation of Methyl-Substituted Phenols: Correlations of Kinetic Parameters with Molecular Properties. *The Journal of Physical Chemistry B*, 110(29), 14283-14291. doi:10.1021/jp057332g

- Mendes, M. J., Santos, O. A. A., Jordão, E., & Silva, A. M. (2001). Hydrogenation of oleic acid over ruthenium catalysts. *Applied Catalysis A: General*, 217(1–2), 253–262. doi:[http://dx.doi.org/10.1016/S0926-860X\(01\)00613-5](http://dx.doi.org/10.1016/S0926-860X(01)00613-5)
- Micromeritics. (2015). TECHNIQUE Temperature Programmed Reduction (TPR). Retrieved from <http://www.micromeritics.com/Repository/Files/Autochem%20II%202920%20technique%20TPR.pdf>
- Modak, A., Deb, A., Patra, T., Rana, S., Maity, S., & Maiti, D. (2012). A general and efficient aldehyde decarbonylation reaction by using a palladium catalyst. *Chemical Communications*, 48(35), 4253–4255. doi:10.1039/C2CC31144E
- Mortensen, P. M., Grunwaldt, J. D., Jensen, P. A., Knudsen, K. G., & Jensen, A. D. (2011). A review of catalytic upgrading of bio-oil to engine fuels. *Applied Catalysis A: General*, 407(1–2), 1–19. doi:10.1016/j.apcata.2011.08.046
- Ochoa-Hernández, C., Yang, Y., Pizarro, P., de la Peña O'Shea, V. A., Coronado, J. M., & Serrano, D. P. (2013). Hydrocarbons production through hydrotreating of methyl esters over Ni and Co supported on SBA-15 and Al-SBA-15. *Catalysis Today*, 210, 81–88. doi:<http://dx.doi.org/10.1016/j.cattod.2012.12.002>
- Olcese, R. N., Bettahar, M., Petitjean, D., Malaman, B., Giovanella, F., & Dufour, A. (2012). Gas-phase hydrodeoxygenation of guaiacol over Fe/SiO<sub>2</sub> catalyst. *Applied Catalysis B: Environmental*, 115–116, 63–73. doi:<http://dx.doi.org/10.1016/j.apcatb.2011.12.005>
- OXFORD Instruments. (2016). XRF - X-ray Fluorescence analysis explained. Retrieved from <http://www.oxford-instruments.com/businesses/industrial-products/industrial-analysis/xrf>
- Pestman, R., Koster, R. M., Pieterse, J. A. Z., & Ponc, V. (1997). Reactions of Carboxylic Acids on Oxides: 1. Selective Hydrogenation of Acetic Acid to Acetaldehyde. *Journal of Catalysis*, 168(2), 255–264. doi:<http://dx.doi.org/10.1006/jcat.1997.1623>
- Popov, A., Kondratieva, E., Goupil, J. M., Mariey, L., Bazin, P., Gilson, J.-P., Travert, A., & Maugé, F. (2010). Bio-oils Hydrodeoxygenation: Adsorption of Phenolic Molecules on Oxidic Catalyst Supports. *The Journal of Physical Chemistry C*, 114(37), 15661–15670. doi:10.1021/jp101949j
- Prasomsri, T., To, A. T., Crossley, S., Alvarez, W. E., & Resasco, D. E. (2011). Catalytic conversion of anisole over HY and HZSM-5 zeolites in the presence of different hydrocarbon mixtures. *Applied Catalysis B: Environmental*, 106(1–2), 204–211. doi:<http://dx.doi.org/10.1016/j.apcatb.2011.05.026>
- Princeton Instruments. (2016). Raman Spectroscopy Basics. Retrieved from <http://www.princetoninstruments.com/spectroscopy/Raman>
- Procházková, D., Zámostný, P., Bejblová, M., Červený, L., & Čejka, J. (2007). Hydrodeoxygenation of aldehydes catalyzed by supported palladium catalysts.

- Rana, M. S., Srinivas, B. N., Maity, S. K., Murali Dhar, G., & Prasada Rao, T. S. R. (2000). Origin of Cracking Functionality of Sulfided (Ni) CoMo/SiO<sub>2</sub>-ZrO<sub>2</sub> Catalysts. *Journal of Catalysis*, 195(1), 31-37. doi:<http://dx.doi.org/10.1006/jcat.2000.2968>
- Ratnasamy, P., & Fripiat, J. J. (1970). Surface chemistry of sulphides. Part 1.-Infra-red study of molybdenum and germanium sulphides and of their reaction with H<sub>2</sub>, H<sub>2</sub>O, thiophene and ethanethiol. *Transactions of the Faraday Society*, 66(0), 2897-2910. doi:10.1039/TF9706602897
- Reiche, M. A., Maciejewski, M., & Baiker, A. (2000). Characterization by temperature programmed reduction. *Catalysis Today*, 56(4), 347-355. doi:[http://dx.doi.org/10.1016/S0920-5861\(99\)00294-1](http://dx.doi.org/10.1016/S0920-5861(99)00294-1)
- Resasco, D. E. (2011). What Should We Demand from the Catalysts Responsible for Upgrading Biomass Pyrolysis Oil? *The Journal of Physical Chemistry Letters*, 2(18), 2294-2295. doi:10.1021/jz201135x
- Roberts, V. M., Stein, V., Reiner, T., Lemonidou, A., Li, X., & Lercher, J. A. (2011). Towards Quantitative Catalytic Lignin Depolymerization. *Chemistry – A European Journal*, 17(21), 5939-5948. doi:10.1002/chem.201002438
- Romero, Y., Richard, F., & Brunet, S. (2010). Hydrodeoxygenation of 2-ethylphenol as a model compound of bio-crude over sulfided Mo-based catalysts: Promoting effect and reaction mechanism. *Applied Catalysis B: Environmental*, 98(3-4), 213-223. doi:<http://dx.doi.org/10.1016/j.apcatb.2010.05.031>
- Ruddy, D. A., Schaidle, J. A., Ferrell Iii, J. R., Wang, J., Moens, L., & Hensley, J. E. (2014). Recent advances in heterogeneous catalysts for bio-oil upgrading via “ex situ catalytic fast pyrolysis”: catalyst development through the study of model compounds. *Green Chem.*, 16(2), 454-490. doi:10.1039/c3gc41354c
- Ruiz, P. E., Leiva, K., Garcia, R., Reyes, P., Fierro, J. L. G., & Escalona, N. (2010). Relevance of sulfiding pretreatment on the performance of Re/ZrO<sub>2</sub> and Re/ZrO<sub>2</sub>-sulfated catalysts for the hydrodeoxygenation of guayacol. *Applied Catalysis A: General*, 384(1-2), 78-83. doi:<http://dx.doi.org/10.1016/j.apcata.2010.06.009>
- Saidi, M., Rostami, P., Rahimpour, H. R., Roshanfekar Fallah, M. A., Rahimpour, M. R., Gates, B. C., & Raeissi, S. (2015). Kinetics of Upgrading of Anisole with Hydrogen Catalyzed by Platinum Supported on Alumina. *Energy & Fuels*, 29(8), 4990-4997. doi:10.1021/acs.energyfuels.5b00297
- Samolada, M. C., Baldauf, W., & Vasalos, I. A. (1998). Production of a bio-gasoline by upgrading biomass flash pyrolysis liquids via hydrogen processing and catalytic cracking. *Fuel*, 77(14), 1667-1675. doi:[http://dx.doi.org/10.1016/S0016-2361\(98\)00073-8](http://dx.doi.org/10.1016/S0016-2361(98)00073-8)

- Sankaranarayanan, T. M., Berenguer, A., Ochoa-Hernández, C., Moreno, I., Jana, P., Coronado, J. M., Serrano, D. P., & Pizarro, P. (2015). Hydrodeoxygenation of anisole as bio-oil model compound over supported Ni and Co catalysts: Effect of metal and support properties. *Catalysis Today*, *243*, 163-172. doi:<http://dx.doi.org/10.1016/j.cattod.2014.09.004>
- Scarano, D., Zecchina, A., Bordiga, S., Geobaldo, F., Spoto, G., Petrini, G., Leofanti, G., Padovan, M., & Tozzola, G. (1993). Fourier-transform infrared and Raman spectra of pure and Al-, B-, Ti- and Fe-substituted silicalites: stretching-mode region. *Journal of the Chemical Society, Faraday Transactions*, *89*(22), 4123-4130. doi:10.1039/FT9938904123
- Schimming, S. M., LaMont, O. D., Konig, M., Rogers, A. K., D'Amico, A. D., Yung, M. M., & Sievers, C. (2015). Hydrodeoxygenation of Guaiacol over Ceria-Zirconia Catalysts. *ChemSusChem*, *8*(12), 2073-2083. doi:10.1002/cssc.201500317
- Şenol, O. İ. (2007). Hydrodeoxygenation of aliphatic and aromatic oxygenates on sulphided catalysts for production of second generation biofuels. (PhD), Helsinki University of Technology, Industrial Chemistry Publication Series, Finland. Retrieved from <http://lib.tkk.fi/Diss/2007/isbn9789512290369>
- Şenol, O. İ., Ryymin, E. M., Viljava, T. R., & Krause, A. O. I. (2007). Effect of hydrogen sulphide on the hydrodeoxygenation of aromatic and aliphatic oxygenates on sulphided catalysts. *Journal of Molecular Catalysis A: Chemical*, *277*(1-2), 107-112. doi:<http://dx.doi.org/10.1016/j.molcata.2007.07.033>
- Sharma, R. K., & Bakhshi, N. N. (1991). Catalytic upgrading of biomass-derived oils to transportation fuels and chemicals. *The Canadian Journal of Chemical Engineering*, *69*(5), 1071-1081. doi:10.1002/cjce.5450690505
- Sheu, Y.-H. E., Anthony, R. G., & Soltes, E. J. (1988). Kinetic studies of upgrading pine pyrolytic oil by hydrotreatment. *Fuel Processing Technology*, *19*(1), 31-50. doi:[http://dx.doi.org/10.1016/0378-3820\(88\)90084-7](http://dx.doi.org/10.1016/0378-3820(88)90084-7)
- Silaghi, M.-C., Chizallet, C., & Raybaud, P. (2014). Challenges on molecular aspects of dealumination and desilication of zeolites. *Microporous and Mesoporous Materials*, *191*, 82-96. doi:<http://dx.doi.org/10.1016/j.micromeso.2014.02.040>
- Song, C. (2006). Global challenges and strategies for control, conversion and utilization of CO<sub>2</sub> for sustainable development involving energy, catalysis, adsorption and chemical processing. *Catalysis Today*, *115*(1-4), 2-32. doi:<http://dx.doi.org/10.1016/j.cattod.2006.02.029>
- Song, W., Liu, Y., Barath, E., Zhao, C., & Lercher, J. A. (2015). Synergistic effects of Ni and acid sites for hydrogenation and C-O bond cleavage of substituted phenols. *Green Chemistry*, *17*(2), 1204-1218. doi:10.1039/C4GC01798F
- Stakheev, A. Y., & Kustov, L. M. (1999). Effects of the support on the morphology and electronic properties of supported metal clusters: modern concepts and progress in 1990s. *Applied Catalysis A: General*, *188*(1-2), 3-35. doi:[http://dx.doi.org/10.1016/S0926-860X\(99\)00232-X](http://dx.doi.org/10.1016/S0926-860X(99)00232-X)

- Subramani, V., & Gangwal, S. K. (2008). A Review of Recent Literature to Search for an Efficient Catalytic Process for the Conversion of Syngas to Ethanol. *Energy & Fuels*, 22(2), 814-839. doi:10.1021/ef700411x
- Suga, M., Asahina, S., Sakuda, Y., Kazumori, H., Nishiyama, H., Nokuo, T., Alfredsson, V., Kjellman, T., Stevens, S. M., Cho, H. S., Cho, M., Han, L., Che, S., Anderson, M. W., Schüth, F., Deng, H., Yaghi, O. M., Liu, Z., Jeong, H. Y., Stein, A., Sakamoto, K., Ryoo, R., & Terasaki, O. (2014). Recent progress in scanning electron microscopy for the characterization of fine structural details of nano materials. *Progress in Solid State Chemistry*, 42(1–2), 1-21. doi:<http://dx.doi.org/10.1016/j.progsolidstchem.2014.02.001>
- Takahashi, R., Sato, S., Sodesawa, T., Kato, M., Takenaka, S., & Yoshida, S. (2001). Structural and Catalytic Properties of Ni/SiO<sub>2</sub> Prepared by Solution Exchange of Wet Silica Gel. *Journal of Catalysis*, 204(2), 259-271. doi:<http://dx.doi.org/10.1006/jcat.2001.3400>
- Thermo Scientific. (2015). XRF Technology Retrieved from <https://www.thermoscientific.com/en/about-us/general-landing-page/xrf-technology.html>
- Toba, M., Abe, Y., Kuramochi, H., Osako, M., Mochizuki, T., & Yoshimura, Y. (2011). Hydrodeoxygenation of waste vegetable oil over sulfide catalysts. *Catalysis Today*, 164(1), 533-537. doi:<http://dx.doi.org/10.1016/j.cattod.2010.11.049>
- Topsøe, H., Clausen, B. S., Massoth, F. E., Anderson, J., & Boudart, M. (1996). *Hydrotreating Catalysis Science and Technology*: Springer, Berlin.
- Tran, N. T. T., Uemura, Y., Chowdhury, S., & Ramli, A. (2016). Vapor-phase hydrodeoxygenation of guaiacol on Al-MCM-41 supported Ni and Co catalysts. *Applied Catalysis A: General*, 512, 93-100. doi:<http://dx.doi.org/10.1016/j.apcata.2015.12.021>
- Travert, A., Nakamura, H., van Santen, R. A., Cristol, S., Paul, J.-F., & Payen, E. (2002). Hydrogen Activation on Mo-Based Sulfide Catalysts, a Periodic DFT Study. *Journal of the American Chemical Society*, 124(24), 7084-7095. doi:10.1021/ja011634o
- Venderbosch, R. H., Ardiyanti, A. R., Wildschut, J., Oasmaa, A., & Heeres, H. J. (2010). Stabilization of biomass-derived pyrolysis oils. *Journal of Chemical Technology & Biotechnology*, 85(5), 674-686. doi:10.1002/jctb.2354
- Viljava, T. R., Komulainen, R. S., & Krause, A. O. I. (2000). Effect of H<sub>2</sub>S on the stability of CoMo/Al<sub>2</sub>O<sub>3</sub> catalysts during hydrodeoxygenation. *Catalysis Today*, 60(1–2), 83-92. doi:[http://dx.doi.org/10.1016/S0920-5861\(00\)00320-5](http://dx.doi.org/10.1016/S0920-5861(00)00320-5)
- Viljava, T. R., Komulainen, S., Selvam, T., & Krause, A. O. I. (1999). Stability of CoMo/Al<sub>2</sub>O<sub>3</sub> catalysts: Effect of HDO cycles on HDS. In G. F. F. B. Delmon & P. Grange (Eds.), *Studies in Surface Science and Catalysis* (Vol. Volume 127, pp. 145-152): Elsevier.

- Wang, L., Li, C., Jin, S., Li, W., & Liang, C. (2014). Hydrodeoxygenation of Dibenzofuran Over SBA-15 Supported Pt, Pd, and Ru Catalysts. *Catalysis Letters*, *144*(5), 809-816. doi:10.1007/s10562-014-1236-2
- Wang, L., Wan, H., Jin, S., Chen, X., Li, C., & Liang, C. (2015). Hydrodeoxygenation of dibenzofuran over SiO<sub>2</sub>, Al<sub>2</sub>O<sub>3</sub>/SiO<sub>2</sub> and ZrO<sub>2</sub>/SiO<sub>2</sub> supported Pt catalysts. *Catalysis Science & Technology*, *5*(1), 465-474. doi:10.1039/C4CY00859F
- Wang, L., Zhang, M., Zhang, M., Sha, G., & Liang, C. (2013). Hydrodeoxygenation of Dibenzofuran over Mesoporous Silica COK-12 Supported Palladium Catalysts. *Energy & Fuels*, *27*(4), 2209-2217. doi:10.1021/ef302166q
- Wang, W.-y., Yang, Y.-q., Bao, J.-g., & Luo, H.-a. (2009). Characterization and catalytic properties of Ni–Mo–B amorphous catalysts for phenol hydrodeoxygenation. *Catalysis Communications*, *11*(2), 100-105. doi:<http://dx.doi.org/10.1016/j.catcom.2009.09.003>
- Wang, W.-y., Yang, Y.-q., Luo, H.-a., & Liu, W.-y. (2010). Effect of additive (Co, La) for Ni–Mo–B amorphous catalyst and its hydrodeoxygenation properties. *Catalysis Communications*, *11*(9), 803-807. doi:<http://dx.doi.org/10.1016/j.catcom.2010.02.019>
- Wang, W., Wang, S., Ma, X., & Gong, J. (2011). Recent advances in catalytic hydrogenation of carbon dioxide. *Chemical Society Reviews*, *40*(7), 3703-3727. doi:10.1039/C1CS15008A
- Wang, W., Yang, Y., Luo, H., Hu, T., & Liu, W. (2011). Amorphous Co–Mo–B catalyst with high activity for the hydrodeoxygenation of bio-oil. *Catalysis Communications*, *12*(6), 436-440. doi:<http://dx.doi.org/10.1016/j.catcom.2010.11.001>
- Wang, W., Yang, Y., Luo, H., & Liu, W. (2010). Characterization and hydrodeoxygenation properties of Co promoted Ni–Mo–B amorphous catalysts: influence of Co content. *Reaction Kinetics, Mechanisms and Catalysis*, *101*(1), 105-115. doi:10.1007/s11144-010-0201-3
- Wang, X., Saleh, R. Y., & Ozkan, U. S. (2005). Reaction network of aldehyde hydrogenation over sulfided Ni–Mo/Al<sub>2</sub>O<sub>3</sub> catalysts. *Journal of Catalysis*, *231*(1), 20-32. doi:<http://dx.doi.org/10.1016/j.jcat.2004.12.010>
- Wang, Y., Fang, Y., He, T., Hu, H., & Wu, J. (2011). Hydrodeoxygenation of dibenzofuran over noble metal supported on mesoporous zeolite. *Catalysis Communications*, *12*(13), 1201-1205. doi:<http://dx.doi.org/10.1016/j.catcom.2011.04.010>
- Wang, Y., He, T., Liu, K., Wu, J., & Fang, Y. (2012). From biomass to advanced bio-fuel by catalytic pyrolysis/hydro-processing: Hydrodeoxygenation of bio-oil derived from biomass catalytic pyrolysis. *Bioresource Technology*, *108*, 280-284. doi:<http://dx.doi.org/10.1016/j.biortech.2011.12.132>
- Wildschut, J., Mahfud, F. H., Venderbosch, R. H., & Heeres, H. J. (2009). Hydrotreatment of Fast Pyrolysis Oil Using Heterogeneous Noble-Metal

Catalysts. *Industrial & Engineering Chemistry Research*, 48(23), 10324-10334. doi:10.1021/ie9006003

- Williams, P. T., & Horne, P. A. (1994). Characterisation of oils from the fluidised bed pyrolysis of biomass with zeolite catalyst upgrading. *Biomass and Bioenergy*, 7(1-6), 223-236. doi:[http://dx.doi.org/10.1016/0961-9534\(94\)00064-Z](http://dx.doi.org/10.1016/0961-9534(94)00064-Z)
- Xinghua, Z., Tiejun, W., Longlong, M., & Chuangzhi, W. (2010). Aqueous-phase catalytic process for production of pentane from furfural over nickel-based catalysts. *Fuel*, 89(10), 2697-2702. doi:<http://dx.doi.org/10.1016/j.fuel.2010.05.043>
- Xu, Y., Wang, T., Ma, L., Zhang, Q., & Liang, W. (2010). Upgrading of the liquid fuel from fast pyrolysis of biomass over MoNi/γ-Al<sub>2</sub>O<sub>3</sub> catalysts. *Applied Energy*, 87(9), 2886-2891. doi:<http://dx.doi.org/10.1016/j.apenergy.2009.10.028>
- Yakovlev, V. A., Khromova, S. A., Sherstyuk, O. V., Dundich, V. O., Ermakov, D. Y., Novopashina, V. M., Lebedev, M. Y., Bulavchenko, O., & Parmon, V. N. (2009). Development of new catalytic systems for upgraded bio-fuels production from bio-crude-oil and biodiesel. *Catalysis Today*, 144(3-4), 362-366. doi:<http://dx.doi.org/10.1016/j.cattod.2009.03.002>
- Yang, Y., Ochoa-Hernández, C., de la Peña O'Shea, V. A., Pizarro, P., Coronado, J. M., & Serrano, D. P. (2014). Effect of metal-support interaction on the selective hydrodeoxygenation of anisole to aromatics over Ni-based catalysts. *Applied Catalysis B: Environmental*, 145, 91-100. doi:<http://dx.doi.org/10.1016/j.apcatb.2013.03.038>
- Yue, Y., Gedeon, A., Bonardet, J.-L., D'Espinose, J.-B., Fraissard, J., & Melosh, N. (1999). Direct synthesis of AISBA mesoporous molecular sieves: characterization and catalytic activities. *Chemical Communications*(19), 1967-1968. doi:10.1039/A904467A
- Zacher, A. H., Olarte, M. V., Santosa, D. M., Elliott, D. C., & Jones, S. B. (2014). A review and perspective of recent bio-oil hydrotreating research. *Green Chemistry*, 16(2), 491-515. doi:10.1039/C3GC41382A
- Zhang, Q., Chang, J., Wang, T., & Xu, Y. (2007). Review of biomass pyrolysis oil properties and upgrading research. *Energy Conversion and Management*, 48(1), 87-92. doi:<http://dx.doi.org/10.1016/j.enconman.2006.05.010>
- Zhang, W., Chen, J., Liu, R., Wang, S., Chen, L., & Li, K. (2014). Hydrodeoxygenation of Lignin-Derived Phenolic Monomers and Dimers to Alkane Fuels over Bifunctional Zeolite-Supported Metal Catalysts. *ACS Sustainable Chemistry & Engineering*, 2(4), 683-691. doi:10.1021/sc400401n
- Zhang, X., Zhang, Q., Wang, T., Ma, L., Yu, Y., & Chen, L. (2013). Hydrodeoxygenation of lignin-derived phenolic compounds to hydrocarbons over Ni/SiO<sub>2</sub>-ZrO<sub>2</sub> catalysts. *Bioresource Technology*, 134, 73-80. doi:<http://dx.doi.org/10.1016/j.biortech.2013.02.039>

- Zhao, C., He, J., Lemonidou, A. A., Li, X., & Lercher, J. A. (2011). Aqueous-phase hydrodeoxygenation of bio-derived phenols to cycloalkanes. *Journal of Catalysis*, 280(1), 8-16. doi:<http://dx.doi.org/10.1016/j.jcat.2011.02.001>
- Zhao, C., & Lercher, J. A. (2012). Selective Hydrodeoxygenation of Lignin-Derived Phenolic Monomers and Dimers to Cycloalkanes on Pd/C and HZSM-5 Catalysts. *ChemCatChem*, 4(1), 64-68. doi:10.1002/cctc.201100273
- Zhao, D., Feng, J., Huo, Q., Melosh, N., Fredrickson, G. H., Chmelka, B. F., & Stucky, G. D. (1998). Triblock Copolymer Syntheses of Mesoporous Silica with Periodic 50 to 300 Angstrom Pores. *Science*, 279(5350), 548-552. doi:10.1126/science.279.5350.548
- Zhao, D., Huo, Q., Feng, J., Chmelka, B. F., & Stucky, G. D. (1998). Nonionic Triblock and Star Diblock Copolymer and Oligomeric Surfactant Syntheses of Highly Ordered, Hydrothermally Stable, Mesoporous Silica Structures. *Journal of the American Chemical Society*, 120(24), 6024-6036. doi:10.1021/ja974025i
- Zhu, X., Lobban, L. L., Mallinson, R. G., & Resasco, D. E. (2011). Bifunctional transalkylation and hydrodeoxygenation of anisole over a Pt/HBeta catalyst. *Journal of Catalysis*, 281(1), 21-29. doi:<http://dx.doi.org/10.1016/j.jcat.2011.03.030>

## LIST OF PUBLICATIONS AND PAPERS PRESENTED

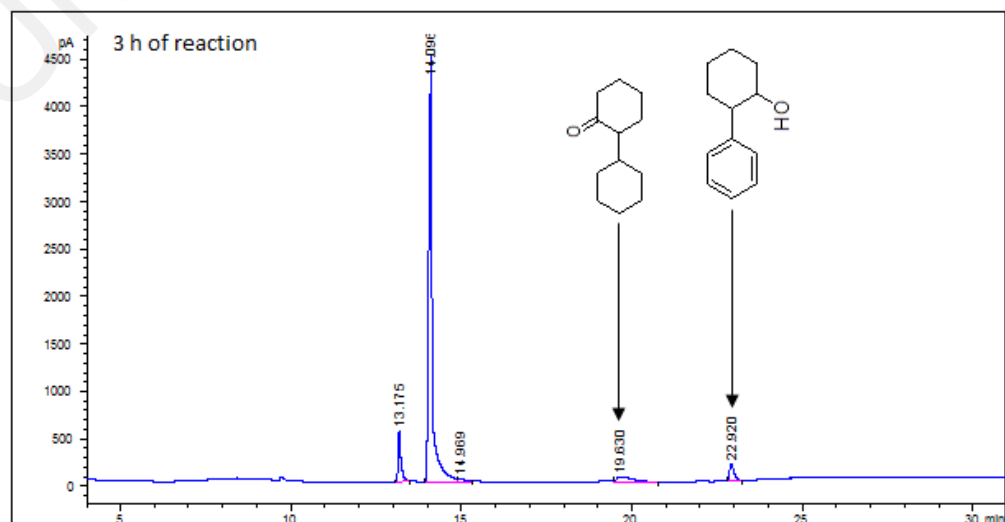
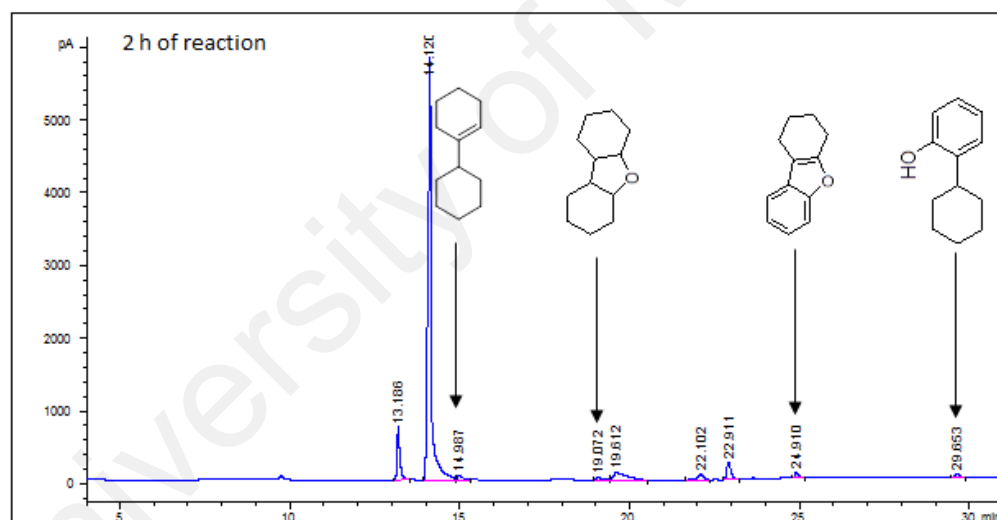
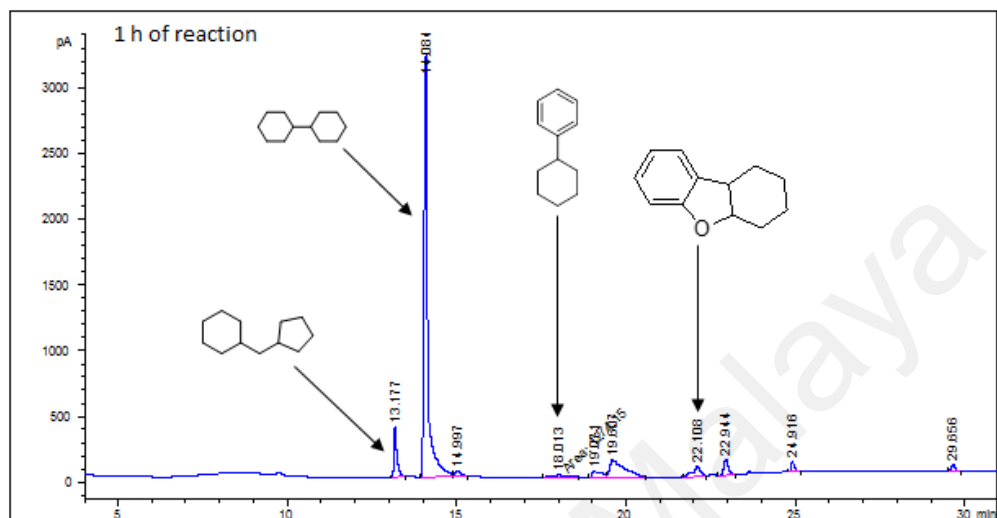
**Gbadamasi, S.**, Ali, T. H., Voon, L. H., Atta, A. Y., Sudarsanam, P., Bhargava, S. K., Abd Hamid, S. B. (2016). Promising Ni/Al-SBA-15 catalysts for hydrodeoxygenation of dibenzofuran into fuel grade hydrocarbons: synergetic effect of Ni and Al-SBA-15 support. *RSC Adv.*, **6**, 25992-26002, **DOI:** 10.1039/C5RA27526A

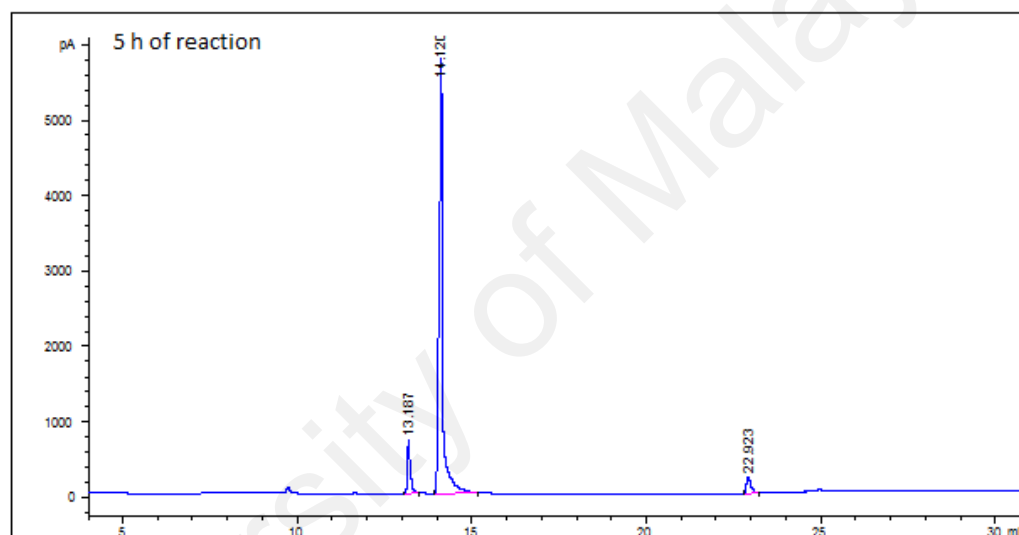
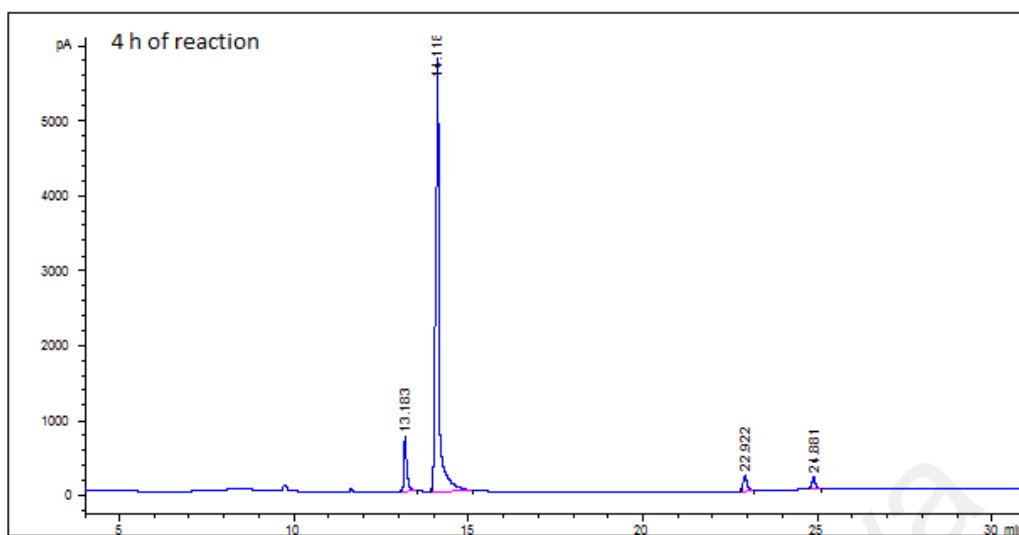
**Gbadamasi, S.**, Abd Hamid, S. B., Voon, L. H., Atta, A. Y. (2016). Hydrodeoxygenation of guaiacol as bio-oil model compound over  $WO_x/Al_2O_3$  supported Ni and Co catalysts. International Conference on Chemistry, Chemical & Petrochemical Engineering (icccpe2016)

Abd Hamid, S. B., Halilu, A., **Gbadamasi, S.**, Hakim, L., (2014). Chapter 11: Opportunities in Utilization of Lignocellulosic Biomass Oil to Bio-Esters: Renewable Energy and Sustainable Developments. Scientific & Academic Publishing, USA, ISBN: 978-1-938681-70-7

## APPENDIX

### Appendix A. GC-FID Chromatograms for product analysis at various reaction time for HDO of DBF at 10 MPa and 260 °C





**Appendix B. Calculation for dibenzofuran conversion at 2 h and 10 MPa**

For the table below, the following equations together with Equation 3.3 were used for the calculations.

$$\text{Response factor} = \frac{\text{DBF Injected (Peak Area)}}{\text{Equivalent amount of DBF feed } (\mu\text{g})} \dots \dots \dots \text{Equation 5.1}$$

$$\text{Equivalent amount of DBF Left } (\mu\text{g}) = \frac{\text{DBF Peak Area Left}}{\text{Response Factor}} \dots \dots \dots \text{Equation 5.2}$$

$$\text{Amount of DBF Consumed } (\mu\text{g}) = \text{Equivalent amount of DBF feed } (\mu\text{g}) - \text{Equivalent amount of DBF Left } (\mu\text{g}) \dots \text{Equation 5.3}$$

| CONVERSION @ 240 °C |                          |                                    |                 |                    |                                    |                             |                |
|---------------------|--------------------------|------------------------------------|-----------------|--------------------|------------------------------------|-----------------------------|----------------|
| Catalyst            | DBF Injected (Peak Area) | Equivalent amount of DBF feed (μg) | Response Factor | DBF Peak Area Left | Equivalent amount of DBF Left (μg) | Amount of DBF Consumed (μg) | Conversion (%) |
| Ni/SBA-15           | 40249.30                 | 39.39                              | 1021.82         | 1123.76            | 1.10                               | 38.29                       | 97.21          |
| Ni/Al-SBA-15(50)    | 40249.30                 | 39.39                              | 1021.82         | 0.00               | 0.00                               | 39.39                       | 100.00         |
| Ni/Al-SBA-15(60)    | 40249.30                 | 39.39                              | 1021.82         | 0.00               | 0.00                               | 39.39                       | 100.00         |
| Ni/Al-SBA-15(70)    | 40249.30                 | 39.39                              | 1021.82         | 695.74             | 0.68                               | 38.71                       | 98.27          |
| Ni/Al-SBA-15(80)    | 40249.30                 | 39.39                              | 1021.82         | 739.12             | 0.72                               | 38.67                       | 98.16          |

| CONVERSION @ 250 °C |                             |  |                    |                       |  |   |                   |
|---------------------|-----------------------------|--|--------------------|-----------------------|--|---|-------------------|
| Catalyst            | DBF Injected<br>(Peak Area) | Equivalent amount<br>of DBF feed ( $\mu\text{g}$ ) | Response<br>Factor | DBF Peak<br>Area Left | Equivalent amount<br>of DBF Left ( $\mu\text{g}$ ) | Amount of DBF<br>Consumed ( $\mu\text{g}$ ) | Conversion<br>(%) |
| Ni/SBA-15           | 40249.30                    | 39.39  | 1021.82            | 817.00                | 0.80   | 38.59                                       | 97.97             |
| Ni/Al-SBA-15(50)    | 40249.30                    | 39.39  | 1021.82            | 0.00                  | 0.00   | 39.39                                       | 100.00            |
| Ni/Al-SBA-15(60)    | 40249.30                    | 39.39  | 1021.82            | 0.00                  | 0.00   | 39.39                                       | 100.00            |
| Ni/Al-SBA-15(70)    | 40249.30                    | 39.39  | 1021.82            | 0.00                  | 0.00   | 39.39                                       | 100.00            |
| Ni/Al-SBA-15(80)    | 40249.30                    | 39.39  | 1021.82            | 276.60                | 0.27   | 39.12                                       | 99.31             |

| CONVERSION @ 260 °C |                             |  |                    |                       |  |   |                   |
|---------------------|-----------------------------|--|--------------------|-----------------------|--|---|-------------------|
| Catalyst            | DBF Injected<br>(Peak Area) | Equivalent amount<br>of DBF feed ( $\mu\text{g}$ ) | Response<br>Factor | DBF Peak<br>Area Left | Equivalent amount<br>of DBF Left ( $\mu\text{g}$ ) | Amount of DBF<br>Consumed ( $\mu\text{g}$ ) | Conversion<br>(%) |
| Ni/SBA-15           | 40249.30                    | 39.39  | 1021.82            | 271.00                | 0.27   | 39.12                                       | 99.33             |
| Ni/Al-SBA-15(50)    | 40249.30                    | 39.39  | 1021.82            | 0.00                  | 0.00   | 39.39                                       | 100.00            |
| Ni/Al-SBA-15(60)    | 40249.30                    | 39.39  | 1021.82            | 0.00                  | 0.00   | 39.39                                       | 100.00            |
| Ni/Al-SBA-15(70)    | 40249.30                    | 39.39  | 1021.82            | 0.00                  | 0.00   | 39.39                                       | 100.00            |
| Ni/Al-SBA-15(80)    | 40249.30                    | 39.39  | 1021.82            | 0.00                  | 0.00   | 39.39                                       | 100.00            |